Ministry of Higher Education and Scientific Research

UNIVERSITÉ ABDELHAMID IBN BADIS - MOSTAGANEM

Faculty of Exact Sciences and Computer Science
Chemistry Department

Field of Study : Applied Chemistry

A dissertation submitted of the

requirements for the degree of Doctor of Philosophy

Specialization: material valorisation

By **BERRAHAL Malika**

THEME :

Synthesis of carbonaceous materials and their use in water treatment.

President : Prof. Benmalti Mohamed El Amine   University of Mostaganem

Examiner : Prof. Belhakem Ahmad   University of Mostaganem

Examiner : Prof. Chougui Abdelkader   University of Tiaret

Supervisor: Prof. Belouatek Aissa   University of Mostaganem

Academic Year : 2023-2024

Dedications

*With my appreciation and all my love, I dedicate this work to: **My beloved parents**, who have devoted their lives to building mine, who have always been there for my joys as well as my sorrows. I express my deep devotion, admiration, and profound respect to them with much emotion. Through this humble work, I hope to give you a small portion of the pride I feel in being your daughter.*

*My little daughter **Yuna***

*My spouse, **Mohamed***

*To my dear brothers : **Nadir**, **Yassine**, and my dear sister **Aya**, I am grateful for their encouragement.*

*To my beloved and dear unt : **Kheira***

To my supportive step family

Appreciation

*First and foremost, I express my gratitude to the Almighty God for granting me the strength, bravery, and resources to complete this humble task. I would like to express my sincere gratitude to my supervisor, Professor **Belouatek Aissa**, for agreeing to guide me and for his understanding nature, patience, availability, valuable guidance, highly valuable advice, and for the time he dedicated to overseeing this work and welcoming me to the Structure, Elaboration, and Application of Molecular Materials (**SEA2M**) laboratory at AbdelHAmid Ibn Bdis Mostaganem University.*

*I would also like to thank Mme. **Nemch Fadhila**, Professor at the University of Mostaganem and Director of the SEA2M laboratory, for providing me with the necessary resources to carry out this thesis. I would also like to acknowledge the members of the laboratory for their teamwork, friendliness, positive attitude, and sense of camaraderie.*

*I would like to thank **Mr Benmalti Mohamed El Amine, professor** at the University of Mostaganem for his interest in this work and for agreeing to chair the Jury for my defence, despite his many occupations.*

*I would like to express my sincere thanks to **Mr Belhakem Ahmad**, Professor at the University of Mostaganem who honoured me by being one of the members of the jury and for agreeing to examine this work.*

*I am also very grateful to **Mr Chougui Abdelkader**, Professor at the University of Tiaret for having very kindly accepted to be part of this jury.*

*A heartfelt thank you to the members of the Research Lab (FSEI faculty), especially Mme. **Hasna** and **Rabiaà**, and to the members of the Pedagogical Lab, as well as all my friends in the cohort, for their assistance, friendship, kindness, and moral support.*

I would also like to express my gratitude to all the teachers who provided me with my education. Finally, my feelings of gratitude and appreciation go to all the individuals who have contributed directly or indirectly to the completion of this project.

Table of content

List of figures

List of tables

Glossary of symbols

NG : natural graphite

MLG : multi-layer graphene

SLG : single-layer graphene sheet

HNO_3 : nitric acid

H_2SO_4 : sulfuric acid

H_3PO_4 : phosphoric acid

HCl : chlorohydric Acid

$KMnO_4$: Potassium permanganate

H_2O_2 : Hydrogen peroxide

EG : exfoliated graphite

MW : microwave

PHB : Porous network hydrogel beads

SA : sodium alginate

$CaCO_3$: calcium carbonate

PVA : Polyvinyl alcohol

$CaCl_2$: calcium chloride

GO : graphene oxide

MGO : magnetic graphene oxide

rGO : reduced graphene oxide

IGO : improved graphene oxide

MWGO : microwave graphene oxide

FTIR : Fourier-transform infrared

XRD : X-ray diffraction

SEM : scanning electron microscopy

TEM : transmission electron microscopy

2D: two dimensional

MG : malachite green

ARS : alizarin red S

CFX : Cefalexin

DMF : N,N-diméthylformamide

MeOH : alcohols methanol

EtOH : ethanol

IPrOH : isopropanol

BnOH : benzyl alcohol

NaCl : sodium chloride

Abstract

This research study presents an academic investigation on the development of a simple, inexpensive, fast, and effective method for synthesising highly expanded graphene. This method utilises thermal shock in an air atmosphere, which allows for simultaneous oxidation, intercalation, and exfoliation to occur within a few seconds. The collected samples underwent analysis using Fourier-transform infrared spectroscopy, X-ray diffraction spectroscopy, and thermogravimetric analyses. A comparative examination was performed at three crucial temperatures (750°C, 820°C, and 870°C), together with microwave-assisted exfoliation. The results showed the efficacy of the thermal shock technique in facilitating swift and substantial expansion of the graphene structure by augmenting the internal forces within an exceptionally brief timeframe. In addition, the samples that were prepared showed exceptional thermal stability, as well as a remarkable ability to retain green malachite (98%) and alizarine red (up to 100%). Single network hydrogel beads and microwave-assisted exfoliated graphene were successfully synthesized and tested for the elimination of Cefalexin from aqueous solutions. The Langmuir model accurately describes adsorption isotherms, with high correlation coefficients and maximum adsorption capacity of 217.39 mg/g and 209.46 mg/g for the hydrogel network and MWGO respectively. The thermodynamic analysis showed exothermic and spontaneous adsorption. This highlights the potential of graphene-based materials in addressing water pollution and scarcity challenges.

Keywords: graphene, Synthesis, Thermal shock, Thermal stability, Filtration, Retention, Adsorption

Résumé

Cette étude présente une recherche universitaire sur le développement d'une méthode simple, peu coûteuse, rapide et efficace pour synthétiser du graphène hautement expansé. Cette méthode utilise un choc thermique dans une atmosphère d'air, ce qui permet l'oxydation, l'intercalation et l'exfoliation simultanées en quelques secondes. Les échantillons collectés ont été analysés par spectroscopie infrarouge à transformée de Fourier, spectroscopie de diffraction des rayons X et analyses thermogravimétriques. Un examen comparatif a été effectué à trois températures cruciales (750°C, 820°C et 870°C), ainsi qu'une exfoliation assistée par micro-ondes. Les résultats ont montré l'efficacité de la technique du choc thermique pour faciliter l'expansion rapide et substantielle de la structure du graphène en augmentant les forces internes dans un laps de temps exceptionnellement court. En outre, les échantillons préparés ont montré une stabilité thermique exceptionnelle, ainsi qu'une capacité remarquable à retenir le vert malachite (98 %) et le rouge alizarine (jusqu'à 100 %). Des billes d'hydrogel à réseau unique et du graphène exfolié à l'aide de micro-ondes ont été synthétisés avec succès. Le modèle de Langmuir décrit avec précision les isothermes d'adsorption, avec des coefficients de corrélation élevés et une capacité d'adsorption maximale de 217,39 mg/g et de 209,46 mg/g pour le réseau d'hydrogel et le MWGO respectivement. L'analyse thermodynamique a montré une adsorption exothermique et spontanée. Ceci met en évidence le potentiel des matériaux à base de graphène pour répondre aux défis de la pollution et de la rareté de l'eau.

Mots-clés : Graphene ; Synthèse ; Choc thermique ; Stabilité thermique ; Filtration ; Rétention ; adsorption

الملخص

تقدم هذه الدراسة بحثًا أكاديميًا في تطوير طريقة بسيطة ومنخفضة التكلفة وسريعة وفعالة لتخليق الجرافين عالي التمدد. وتستخدم هذه الطريقة الصدمة الحرارية في جو هوائي، مما يسمح بالأكسدة والإقحام والتقشير المتزامن في غضون ثوانٍ معدودة. وقد تم تحليل العينات التي تم جمعها باستخدام التحليل الطيفي بالأشعة تحت الحمراء المحولة فورييه والتحليل الطيفي لحيود الأشعة السينية والتحليل الحراري للوزن الثقيل. وأُجري فحص مقارن عند ثلاث درجات حرارة حاسمة (750 درجة مئوية و820 درجة مئوية و870 درجة مئوية)، بالإضافة إلى التوسيع بمساعدة الموجات الدقيقة. وأثبتت النتائج فعالية تقنية الصدمة الحرارية في تسهيل التمدد السريع والكبير لبنية الجرافين من خلال زيادة القوى الداخلية في فترة زمنية قصيرة للغاية. وبالإضافة إلى ذلك، أظهرت العينات المحضرة ثباتًا حراريًا استثنائيًا، بالإضافة إلى قدرة ملحوظة على الاحتفاظ باللون الأخضر الملكيت (98%) والأحمر الأليزارين (حتى 100%). تم بنجاح تصنيع خرزات هيدروجيل أحادية الشبكة والجرافين بالموجات الدقيقة. وقد وصف نموذج لانجموير بدقة متساوي الامتزاز، مع وجود معاملات ارتباط عالية وقدرة امتصاص قصوى تبلغ 217,39مجم/جم و 209,46 مجم/جم لشبكة الهيدروجيل والجرافين الموسع بالموجات الدقيقة على التوالي. أظهر التحليل الديناميكي الحراري أن الامتزاز كان طاردًا للحرارة و تلقائيًا. وهذا يسلط الضوء على إمكانات المواد القائمة على الجرافين لمواجهة تحديات تلوث المياه وندرتها.

الكلمات المفتاحية : الجرافين ؛ الصدمة الحرارية؛ الاستقرار الحراري؛ الترشيح؛ الاحتباس؛ الامتزاز

General introduction

Since its discovery in 2004 by Novoselov and Geim, an extraordinary allotrope of carbon with a single-layer material formed by the sp^2 electron orbital hybridization, tightly packed into a two-dimensional (2D) honeycomb lattice of carbon atoms with an atomic spacing of 1.42°, graphene has captivated the attention of scientists, engineers, and researchers across various disciplines due to its exceptional properties and diverse applications [1, 2, 3].

Thanks to graphene's unique properties including high specific surface area, storage modulus being two of the highest values reported at about 2,600 m^2 /g and 130 Gpa respectively, superior thermal, mechanical, electronic and optical characteristics, it has spurred extensive investigations into its synthesis and multifaceted applications such as electronics and batteries, energy storage, water treatment and many more [4, 5, 6].

Synthesizing graphene can be achieved using different approaches such as chemical vapor deposition, mechanical exfoliation, epitaxial growth on silicon carbide, and other innovative techniques. However, nowadays, most bulk-scale graphene is produced by a top-down approach, exfoliating graphite, oxidizing graphite via the Hummers' method or Brodie's method, followed by chemical or thermal reduction of graphite oxide (GO) which has always been one of the most advantageous and preferred method to obtain graphene in significant yields [1, 7, 8].

Each technique presents its unique advantages and disadvantages in terms of scalability, cost-effectiveness, and the quality of resultant graphene products produced. Gaining a comprehensive understanding of these synthesis techniques is essential for improving the efficiency of graphene manufacturing intended for various applications including water treatment purposes.

As the global demand for efficient water treatment solutions intensifies, the potential of graphene-based materials to address these challenges becomes increasingly promising by offering innovative solutions for tackling water contamination challenges. Its exceptional properties such as high surface area, electrical conductivity, and chemical stability made graphene a promising candidate for various water treatment applications including desalination, water purification, and wastewater treatment [9,10].

Through a comprehensive exploration of synthesis methodologies, structural analyses, and water treatment evaluations, this Ph.D. thesis aspires to contribute valuable insights to graphene research, with potential implications for sustainable and effective water management practices.

Therefore, novel methods of graphene synthesis must be developed in order to improve the important characteristics for further applications.

The work is divided into three chapters.

✓ First, literature review, is it divided into two sections : the first was sacrificed to some important considerations about graphene and graphene based materials, while the second section is about some novel strategies and technologies for water effluents' management.

✓ Second, synthesis and characterization. This chapter was sacrificed to the synthesis of five different graphene and graphene based materials including a one-step approach integrating oxidation, reduction and exfoliation where the key aspect of this method involves rapid heating at three carefully selected critical temperatures, graphene oxide synthesis via the improved Hummer's method, microwave assisted exfoliation, magnetic graphene and finally graphene based hydrogel beads. Some of these synthesis were followed-up by physico-chemical characterisation using Fourier transform Infra-Red spectroscopy FTIR, X-Rays Diffraction and thermogravimetric analyses.

✓ Finally, some water treatment applications where a vertical filtration of two different dyes with three different initial concentrations each was evaluated, and a comparative adsorption of an antibiotic study between MWGO and PHB has been chosen in order to evaluate the efficacity of the as obtained materials, and that was the subject of chapter III.

References

[1]   A.L. Olatomiwa, T. Adam, S.C.B. Gopinath, S.Y. Kolawole, O.H. Olayinka, U. Hashim, Graphene synthesis, fabrication, characterization based on bottom-up and top-down approaches: An overview, J. Semicond. 43 (2022) 061101. https://doi.org/10.1088/1674-4926/43/6/061101.

[2]   M. Liu, X. Zhang, W. Wu, T. Liu, Y. Liu, B. Guo, R. Zhang, One-step chemical exfoliation of graphite to ∼100% few-layer graphene with high quality and large size at ambient temperature, Chem. Eng. J. 355 (2019) 181–185. https://doi.org/10.1016/j.cej.2018.08.146.

[3]   V.B. Mbayachi, E. Ndayiragije, T. Sammani, S. Taj, E.R. Mbuta, Results in Chemistry Graphene synthesis , characterization and its applications : A review, Results Chem. 3 (2021) 100163. https://doi.org/10.1016/j.rechem.2021.100163.

[4]   H. Jahandideh, J.-R. Macairan, A. Bahmani, M. Lapointe, N. Tufenkji, Fabrication of graphene-based porous materials: traditional and emerging approaches, Chem. Sci. 13 (2022) 8924–8941. https://doi.org/10.1039/D2SC01786E.

[5]   C. Zhang, W. Lv, X. Xie, D. Tang, C. Liu, Q.H. Yang, Towards low temperature thermal exfoliation of graphite oxide for graphene production, Carbon N. Y. 62 (2013) 11–24. https://doi.org/10.1016/j.carbon.2013.05.033.

[6]   F.S. Al-Hazmi, G.H. Al-Harbi, G.W. Beall, A.A. Al-Ghamdi, A.Y. Obaid, W.E. Mahmoud, One pot synthesis of graphene based on microwave assisted solvothermal technique, Synth. Met. 200 (2015) 54–57. https://doi.org/10.1016/j.synthmet.2014.12.028.

[7]   D.X. Luong, K. V. Bets, W.A. Algozeeb, M.G. Stanford, C. Kittrell, W. Chen, R. V. Salvatierra, M. Ren, E.A. McHugh, P.A. Advincula, Z. Wang, M. Bhatt, H. Guo, V. Mancevski, R. Shahsavari, B.I. Yakobson, J.M. Tour, Gram-scale bottom-up flash graphene synthesis, Nature. 577 (2020) 647–651. https://doi.org/10.1038/s41586-020-1938-0.

[8]   Y. Hu, C. bao Sun, J. Kou, Exfoliation of poly(ethylene glycol)-intercalated graphite oxide composite in water without sonication, Int. J. Miner. Metall. Mater. 27 (2020) 840–845. https://doi.org/10.1007/s12613-019-1932-4.

[9]   W.T. Tee, N.Y.L. Loh, K.C. Lai, B.Y.Z. Hiew, S. Gan, L.Y. Lee, Application of 3D heteroatom-doped graphene in adsorptive removal of water pollutants: Review on hydrothermal synthesis and its influencing factors, Sep. Purif. Technol. 320 (2023) 124072. https://doi.org/10.1016/j.seppur.2023.124072.

[10]   B. Wang, Q. Liu, Z. Fan, A Mini Review : Application Progress of Magnetic Graphene Three-Dimensional Materials for Water Purification, 8 (2020). https://doi.org/10.3389/fchem.2020.595643.
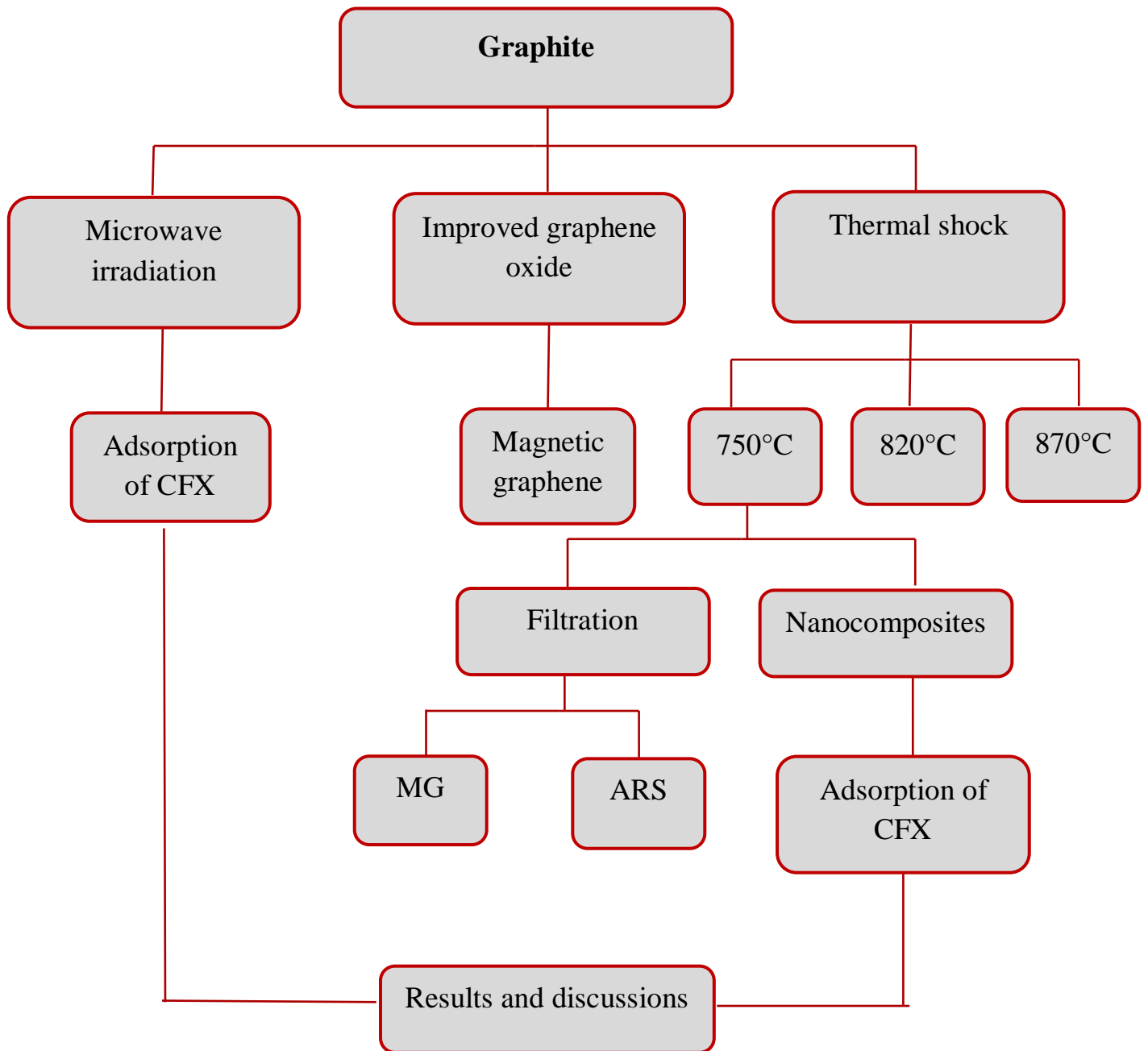
Figure I. 1. Flow chart showing the planning process for this project.

Part I

I. Generalities about graphene and graphene based materials

II. Discovery

Although graphene was initially discovered in 1859 by Benjamin Collins Brodie [1], Wallace has dedicated many years studying it theoretically. Graphene was first investigated in 1947, at that time it was only examined theoretically, with only a few the electronic structure predictions made. In 1962, graphene was first observed under an electron microscope. Boehm et al. first proposed that name in 1994 [2]. But according to Mouras et al. (1987) [1], the name "graphene" was initially used to describe a single sheet of graphite, which is the fundamental component of graphitic materials including carbon nanotubes, graphite, and fullerene. Consequently, graphene, a two-dimensional (2D) honeycomb lattice, may be compactly constructed from the single carbon atom layer of graphite.

Later, Ruoff et al. proposed a method for extracting graphene from graphite utilising simple mechanical exfoliation using Scotch tape [3]. But this effort resulted in the separation of multi-layer graphene MLG. By using the same method, Geim and Novoselov were able to successfully isolated and studied a single-atom-thick crystallite (graphene) from highly-oriented pyrolytic graphite in Manchester University and transferred them onto thin silicon dioxide on a silicon wafer using the well-known Scotch Tape Technique in 2004 [4, 5].

The properties of graphene material were, however, achieved in 2004 when Novoselov and Geim successfully isolated and studied a single-atom-thick crystallite (graphene) from bulk graphite and transferred them onto thin silicon dioxide on a silicon wafer using the Scotch Tape technique known as micromechanical cleavage. Konstantin Novoselov and Andre Geim were awarded jointly the 2010 Nobel Prize in Physics "for groundbreaking experiments on the two-dimensional material graphene" [1]. Since then, graphene has garnered significant attention in the scientific community ,and its production has been categorized into two key methods : top-down and bottom-up.

III. Graphene's Structure

With a molecular bond length of approximately 0.142 nm, graphene is a carbon allotrope consisting of a single-atom-thick sheet of sp^2 hybridised carbon atoms. Due to its structure which extends beyond the nanoscale range (< 100 nm) in two dimensions, it is classified as a 2D nanomaterial. Graphene sheets are packed tightly into a hexagonal honeycomb lattice crystal, with each carbon atom strongly bound to three neighbouring carbon atoms forming σ-bonds through strong covalent bonds [6].

A conducting π band, formed by the fourth valent electron that is perpendicular to the graphene sheet, gives graphene its unique chemical and electronic properties. Its distinctive structure resembles numerous joined benzene rings without hydrogen atoms, resulting in graphene's hydrophobicity [1, 4, 7]. In addition to the 0.335 nm thick single-layer graphene sheet (SLG) with an interlayer bonding energy of 2.1 EVnm^{-2} [8], graphene may also be in the form of bi-, few-, and multi-layer graphene sheets (MLG) consisting of up to ten well defined stacked graphene layers joined by van der Waals interactions [4].

Graphene sheets are building blocks for other graphitic materials stacked on top of each other they make graphite (1 mm thick graphite contains about 3 million layers of graphene) rolled up they make a carbon nanotube, cut and folded into a spherical shape they make a fullerene.
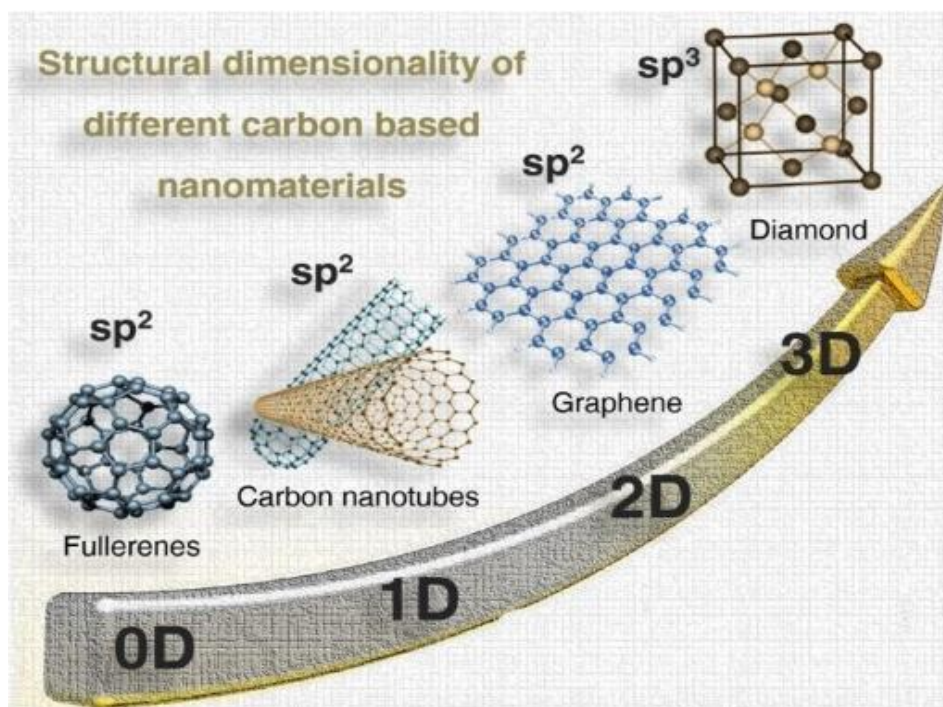
Figure I. 2. Different nanoscaled carbon allotropes with appropriate hybridization and dimensionality [4].
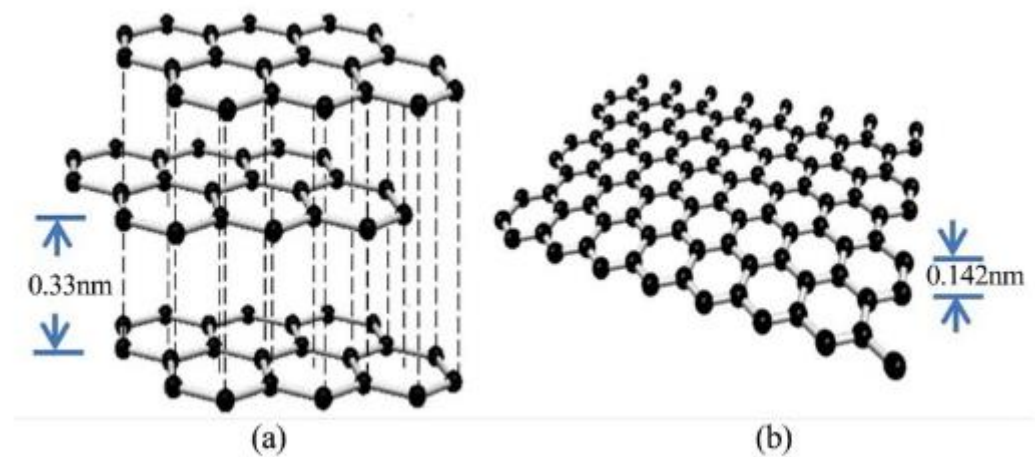
Figure I. 3. Schematic diagram of (a) Graphite and (b) Single layer of graphene from graphite [9].

IV. Unique properties

This section highlights several key essential qualities of graphene, emphasizing its unique characteristics that have drawn so much attention to the material.

IV.1 Atomic thickness : A single layer is only one atom thick therefore called "2D" is about 0.335 nanometers making it the world's thinnest material [10].

IV.2 Exceptional mechanical and tensile strength : monolayer graphene is the strongest nanomaterial ever tested with a strength of 42 N/m which equates to Young's elastic modulus close to 1 Tpa this makes the strength of graphene to be 100 times more than that of steel [8].

IV.3 Transparency : It has high optical transmittance of approximately 97.7% with negligible reflectance (<0.1%) better than ITO [9].

IV.4 Large specific surface area : Graphene possesses a high theoretical specific surface area of approximately 2630 m^2/g with less than 3 grams you could cover an entire soccer field [10, 11].

IV.5 Enhanced Thermal Conductivity : It exhibits high thermal conductivity ranging from 3000 to 5000 W/mK at room temperature, henceforth 10 times higher than that of copper (401 W/mK) [4, 10].

IV.6 Ultra-high Electron mobility : It exhibits the highest electron mobility of all electronic materials with theoretical limit of 200,000 cm²/Vs that is 140 more than that of silicon [6] .Graphene's electron mobility has a conductivity of 106 S/m, and resistance of 31 Ω/ Ω/sq [8, 10].

IV.7 Charge Carrier Mobility : Graphene has a charge carrier mobility at room temperature of up to 106 $cm^2V^{-1}s^{-1}$ for suspended graphene.

IV.8 Toughness and Stretchability : Although graphene is relatively brittle, it can be stretched by up to 25%, highly relevant for flexible electronics.

IV.9 Impermeability : It shows complete gas impermeability where even the smallest atoms (helium atom) cannot pass through a sheet of graphene [5].

IV.10 Electrical resistivity : 1×10^{-8} Ω•m among the lowest of any known material at room temperature (~35% less than copper).

IV.11 Zero Band Gap Semiconductor : Unlike most 2D materials, graphene is a semiconductor with valence and conduction bands symmetrically distributed on the two sides of the Fermi level, making it a zero band gap semiconductor [6].
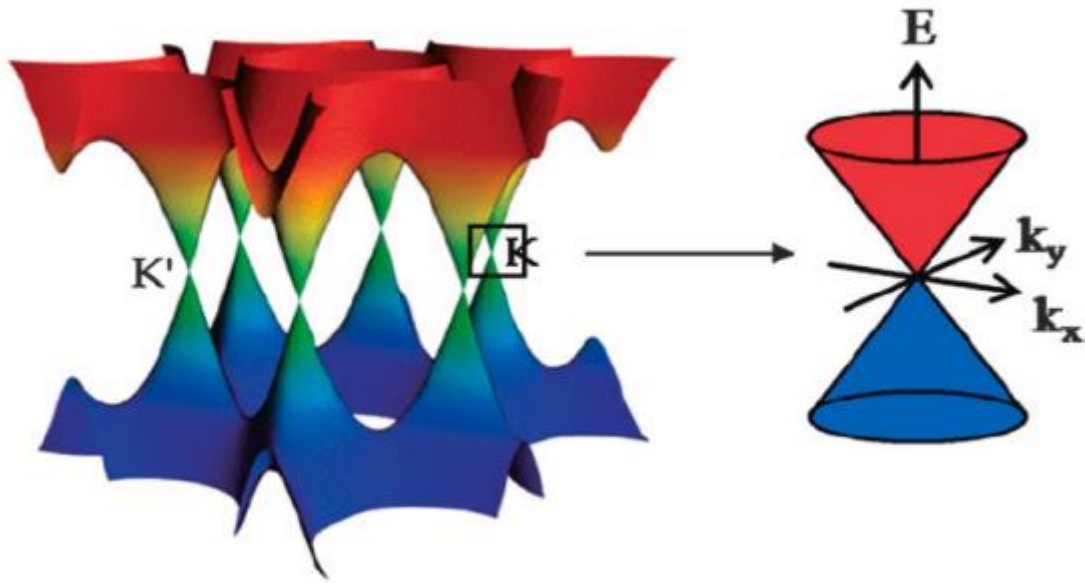
Figure I. 4. Electronic band structure of single-layer graphene [6].

These properties collectively contribute to the versatility and potential applications of graphene in various fields including energy storage and conversion, electrochemical catalysis, and environmental remediations.

V. Synthesis routes of graphene

After its discovery in 2004, different techniques were developed to produce layers and thin films of graphene. The production was divided into two key categories, top-down and bottom-up, which offered from the simplest to state-of-the-art technologies synthesis methods. However, the impact on large-scale industrial production is closely connected to the development of methods for scalable synthesis of high-quality graphene . However, each of the mentioned methods shows several extraordinary advantages in graphene synthesis but also some substantial drawbacks [4].

The top-down approach involves breaking down larger graphite structures into graphene, while the bottom-up approach involves building up graphene from smaller molecular precursors. Each approach has its advantages and challenges, and the choice of method depends on the specific requirements of the application [12].

 In this section both top-down and bottom-up synthesis methods as well as some of their advantages and disadvantages are discussed.

V.1   Top-down approach

This method involves peeling off or reducing graphite and its derivatives (pyrolytic carbon in graphite, graphite single-crystal) from one another into nano-sized graphene sheets of various thicknesses [4].

The benefits of top-down methods include substrate transfer, cost-effectiveness, and high dependability compared to the bottom-up approach [12].

V.1.1 Micromechanical exfoliation/cleavage Mechanical exfoliation

This is the first known mechanical processing technique used to produce graphene from highly oriented pyrolytic graphite (HOPG) as demonstrated by Gein and Noveselov in 2004. It is also known as Scotch tape or peel-off method [13].

The concerned top-down nanotechnology method stresses the materials that make up the layered structure's surface longitudinally or transversely [8]. To separate layers that are defined as single mono-atomic from graphite mechanical external force of 3001 nNμm^{-2} is needed [4].

The method for the simple separation of graphene layers from bulk graphite through multiple exfoliation steps using Scotch tape is based on overcoming van der Waals forces between adjacent layers of graphene. Separated mono-layer or multiple layers of graphene remain on the tape after peeling off then attached to certain substrate such as acetone and finally deposited on different substrates such as silicon wafers SiO_2/Si.

The most accurate yet the simplest way to control the thickness of graphene flakes and determine how crystalline they are is the spectroscopic method.

Although this process is slow and imprecise, it shows restrictions in precise control of the size and quality of stacked graphene layers and limitations in term of scalability. The diameter of several microns, as well as the irregular shape and low quality of produced graphene sheets, rise as a result of the residues left on the graphene surface after Scotch tape removal [4].

Hence the material produced is most often used to study the properties of graphene rather than actually using it commercially.

Mechanical exfoliation can also be performed by using different agents such as electric field, epoxy resin , and by transfer printing technique [6].
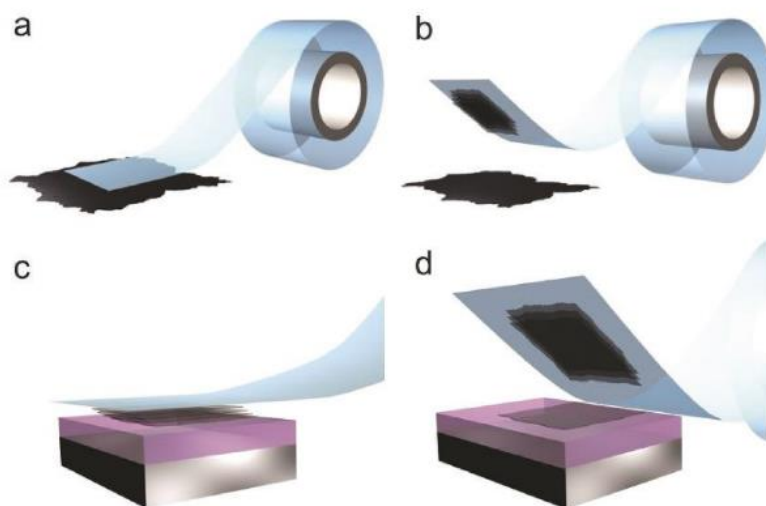
Figure I. 5. A mechanical exfoliation procedure step by step top few layers of adhesive tape are bond to tape when it is placed against a HOPG surface in (a), tape with layered crystal material pressed against a surface of choice in (b), and (d) Tape is peeled off, bottom layer is left on the substrate [8].

V.1.2   Chemical synthesis and exfoliation method

Chemical synthesis and exfoliation method are ones of the common methods for producing significant graphene amounts.

The chemical technique has already been used to make several types of graphene paper, graphene derived materials , graphene polymer composites, and magnetic transparent electrodes… etc

Exfoliation by chemicals is a two-step procedure :

- First, Increases the interlayer separation by first diminish the between layers of van der Waals forces. Thus, graphene intercalated compounds (GICs) are created.

- Furthermore, sonication and fast heating are implemented in the exfoliated layers of graphene [8].

Brodie was the first to prepare graphite oxide by oxidation of graphite in a mixture of potassium chlorate in the year of 1860. Later on, Staudenmaier used a specific ration of nitric acid : sulphuric acid in an ice bath where amounts of graphite were added with potassium chlorate as an oxidizing agent. Staudenmaier's method is considered safer than the Brodie method, but toxic gasses are still created [14, 15]**.**

In 1958, Hummer developed a new method for preparing graphene oxide within a few hours using $KMnO_4$ instead of $KClO_3$, $NaNO_3$, and H_2SO_4. This method improved reaction safety by avoiding the evolution of explosive ClO_2 and $KClO_3$ [14].

The sonication and graphene oxide reduction are other method for preparation of graphene [8].
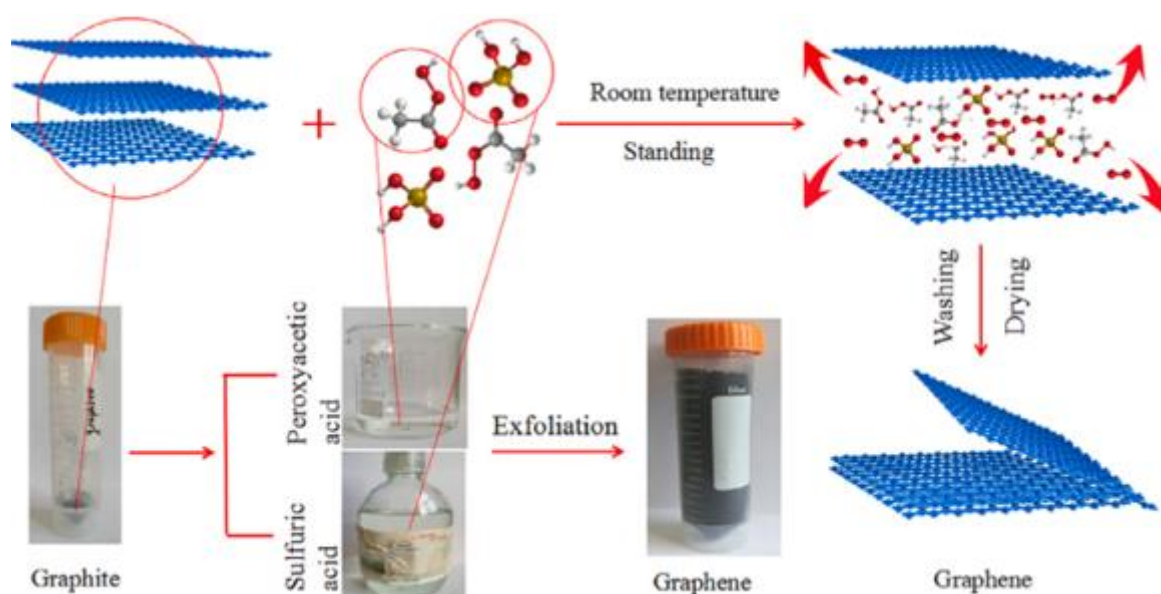
Figure I. 6. Schematic of chemical exfoliation mechanism of graphite into graphene [8].

a) Sonication

Sonication is a typical technique for exfoliating graphene oxide (GO) layers. Sonication, which involves the application of high-frequency sound waves to a GO suspension or solution, offers the mechanical energy required to break down GO flakes into individual or few layers. This exfoliation technique is vital for increasing the surface area and improving the characteristics of GO for various applications, such as the production of efficient water purification membranes.

Optimising sonication parameters, such as time and intensity, is crucial for achieving the optimum level of exfoliation without causing significant damage to the GO sheets. Proper sonication can produce well-exfoliated GO with better characteristics, such as increased permeability, selectivity, and efficient removal of contaminants in water purification processes [16]. However, shear forces and cavitation created during sonication would inevitably damage and fragment the GO nanosheets, affecting the intrinsic characteristics of the final formed nanosheet material.

b) Ball milling

Ball milling is a mechanical technique to produce high-quality graphene by separating stacked graphite into graphene layers. The technique involves the use of a ball mill equipment made of stainless steel or other, which ensures facile and very effective crush and grind several materials into fine powder and synthesizing nanocomposites and oxides at room temperature.

During ball milling, shear and normal stresses are applied to large graphite sheets, reducing graphite flakes to nano-sized materials and introducing defects in the graphite structure's basal plane. The technique can be performed under wet or dry conditions, depending on the desired results. Ball milling has been shown to be an excellent solid-state approach for fine grinding of various materials as well as the synthesis of nanocomposites and oxides. The size and quality of graphene produced during ball milling are determined by parameters such as milling media and milling time. Researchers explored several ball milling variations, including wet ball milling in a liquid medium, which yielded encouraging results in the production of graphene flakes of controlled thickness. Overall, ball milling is a versatile and frequently used method for producing graphene and other nanomaterials, with potential applications in a wide range of academic fields [12].
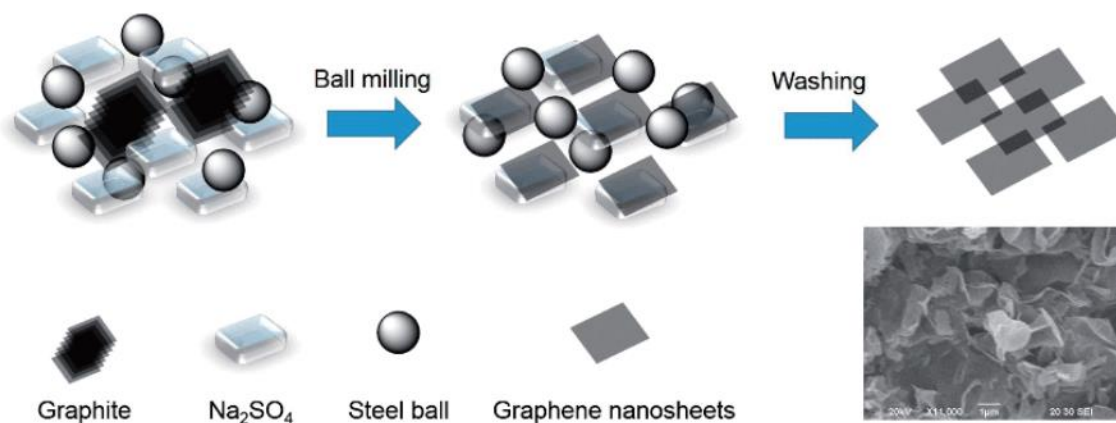
Figure I. 7. Schematic diagram of the soluble salt assisted (Na_2SO_4) wet ball milling approach for synthesis of graphene nanosheet powder [12].
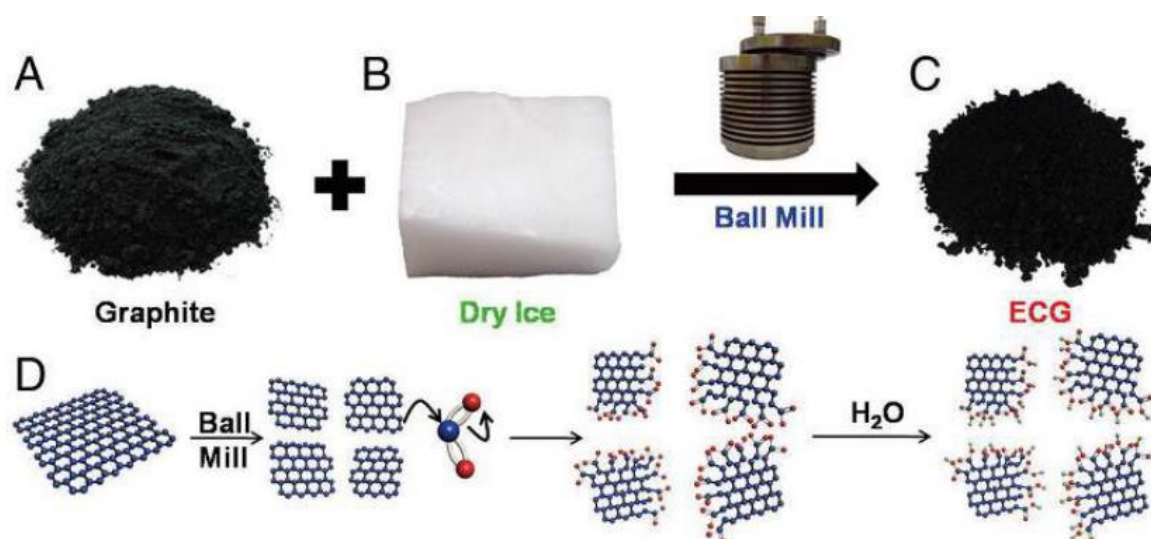
Figure I. 8. (a) Pure graphene. (b) Dry ice. (c) Edge-carboxylated graphite prepared by ball milling for 48 h. (d) Schematic view of physical cracking and edge-carboxylation of graphite by ball milling in the presence of dry ice, and protonation [12].

V.1.3   Electrochemical exfoliation

Electrochemical exfoliation is an eco-friendly manufacturing process, relatively simple that does not require complex equipments used to produce graphene with controlled properties. It involves applying a fixed potential or electrical current to a graphite electrode in an appropriate electrolyte solution to weaken the van der Waals force among the layers. This process involves the intercalation of ions between graphite layers, promoting the separation and shedding of graphite to form graphene sheets. The quality, yield, and characteristics of graphene can be influenced by the electrolyte, solvent, and experimental conditions employed. This technology provides advantages like as scalability, simplicity, and the potential for large-scale graphene manufacturing [17, 18].
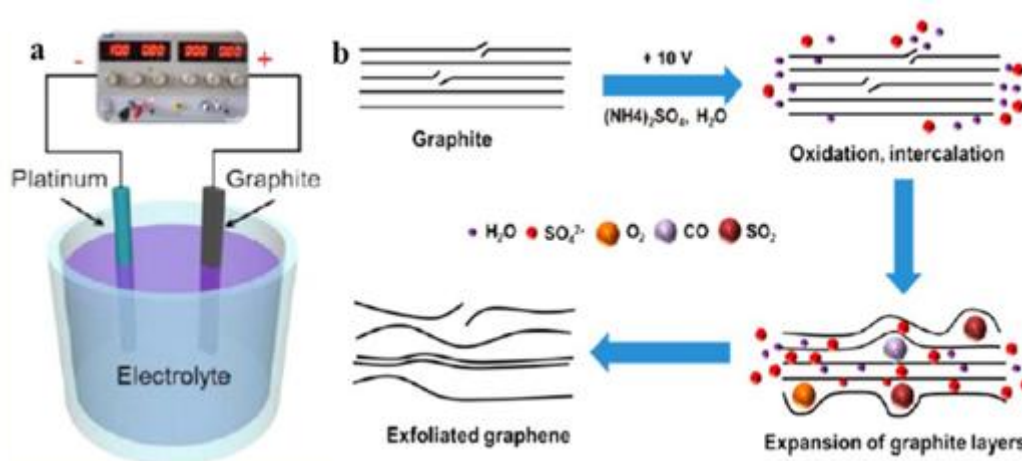
Figure I. 9. Schematic illustration of (a) anode exfoliation device (b) the mechanism of anode electrochemical exfoliation [17].
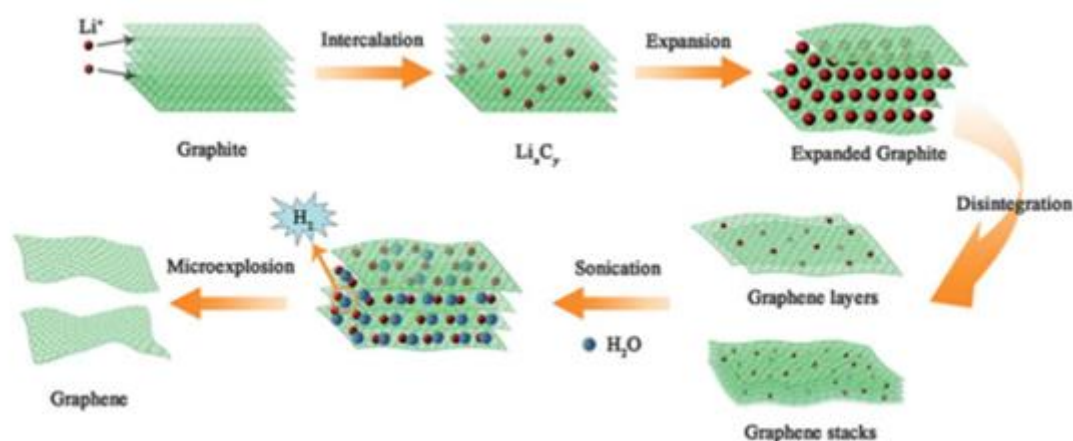
Figure I. 10. Schematic illustration of the mechanism of cathode electrochemical exfoliation [18].

Electrolytes often utilised in electrochemical exfoliation of graphene are : Sodium sulfate (Na_2SO_4), Potassium bisulfate (KH_SO_4) and Ammonium sulfate ((NH_4)2SO_4). The choice of electrolytes can impact the formation of defects, purity, and uniformity of the graphene sheets obtained through electrochemical exfoliation. This can by consequence influence the quality, yield, and properties of the produced graphene [17].

The electrochemical exfoliation process can also be used to introduce functional groups or modify the surface chemistry of graphene, enhancing its compatibility with various applications.

This method offers three main methods for producing graphene-based materials: anodic exfoliation, cathodic exfoliation, and double-electrode exfoliation. Here is a summary of these three methods :

V.1.3.1 Anodic electrochemical exfoliation

The graphite or layered material serves as the anode e. Under an electric field, the anion in the electrolyte migrate towards the graphite layer, increasing the interlayer distance, while the anode expands and produces gas. The interlayer van der Waals force is reduced and peeled off to produce graphene. Anodic exfoliation is known for its high peeling efficiency, but the obtained graphene may contain oxygen-containing functional groups and structural defects due to oxidation reactions [1, 18].

V.1.3.2 Cathodic electrochemical exfoliation

Unlike anodic exfoliation, cathode exfoliation involves using the graphite or layered material as the cathode where cations from the electrolyte solution migrate towards the cathode, promoting intercalation within the graphite layers and expansion of the material. The cationic electrolytes usually utilised in this procedure are metallic lithium ions, sodium chloride and dimethyl sulfoxide, quaternary ammonium salt, and $BMPTF_2N$.

Cathodic exfoliation is generally less efficient than anodic exfoliation [18].

V.1.3.3 Double-Electrode Exfoliation

Double-electrode exfoliation combines anodic and cathodic potentials in the electrochemical cell setup. The initial potential drives intercalation, while the reverse potential facilitate exfoliation. This exfoliation method employs a graphite electrode as both a cathode and an anode.

By selecting an appropriate electrolyte or alternating positive and negative voltages, simultaneous exfoliation of the cathode and anode can be achieved, resulting to the generation of high-quality graphene. The Efficiency of the double-electrode exfoliation depend on the critical choice of electrolyte and voltage application.

To summarise, anodic exfoliation, cathodic exfoliation, and double-electrode exfoliation are three independent electrochemical exfoliation processes, each with its own set of mechanisms and advantages for producing graphene-based materials with specific features [18].

V.2 Bottom up approach

This methodology is a layer-by-layer procedure that begins with the formation of alternative carbon containing sources to derive graphene. The benefit of bottom-up approach is the controlled thickness of the graphene layer achieved with the use of distinct surface catalysts and growth criteria [12, 19].

V.2.1   Pyrolysis

Pyrolysis is a process used for synthesizing graphene by thermal decomposition of certain carbon containing materials such as organic compounds or polymers which are heated in an inert atmosphere to prevent oxidation. The term "pyrolysis" originates from the Greek words "pyro," meaning fire, and "lysis," meaning separating.

One common technique of graphene (or carbon-based materials) synthesis through pyrolysis is the thermal decomposition of silicon carbide (SiC). During this process, the silicon (Si) component of SiC is desorbed at high temperatures, leaving behind carbon atoms that arrange themselves into few-layer graphene structures.

The properties of graphene synthesised using pyrolysis vary depending on the precursor material employed, the heating settings, and the cooling procedure. Pyrolysis is a simple yet scalable method for producing graphene on a large scale for various applications in electronics, energy storage, composites, and more [1].

V.2.2   Chemical vapor deposition

Chemical Vapor Deposition (CVD) ; a bottom-up synthesis technique ; is a widely used technique for synthesizing high-quality graphene and other thin films on a large scale basis by combining a gas molecule with a surface substrate inside a reaction chamber. In CVD, a chemical reaction takes place in a gas phase, leading to the deposition of thin film of materials onto a substrate surface.

 In this process, methane (CH_4) and acetylene (C_2H_2) are commonly used as precursor gases, flowed into a reactor containing commonly metals substrate ;especially copper ; at high temperatures. The gases decompose, and graphene is deposited on the substrate. The choice of precursor gases, reaction conditions, and substrate materials influence the quality and properties of the synthesized graphene [1, 9, 20].

 While Cu substrates have demonstrated favourable graphene development, Ni substrates have been connected with problems such as non-self-limiting growth and the creation of wrinkles and folds [9].

Carbon source decomposes at high temperature into hydrogen and carbon atoms.

$CH_{4(g)}$ $=$ $2H_{2\,(g)} + C_{(S)}$; $C_2H_{2(g)}$ $=$ $H_{2(g)} + 2C_{(s)}$ [6]
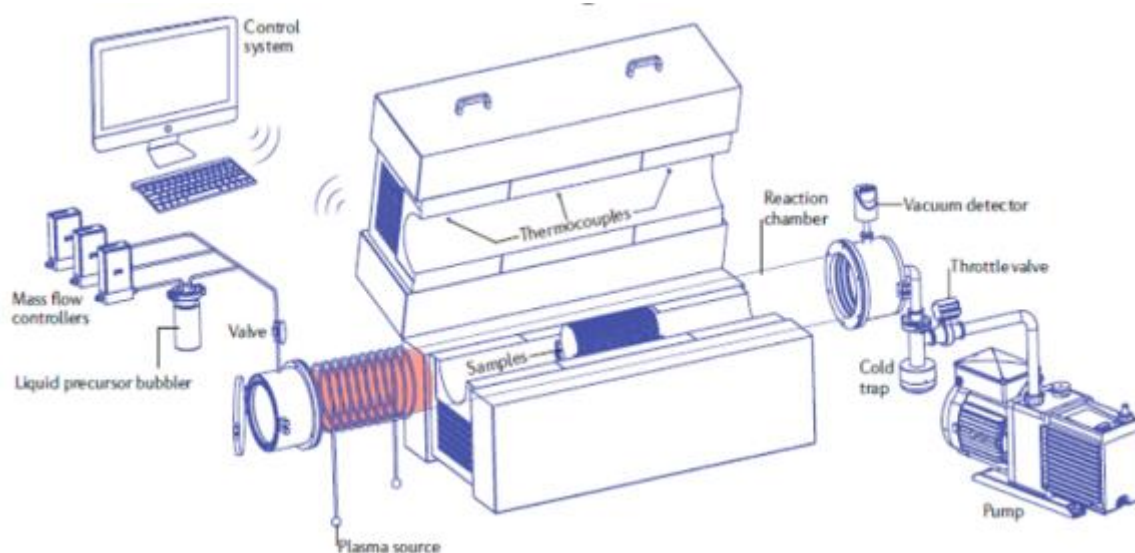
Figure I. 11. Schematic diagram of a typical CVD equipment [1].
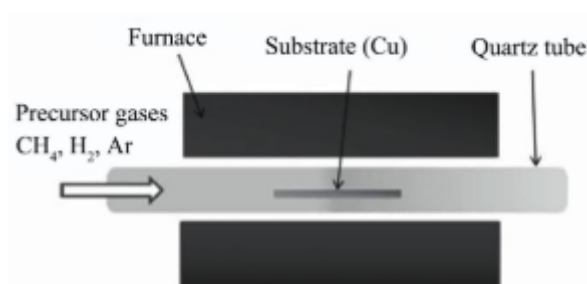
Figure I. 12. Schematic of (a) thermal CVD [9].

The Chemical Vapor Deposition (CVD) technique offers numerous benefits for synthesizing of graphene:

- High quality : CVD can yield relatively high-quality graphene.
- Scalability : This method has the potential to produce graphene on a large scale.
- Established Technique : CVD is a well-established technique for graphene synthesis.
- Facile Process : The CVD process is known for its relative simplicity.
- Controlled Growth : CVD enables controlled growth of graphene layers.
- Versatility : CVD can be utilized to grow graphene on a variety of substrates, including metals and nonmetals.

- Potential for Direct Growth : CVD offers the potential to directly grow graphene on crucial materials, reducing the necessity for transfer processes [20].

Overall, CVD techniques play a crucial role in the synthesis of high-quality graphene in both research and industrial settings such as electronics, energy storage, and composite materials. Researchers continue to explore and optimize CVD methods to achieve uniform large-scale and single-layer graphene production [9, 20].

V.2.3   Epitaxial growth

Epitaxial growth entails depositing a crystalline film on a substrate and aligning its crystallographic orientation with that of the substrate, resulting in a well-ordered structure. It is categorized into two categories :

Homoepitaxy, in which the film matches the substrate material, and

Heteroepitaxy, in which alternative materials are employed.

Epitaxial growth allows precise control of crystal structure, which is crucial for high-quality materials. It is widely utilised in the semiconductor industry to optimise device performance by aligning crystal structures. In graphene production, epitaxial growth on substrates such as SiC results in high-quality films with specified characteristics. Overall, epitaxial growth is a versatile process in materials science, nanotechnology, and semiconductor manufacturing [9].
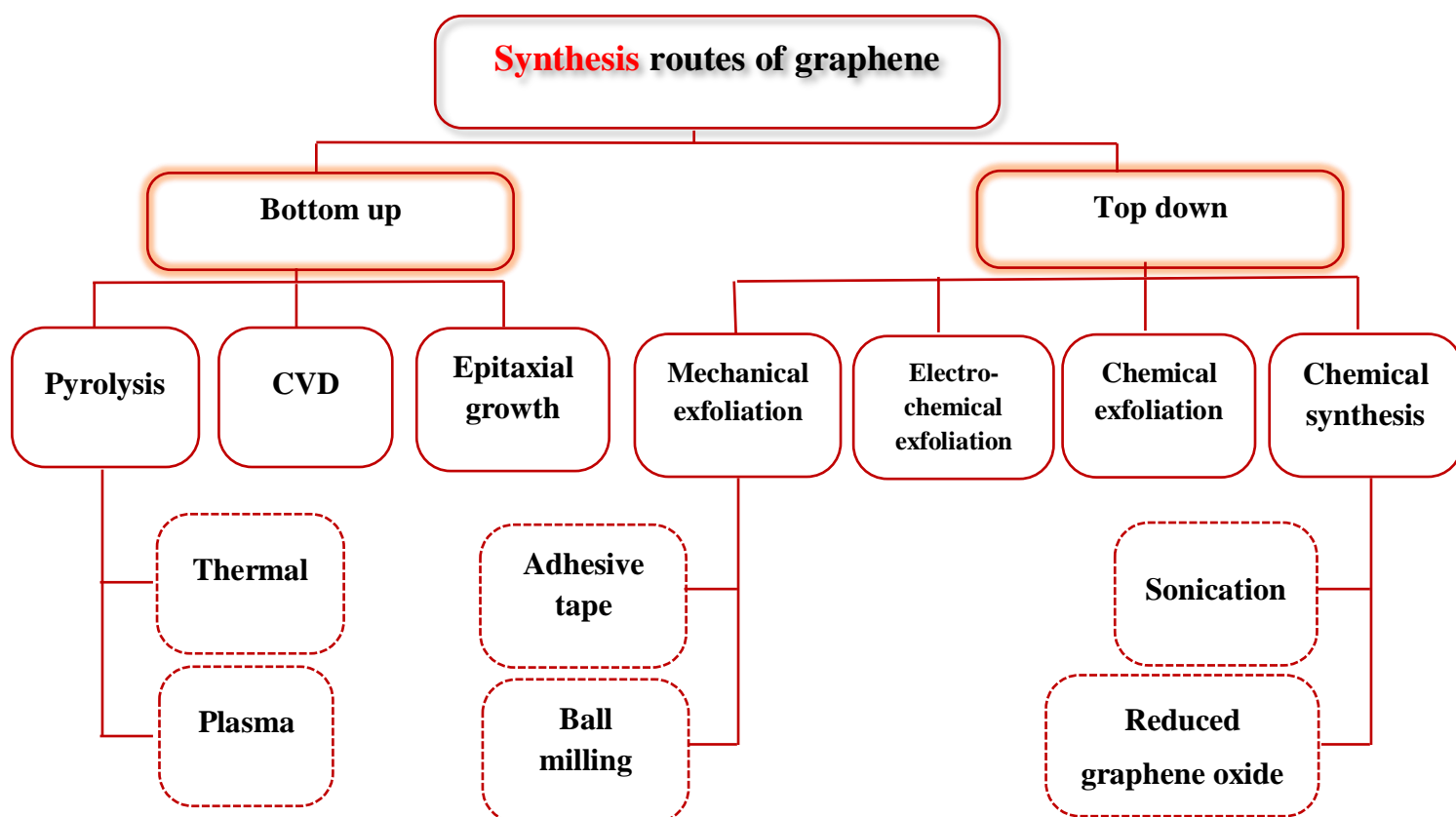
Figure I. 13. Schematic representation of different routes of graphene synthesis.

VI.   Graphene oxide

Graphene oxide (GO) is a derivative of graphene. It is a layered material with oxygen functional groups attached to both sides of the carbon layer and at the edges. The preparation of graphene oxide via chemical recipe is mainly based on the strong oxidation using sulfuric, nitric and phosphoric acids to create hydroxyl (-OH), epoxy (-O-) carboxyl (-COOH) and carbonyl (C=O) groups on the graphite surface. The oxidation   disrupt the sp^2 hybridization and introduce defects in the lattice structure. These functional groups also make graphene oxide more hydrophilic [7].

Nevertheless, these functional groups can be easily removed by thermal or chemical reduction and the resulting reduced GO (rGO) is very similar to pristine graphene [21].

GO is generally prepared by oxidizing graphite via the Hummers' method or Brodie's method, followed by an exfoliation process to remove the resultant graphite oxide (GrO) in a polar solvent such as water [22].

Conventional routes of GO synthesis have been widely studied and optimized to control the degree of oxidation, functional groups presence and the properties of the resulting graphene oxide for various applications. Some typical conventional approaches are the following :

1. **Hummers Method** : The Hummers method, developed by Hummers and Offeman in 1958, entails oxidizing graphite using a mixture of sulfuric acid, potassium permanganate, and sodium nitrate. This method is widely employed for large-scale production of GO [7].

2. **Brodie Method :** The Brodie method, introduced by B. C. Brodie in 1859, involves using a mixture of potassium chlorate and fuming nitric acid to oxidize graphite. This method was one of the earliest attempts to synthesize graphene oxide [7].

3. **Staudenmaier Method :** The Staudenmaier method involves the use of a combine mixture of nitric acid, sulfuric acid, and potassium chlorate to oxidize graphite and produce graphene oxide [7].

4. **Improved Hummers Method :** Variations on the original Hummers method have been developed to improve the efficiency and safety of the oxidation process. These alterations may include changes in the reaction conditions or the introduction of alternative oxidising agents [23].

VI.1 Modern methods of synthesizing graphene oxide (GO)

Researchers have developed alternative approaches to GO synthesis with additional tools and techniques to tailor its properties for specific applications and to address environmental concerns associated with traditional synthesis routes. Some of the modern ways of GO synthesis include

VI.1.1 Tour's Method : Tour's method, introduced in 2010, involves the use of 1 : 9 ratio of phosphoric acid : sulfuric acid , potassium permanganate, and graphite. approach enables the manufacture of GO with higher levels of oxidation and a more regular structure [7].

VI.1.2 Electrochemical Synthesis : Electrochemical techniques provide an environmentally friendly approach to GO synthesis, as they use aqueous electrolytes and do not require oxidizing chemicals. This approach improves the quality control of GO by adjusting the level of oxidation and defect's density [24].

VI.1.3 Microbial Synthesis : Some research has explored the use of microbial processes to produce GO, offering a potentially sustainable and environmentally friendly method of synthesis [7].
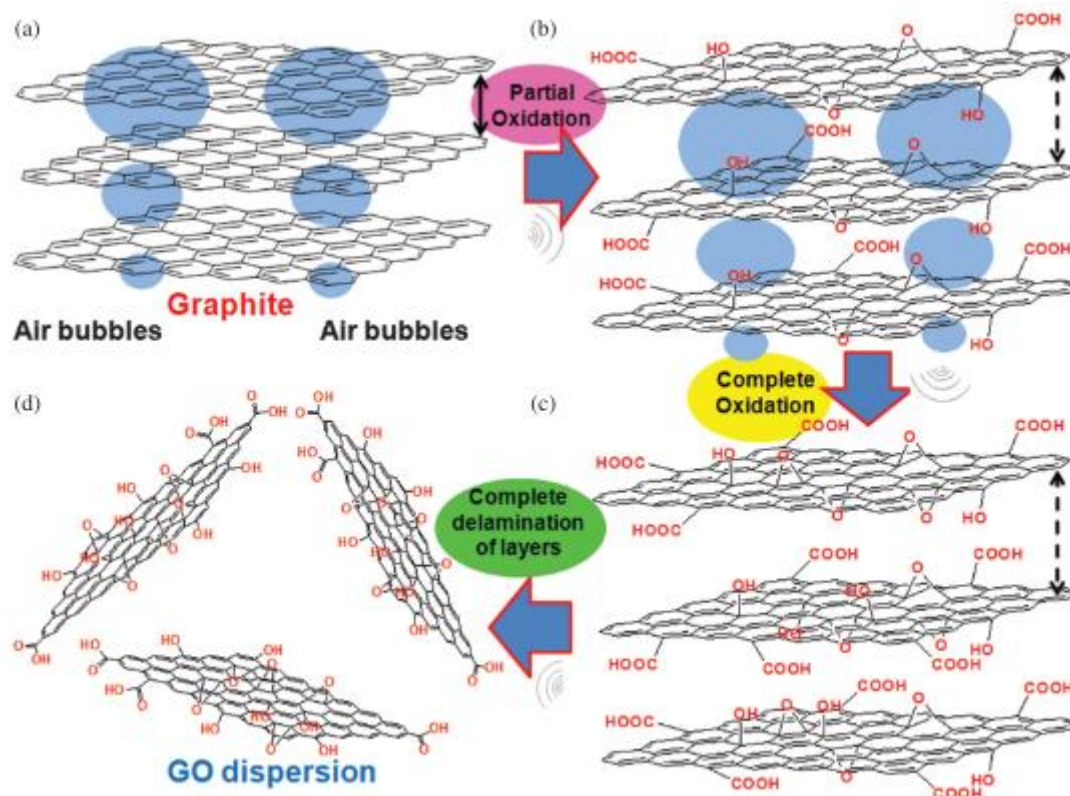
Figure I. 14. Schematic representation of sonication assisted mechanochemical process by chemical structure: (a) Graphite (b) partially oxidized graphite oxide (c) fully oxidized graphite oxide (d) exfoliated graphene oxide [15].

VI.2 Graphene oxide reduction

Reduction of graphene oxide (GO) is considered the most viable alternative approach to produce higher quality of graphene. It involves typically the removal of oxygen-containing functional groups from the graphene oxide sheets.

The reduction rates of graphene oxide (GO) are determined by a variety of parameters, including the reduction process, reaction conditions, and the desired qualities of the resulting reduced graphene oxide (rGO). Some popular reduction processes include chemical reduction with reducing agents such

as hydrazine, hydrothermal reduction, thermal reduction, and electrochemical reduction. There have been numerous reports documenting a variety of reductants in the literature.

X-ray photoelectron spectroscopy (XPS), Raman spectroscopy, and Fourier-transform infrared spectroscopy (FTIR) can be employed to control the oxidation degree and the quality of the resulted material.

VI.2.1 Chemical reduction

1. **Hydrazine hydrate :** The most commonly used chemical reductant is hydrazine monohydrate ($N_2H_4 \cdot H_2O$). Reduced graphene oxide (rGO) produced using this method is thought to be the most similar to pure graphene in terms of electrical and structural properties. They revealed that hydrazine treatment promotes the incorporation of nitrogen within the rGO chemical structure [25, 26].

2. **Organic solvents :** To synthesise rGO, solvents such DMF, alcohols methanol (MeOH), ethanol (EtOH), isopropanol (iPrOH), or benzyl alcohol (BnOH), and water were employed [25].

3. **Catalysts :** Catalysts such as aluminium and zinc have been utilised in acidic circumstances to obtain an important reduction of GO in less than an hour. Aluminium (Al) reacts with acid (HCl) to produce aluminium chloride and hydrogen gas, as illustrated in reactions below :

   $2Al + 6HCl \rightarrow 2AlCl_3 + 3H_2$

   $GO + H_2 \rightarrow rGO + H_2O$

   In an exothermic reaction, the generated hydrogen interacts with oxygen-containing functional groups on GO, forming rGO sheets [25].

4. **Sodium compounds :** Different sodium based reducing agents have also been employed to synthesise rGO such as sodium borohydride, sodium hypophosphite monohydrate, sodium cholate (NaC), sodium citrate, sodium tetraborate decahydrate, sodium bisulfite ($NaHSO_3$) and sodium sulfide (Na_2S) [25].

5. **Ascorbic acid :** Ascorbic acid is the most studied 'green' reducing agent for rGO synthesis [26].

VI.2.2. Microwave reduction

Microwave (MW) irradiation has been used as an alternative thermal approach for rapid reduction of GO. One of the key advantages of this approach is its short reduction time. Selective microwave power and time are imperative for the quality of the resulted material [27].

VI.2.3. Thermal reduction

Given the toxicity, elemental impurities, and environmental impact of some reducing agents, such as hydrazine or sodium borohydride, thermal reduction of GO to rGO has been receiving attention for its simplicity, rapidity, non-toxicity, and mass-production possibility [28].

Temperature plays an important role in oxygen-containing functional groups removal from GO in order to obtain reduced graphene sheets with structural and electrical properties similar to pristine graphene sheets. The reduction temperature is mainly dependent by the end-use application of rGO, since is a delicate balance to be maintained between the extent of reduction and structural decomposition of the GO basal plane [25].

High temperatures of the thermal reduction lead to the transformation of oxygen-containing groups into emissions of gases resulting splitting wide sheets of graphene oxide into small-sized graphene sheets [7].

Annealing temperature plays an important role in oxygen atoms removal from GO. Researches showed that the C/O ratio can shift from about 2:1 in virgin GO to more than 13:1 at temperatures above 750°C, but less than 7:1 at temperatures below 500°C. An additional factor to consider during thermal reduction of GO is the annealing atmosphere [28]. However, studies are is still required to standardise this reduction technique due to current difficulties connected with the formation of defects during high-temperature annealing, and residual oxygen-containing functional groups when reduced at low temperatures [25].
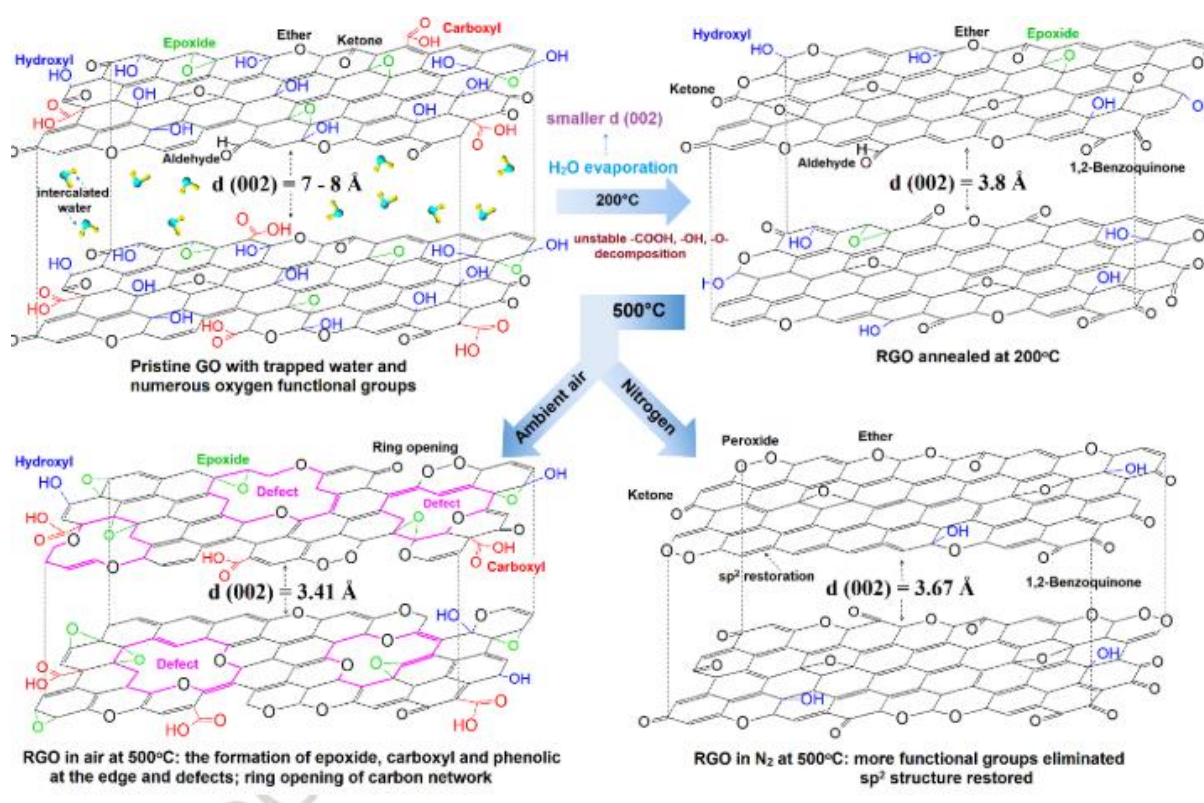
Figure I. 15. Schematic diagram of the temperature evolution of GO in nitrogen and ambient air [28].

Part II

I.   Managing water effluents: strategies and treatment technologies

I.1   Introduction

Water effluents, which are the wastewater often discharged from various sources such as industries, agriculture, municipal activities and sewage systems, pose significant impacts on the environment and human health when released untreated or inadequately treated into natural water. These effluents contain a wide range of pollutants, including organic matter, heavy metals, dyes, oils, pathogens and many other contaminants [29, 30, 31].

When released into water bodies without proper treatment, water effluents can degrade water quality, harm aquatic ecosystems, and threaten public health. Although, effective management of water effluents is required to address these challenges [29].

I.2   Sources and Composition of Water Effluents

2.   Industrial effluents : Industrial discharged from battery manufacturing, chemical manufacturing, textile, metal smelting, paper industries, pesticides, pharmaceutic and other industries frequently contain a wide variety of contaminants including heavy metals, organic compounds, dyes and hazardous chemicals that originate from manufacturing, mining, and energy production activities [32, 33, 34]. By way of example, more than 0.8 million tonnes of organic dye get disposed of each year [29].

3.   Agricultural effluents : consist of pesticides, fertilisers, and organic remains that are carried out of fields. These substances contribute to the contamination of nutrients and the process of eutrophication in water bodies [35].

4.   Domestic sewage : consisting of organic substances, nutrients, pathogens, and household chemicals are released from residential areas. During rainfall events, stormwater runoff carries contaminants like silt, oil, grease, and trash from urban areas, exacerbating water quality problems [35].

I.3   Micropollutants

Micropollutants, also known as emerging contaminants, are large quantities of man-made substances such as pharmaceuticals, steroid hormones, agrochemicals and dyes. These substances are generally present in water in low concentrations [36].

I.3.1   Antibiotics

Antibiotics are pharmaceutical agents widely recognized for bacteriostatic properties which effectively prevent proliferation of bacteria and reduce the risk of death caused by bacterial infections. Antibiotics are used in human and animal healthcare, as well as in agriculture as feed additives [37, 38]. The presence of antibiotics in wastewater is a significant environmental concern due to their potential impact on aquatic ecosystems and human health. Antibiotics can enter wastewater systems through various pathways such as hospital or pharmaceutical wastewater discharge, aquaculture and biological metabolism [39, 40]. About 50–90% of antibiotic drugs are released to the aquatic media via the domestic sewage, coming from human urine and faeces, due to incomplete metabolism in human body [41].

Different levels of antibiotics' concentrations are detected in wastewater ranging from several hundred mg L^{-1} to less than 20 mg L^{-1} in developing and developed countries respectively [39]. Although antibiotic concentrations in wastewater are not too high in some areas, antibiotics are difficult to remove and gradually accumulate [39, 40].

Cephalosporins are one of the most widely used antibiotics, which are divided into four major groups based on the antimicrobial activity. Cephalexin (CFX) is considered as the first-generation cephalosporin antibiotic that is used to treat a number of infections [42].

The next table shows the 1st generation of Cephalosporins.

Table I. 1 . 1st generation of cephalosporins

Substance	Frequent utilization
1 st generation	
Céfadroxile	Mainly skin and soft tissue infections
Céfazoline	Administered prior to surgery to prevent infection
Céfalexine	Treat infections caused by bacteria

I.4.2. Dyes

Different kinds of coloured compounds, known as dyes, are found in wastewater that is produced by various types of industries, including tanning, printing, leather, and textile sectors. Many of these dyes, including acid blue, Eriochrome black-T, malachite green, methylene blue, methyl orange, and alizarine red S… etc

These dyes are carcinogenic, mutagenic, and teratogenic, which means that they pose a risk to both humans and animals. The dye that is found in wastewater contains pigment that blocks the passage of light through water. As a result, the amount of photosynthesis that occurs in aquatic creatures diminishes, which has a negative impact on the growth of these organisms.

In addition to its usage as an antibacterial and antifungal agent in the food business, malachite green (MG) dye is one of the most widely used dyes for colouring a variety of materials, including cotton, jute, wool, leather, and cloth, among other things. Because of the presence of MG dye in water, the amount of food that is consumed is reduced, damage is caused to the kidneys and liver, heart failure occurs, the fertility rate is decreased, and human cells are subjected to mutagenic, carcinogenic, and

teratogenic effects. Because of this, it is of the utmost importance for enterprises to remove MG dye from the wastewater discharge they produce

I.4 Environmental Impacts of Water Effluents

Discharging untreated or inadequately treated water effluents may end up with significant consequences for the environment.

I.4.1 Environmental Impact

Organic pollutants have a tendency to reduce the amount of dissolved oxygen in water bodies, which can result in the deterioration of aquatic ecosystems and the death of fish. Agricultural and sewage effluents contribute to nutrient pollution, which stimulates the proliferation of algae. This excessive development of algae leads to the formation of hazardous algal blooms, eutrophication, that can release toxins that are harmful to aquatic organisms [30,43].

I.4.2 Human Health Impact

Industrial effluents containing heavy metals and harmful compounds accumulate up in soils and living organisms, which may threaten the health of ecosystems and lead to pollution of the food chain. Sewage effluents containing pathogens can transmit waterborne diseases, posing a threat to public health, particularly in populations without access to safe drinking water and sanitation infrastructure [43].

II. Graphene based water treatment technologies

Graphene oxide and its derivatives are being extensively researched for their potential in tackling water scarcity and pollution. Their use in water treatment technologies is driven by their distinctive characteristics, including a large surface area, impressive adsorption capabilities, exceptional electrical conductance and potent antibacterial properties.

Their large surface area allows for enhanced adsorption of various contaminants including heavy metal ions, organic impurities, and microbial contaminants from water. Additionally, graphene-based membranes exhibit significant potential in water filtration.

II.1 . Graphene-based membranes

Graphene oxide membranes have been developed as ionic and molecular sieves, or for selective gas transport. These membranes are able to restrict and block most substances, allowing only water vapor to pass through while effectively blocking other molecules such as ethanol and alcohol [7].

Graphene and graphene oxide membranes exhibit significant promise in water filtration owing to their remarkable permeability and selectivity demonstrating their ability to remove salts. Graphene membranes have the capacity to reject 97 % of NaCl from seawater, organic compounds, and other impurities from water. Graphene nanoporous membranes can ideally be used for water desalination and filtration with an efficiency of 33 % to 100 % depending on the pore size and the applied pressure [3]. These materials have a potential to improve the rejection efficiencies, suppress the accumulation of pollutants and foulants. They can boost the strength and stability of the membranes [15].
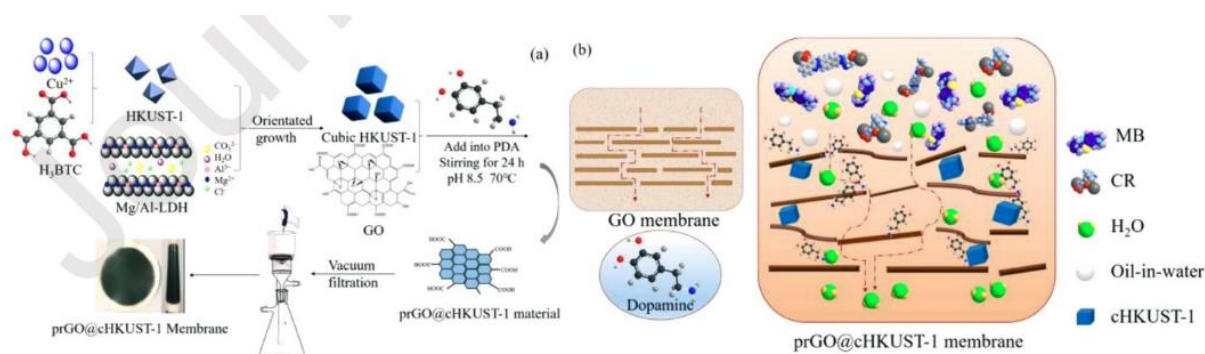
Figure I. 16. Preparation procedures of prGO@cHKUST-1 membrane and mechanism of dye removal and oil–water emulsion separation [48].

II.2 Removal of toxic gases

By exploiting its adsorption capacity, catalytic properties, and gas separation capabilities, graphene oxide offers a versatile and efficient solution for the removal of harmful gases from the environment. This application of GO contributes to environmental preservation enhancement of air quality.

The interactions between the oxygen-containing functional groups on GO and the gas molecules promote the ability to adsorb a variety of toxic gases, including carbon dioxide (CO_2), carbon monoxide (CO), nitrogen dioxide (NO_2) …etc . These interactions leads to the physical or chemical binding of the gases to the surface of GO. As a result, graphene oxide effectively removes these toxic gases from the

environment, highlighting its potential for environmental remediation. Graphene oxide has the ability to catalyse the transformation of toxic gases into safer compounds via chemical reactions [15].

II.3 Water Purification

Its extensive surface area and the presence of functional groups create sites for the attachment of pollutants, making it highly efficient in water treatment procedures. Graphene and its derivatives has the ability to remove heavy metal ions [9], organic contaminants [49, 50], and dyes from polluted water sources through the process of adsorption [37]. The extensive surface area and presence of functional groups create sites for the attachment of contaminants, hence enhancing its efficacy in water treatment procedures [10].

II.4 Graphene based nanocomposites

II.4.1 Graphene-based hydrogels

Hydrogels are a class of materials that combine the unique properties of graphene with the structural characteristics of hydrogels. Hydrogels are three-dimensional networks of hydrophilic polymers that can absorb and retain large amounts of water. When graphene with its tunable properties is incorporated into hydrogels, it leads to the formation of graphene-based hydrogels with enhanced functionalities. Graphene-based hydrogels have found applications in diverse fields, including environmental remediation [49, 51, 52]**,** drug delivery [51], tissue engineering [11], energy storage, and catalysis.

II.4.1.1 Graphene-based hydrogels synthesis and characterization

Graphene-based hydrogels are synthesized via a multi-step process. Graphene Oxide (GO) is first synthesised from graphite using techniques like the Hummers' method, taking advantage of its functional groups to facilitate further modifications. Subsequently, the process of hydrogel production occurs, utilising polymers such as alginate to provide structural reinforcement and water-absorbing abilities. To achieve a consistent composite, the incorporation of graphene oxide into the hydrogel matrix is performed either by physically chemical techniques. Afterwards, crosslinking chemicals such as calcium ions Ca^{2+} are added to stabilise the hydrogel structure, enhance mechanical characteristics, and secure graphene inside the network. Graphene oxide is then subjected to thermal or chemical reduction. Ultimately, the synthesised hydrogel undergoes thorough detailed characterisation using techniques such as scanning electron microscopy (SEM), transmission electron microscopy (TEM), X-ray diffraction (XRD), Fourier-transform infrared spectroscopy (FTIR), and thermogravimetric analysis (TGA) to

analyse   its   structure,   shape,   and   characteristics   [52,   50]**.**   .
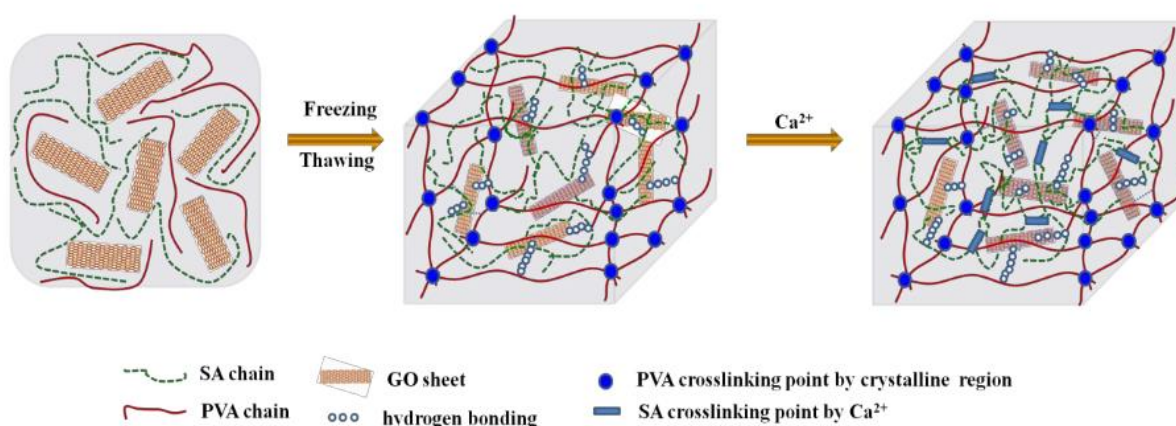
Figure I. 17. Schematic of crosslinking mechanism of graphene oxide (GO) reinforced double network (DN) hydrogel [49].

The synthesis of graphene-based hydrogels can involve various methods, such as chemical crosslinking, physical blending, or in situ reduction of graphene oxide within the hydrogel matrix. These methods allow for the control of the structure, porosity, and properties of the resulting hydrogel. The materials' adaptability make them particularly attractive for diverse technological advancements [52].

II.4.2 Magnetic graphene based materials

Due to the π–π interactions between neighbouring sheets, graphene sheets usually suffer from serious agglomeration and restacking during utilization leading to a great loss of effective surface area and consequently a lower adsorption capacity than expected. Consequently, by loading magnetite nanoparticles, the occurrence of significant agglomeration and restacking of the graphene sheets can be avoided or reduced. This leads to an increase in higher available surface area and enhancement of adsorption capacity [53].

Compared with traditional methods, such as filtration, centrifugation or gravitational separation, magnetic separation requires less energy allowing for convenient separation and recovery of the graphene from wastewater using an external magnetic field [53, 54].

The synthesis of magnetic graphene oxide involves incorporating magnetic nanoparticles ; typically iron oxide (Fe_3O_4) or magnetite ; onto the surface of graphene oxide through various chemical or physical methods such as co-precipitation, sol-gel techniques, or chemical reduction [55].
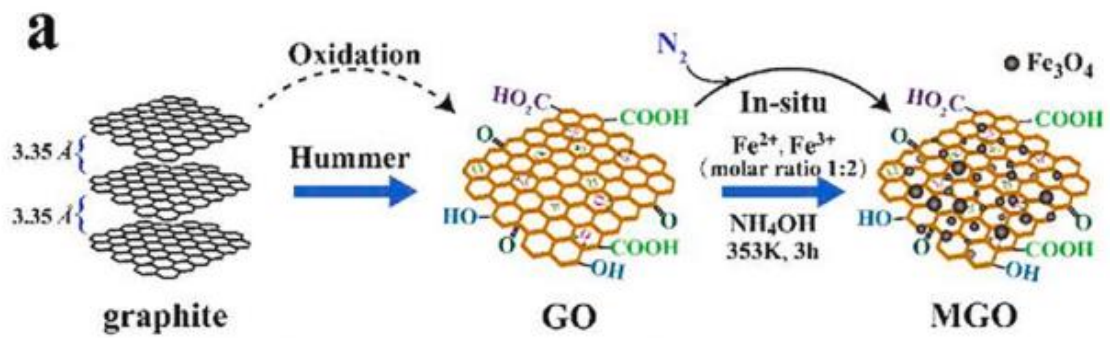
Figure I. 18. Synthesis of Graphene oxide based Nanocomposites using Co-precipitation Method [56].
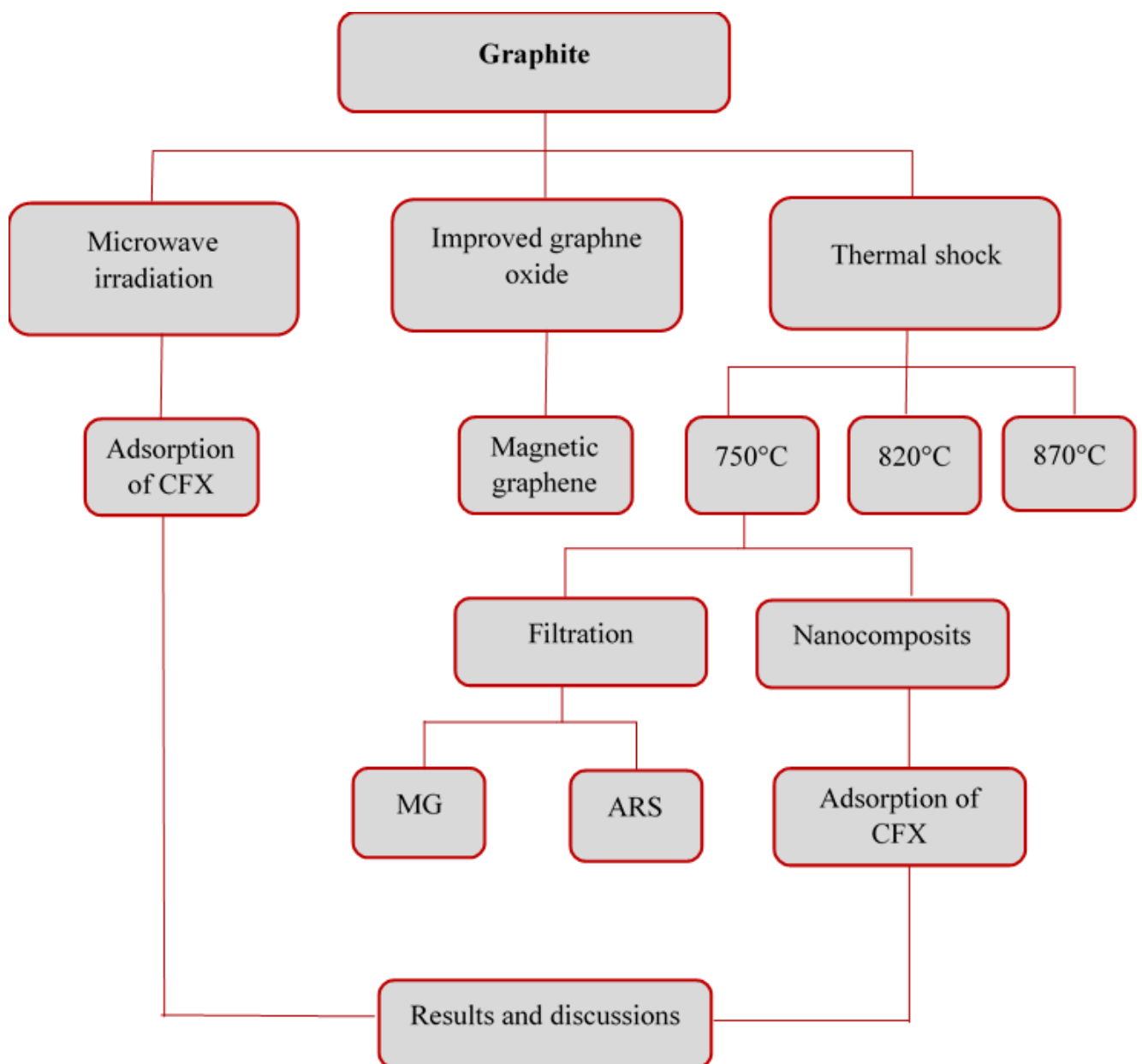
Figure I. 19. Flowchart of the planning process for this project.

References

[1]   V.B. Mbayachi, E. Ndayiragije, T. Sammani, S. Taj, E.R. Mbuta, Results in Chemistry Graphene synthesis , characterization and its applications : A review, Results Chem. 3 (2021) 100163. https://doi.org/10.1016/j.rechem.2021.100163.

[2]   H. Boehm, R. Setton, E. Stumpp, INTERNATIONAL UNION OF PURE AND SOLID STATE CHEMISTRY * NOMENCLATURE AND TERMINOLOGY Nomenclature and terminology of graphite, 66 (1994) 1893–1901.

[3]   X. Lu, M. Yu, H. Huang, R.S. Ruoff, Tailoring graphite with the goal of achieving single sheets, 10 (1999) 269–272.

[4]   D.A.G. and S.P.J. Jovana R Prekodravac, Dejan P Kepić, Juan Carlos Colmenares, Materials Chemistry C, Mater. Chem. C. (2021) 45. https://doi.org/10.1039/D1TC01316E.

[5]   X. Zhao, D.G. Papageorgiou, L. Zhu, F. Ding, J. Robert, The Strength of Mechanically-Exfoliated Monolayer Graphene, (n.d.) 1–16.

[6]   V.B. Mbayachi, E. Ndayiragije, T. Sammani, S. Taj, E.R. Mbuta, A. ullah Khan, Graphene synthesis, characterization and its applications: A review, Results Chem. 3 (2021) 100163. https://doi.org/10.1016/j.rechem.2021.100163.

[7]   C. Republic, Synthesis and Applications of Graphene Oxide, (2022).

[8]   L.S. Sundar, M.A. Mir, M.W. Ashraf, F. Djavanroodi, Synthesis and characterization of graphene and its composites for Lithium-Ion battery applications : A comprehensive review, Alexandria Eng. J. 78 (2023) 224–245. https://doi.org/10.1016/j.aej.2023.07.044.

[9]   A. Adetayo, D. Runsewe, Synthesis and Fabrication of Graphene and Graphene Oxide : A Review, (2019) 207–229. https://doi.org/10.4236/ojcm.2019.92012.

[10]   A.R. Urade, I. Lahiri, K.S. Suresh, Graphene Properties , Synthesis and Applications : A Review, JOM. 75 (2023) 614–630. https://doi.org/10.1007/s11837-022-05505-8.

[11]   H. Jahandideh, J.-R. Macairan, A. Bahmani, M. Lapointe, N. Tufenkji, Fabrication of graphene-based porous materials: traditional and emerging approaches, Chem. Sci. 13 (2022) 8924–8941. https://doi.org/10.1039/D2SC01786E.

[12]   A.L. Olatomiwa, T. Adam, S.C.B. Gopinath, S.Y. Kolawole, O.H. Olayinka, U. Hashim, Graphene synthesis, fabrication, characterization based on bottom-up and top-down approaches: An overview, J. Semicond. 43 (2022) 061101. https://doi.org/10.1088/1674-4926/43/6/061101.

[13]   M. Li, B. Yin, C. Gao, X. Guo, J. Guo, Graphene : Preparation , tailoring , and modification, (2023). https://doi.org/10.1002/EXP.20210233.

[14]   A. Moosa, Graphene preparation and graphite exfoliation, 45 (2021). https://doi.org/10.3906/kim-2101-19.

[15]   M. Bera, Chandravati, P. Gupta, P.K. Maji, Facile One-Pot Synthesis of Graphene Oxide by Sonication Assisted Mechanochemical Approach and Its Surface Chemistry, J. Nanosci. Nanotechnol. 18 (2017) 902–912. https://doi.org/10.1166/jnn.2018.14306.

[16]   S. Kumar, A. Garg, A. Chowdhuri, Sonication effect on graphene oxide (GO) membranes for water purification applications, Mater. Res. Express. 6 (2019). https://doi.org/10.1088/2053-1591/ab1ffd.

[17]   V. Nagyte, D.J. Kelly, A. Felten, G. Picardi, Y.Y. Shin, A. Alieva, R.E. Worsley, K. Parvez, S. Dehm, R. Krupke, S.J. Haigh, A. Oikonomou, A.J. Pollard, C. Casiraghi, Raman fingerprints of graphene produced by anodic electrochemical exfoliation, Nano Lett. 20 (2020) 3411–3419.

https://doi.org/10.1021/acs.nanolett.0c00332.

[18] L. Li, D. Zhang, J. Deng, J. Fang, Y. Gou, Review—Preparation and Application of Graphene-Based Hybrid Materials through Electrochemical Exfoliation, J. Electrochem. Soc. 167 (2020) 086511. https://doi.org/10.1149/1945-7111/ab933b.

[19] G. Surekha, K.V. Krishnaiah, N. Ravi, R. Padma Suvarna, FTIR, Raman and XRD analysis of graphene oxide films prepared by modified Hummers method, J. Phys. Conf. Ser. 1495 (2020) 012012. https://doi.org/10.1088/1742-6596/1495/1/012012.

[20] Q. Shi, K. Tokarska, H.Q. Ta, X. Yang, Y. Liu, S. Ullah, L. Liu, B. Trzebicka, A. Bachmatiuk, J. Sun, L. Fu, Z. Liu, M.H. Rümmeli, Substrate Developments for the Chemical Vapor Deposition Synthesis of Graphene, Adv. Mater. Interfaces. (2020) 10. https://doi.org/10.1002/admi.201902024.

[21] A.J. Sellathurai, S. Mypati, M. Kontopoulou, High Yields of Graphene Nanoplatelets by Liquid Phase Exfoliation using Graphene Oxide as a Stabilizer, Chem. Eng. Journa. (2022). https://doi.org/10.1016/j.cej.2022.138365.

[22] Y. Hu, C. bao Sun, J. Kou, Exfoliation of poly(ethylene glycol)-intercalated graphite oxide composite in water without sonication, Int. J. Miner. Metall. Mater. 27 (2020) 840–845. https://doi.org/10.1007/s12613-019-1932-4.

[23] D.C. Marcano, D. V. Kosynkin, J.M. Berlin, A. Sinitskii, Z. Sun, A. Slesarev, L.B. Alemany, W. Lu, J.M. Tour, Improved synthesis of graphene oxide, ACS Nano. 4 (2010) 4806–4814. https://doi.org/10.1021/nn1006368.

[24] Y. Nishina, Chemical and Electrochemical Synthesis of Graphene Oxide Chemical and Electrochemical Synthesis of Graphene Oxide - A, R. Soc. Chem. (2020) 10. https://doi.org/10.1039/x0xx00000x.

[25] V. Agarwal, P.B. Zetterlund, Strategies for reduction of graphene oxide – A comprehensive review, Chem. Eng. J. 405 (2021) 127018. https://doi.org/10.1016/j.cej.2020.127018.

[26] I.O. Faniyi, O. Fasakin, B. Olofinjana, A.S. Adekunle, T. V. Oluwasusi, M.A. Eleruja, E.O.B. Ajayi, The comparative analyses of reduced graphene oxide (RGO) prepared via green, mild and chemical approaches, SN Appl. Sci. 1 (2019) 1–7. https://doi.org/10.1007/s42452-019-1188-7.

[27] F.S. Al-Hazmi, G.H. Al-Harbi, G.W. Beall, A.A. Al-Ghamdi, A.Y. Obaid, W.E. Mahmoud, One pot synthesis of graphene based on microwave assisted solvothermal technique, Synth. Met. 200 (2015) 54–57. https://doi.org/10.1016/j.synthmet.2014.12.028.

[28] G.T.T. Le, J. Manyam, P. Opaprakasit, N. Chanlek, N. Grisdanurak, P. Sreearunothai, Divergent mechanisms for thermal reduction of graphene oxide and their highly different ion affinities, Diam. Relat. Mater. 89 (2018) 246–256. https://doi.org/10.1016/j.diamond.2018.09.006.

[29] B. Basha, M. Ikram, Z.A. Alrowaili, M.S. Al-buriahi, M. Anwar, Wet chemical route synthesis of Cr doped CoFe2O4 @ rGO nanocomposite for photodegradation of organic effluents present in drinking water Wet chemical route synthesis of Cr doped CoFe 2 O 4 @ rGO nanocomposite for photodegradation of organic effluents pres, Ceram. Int. 49 (2024) 30049–30059. https://doi.org/10.1016/j.ceramint.2023.06.262.

[30] P.L. Yap, J. Nine, K. Hassan, T.T. Tung, D.N.H. Tran, D. Losic, Graphene-Based Sorbents for Multipollutants Removal in Water : A Review of Recent Progress, 2007356 (2020) 1–25. https://doi.org/10.1002/adfm.202007356.

[31] V. Karthik, P. Selvakumar, P.S. Kumar, D.N. Vo, M. Gokulakrishnan, P. Keerthana, V.T. Elakkiya, R. Rajeswari, Graphene-based materials for environmental applications : a review Graphene - based materials for environmental applications : a review, Environ. Chem. Lett.

(2021). https://doi.org/10.1007/s10311-021-01262-3.

[32] N. Chandra, P. Gururani, Current Research in Green and Sustainable Chemistry Advances of graphene oxide based nanocomposite materials in the treatment of wastewater containing heavy metal ions and dyes, Curr. Res. Green Sustain. Chem. 5 (2022) 100306. https://doi.org/10.1016/j.crgsc.2022.100306.

[33] G. Yin, Z. Sun, Y. Gao, S. Xu, Preparation of expanded graphite for malachite green dye removal from aqueous solution, Microchem. J. 166 (2021) 106190. https://doi.org/10.1016/j.microc.2021.106190.

[34] G. Wernke, Q.L. Shimabuku-Biadola, T.R.T. dos Santos, M.F. Silva, M.R. Fagundes-Klen, R. Bergamasco, Adsorption of cephalexin in aqueous media by graphene oxide: kinetics, isotherm, and thermodynamics, Environ. Sci. Pollut. Res. 27 (2020) 4725–4736. https://doi.org/10.1007/s11356-019-07146-y.

[35] T. Paramasivan, N. Sivarajasekar, S. Muthusaravanan, R. Subashini, Graphene Family Materials for the Removal of Pesticides from Water, Springer International Publishing, 2019. https://doi.org/10.1007/978-3-319-75484-0.

[36] A. Bentouami, A. Khelifa, M me SALAA Fahima Intercalation d ' une argile de type 1 : 1 par HDTMA et application à la coadsorption de produits pharmaceutiques A mes très chers et tendres parents Pour leurs encouragement et soutien A mon mari Hamza A tous ceux qui me sont chers : Me, (2021).

[37] Removal of ceftriaxone and ciprofloxacin antibiotics from aqueous solutions using graphene oxide derived from corn cob, 10 (2024) 573–588. https://doi.org/10.22035/gjesm.2024.02.10.

[38] M. Li, Y. Liu, G. Zeng, N. Liu, S. Liu, Chemosphere Graphene and graphene-based nanocomposites used for antibiotics removal in water treatment : A review, Chemosphere. 226 (2019) 360–380. https://doi.org/10.1016/j.chemosphere.2019.03.117.

[39] J. Ma, Z. Jiang, J. Cao, F. Yu, Chemosphere Enhanced adsorption for the removal of antibiotics by carbon nanotubes / graphene oxide / sodium alginate triple-network nanocomposite hydrogels in aqueous solutions, Chemosphere. 242 (2020) 125188. https://doi.org/10.1016/j.chemosphere.2019.125188.

[40] R. Rostamian, H. Behnejad, Ecotoxicology and Environmental Safety A comprehensive adsorption study and modeling of antibiotics as a pharmaceutical waste by graphene oxide nanosheets, Ecotoxicol. Environ. Saf. 147 (2018) 117–123. https://doi.org/10.1016/j.ecoenv.2017.08.019.

[41] S. Yadav, A. Asthana, A.K. Singh, R. Chakraborty, S.S. Vidya, Methionine-Functionalized Graphene Oxide / Sodium Alginate Bio-Polymer Nanocomposite Hydrogel Beads : Synthesis , Isotherm and Kinetic Studies for an Adsorptive Removal of Fluoroquinolone Antibiotics, (2021). https://doi.org//doi.org/10.3390/ nano11030568 Academic.

[42] G. Nazari, H. Abolghasemi, M. Esmaieli, Batch adsorption of cephalexin antibiotic from aqueous solution by walnut shell-based activated carbon, J. Taiwan Inst. Chem. Eng. 000 (2015) 1–9. https://doi.org/10.1016/j.jtice.2015.06.006.

[43] S.S. Sonone, S. V Jadhav, M.S. Sankhla, R. Kumar, Water Contamination by Heavy Metals and their Toxic Effect on Aquaculture and Human Health through Food Chain, (2020). https://doi.org/10.33263/LIANBS102.21482166.

[44] N.F.D. Junaidi, N.H. Othman, N.S. Fuzil, M.S. Mat Shayuti, N.H. Alias, M.Z. Shahruddin, F. Marpani, W.J. Lau, A.F. Ismail, N.F.D. Aba, Recent development of graphene oxide-based membranes for oil–water separation: A review, Sep. Purif. Technol. 258 (2021) 118000.

https://doi.org/10.1016/j.seppur.2020.118000.

[45] W.T. Tee, N.Y.L. Loh, K.C. Lai, B.Y.Z. Hiew, S. Gan, L.Y. Lee, Application of 3D heteroatom-doped graphene in adsorptive removal of water pollutants: Review on hydrothermal synthesis and its influencing factors, Sep. Purif. Technol. 320 (2023) 124072. https://doi.org/10.1016/j.seppur.2023.124072.

[46] E. Freitas, D. Janu, Y. Jaqueline, G. Wernke, G. Maria, M. Demiti, L. Bergamasco, S. Vieira, Chemosphere Application of activated carbon functionalized with graphene oxide for efficient removal of COVID-19 treatment-related pharmaceuticals from water, Chemosphere. 289 (2022) 9. https://doi.org/https://doi.org/10.1016/j.chemosphere.2021.133213.

[47] A. Carolina, S. Guerra, M.B. De Andrade, T. Rhuna, Adsorption of sodium diclofenac in aqueous medium using graphene oxide nanosheets, Environ. Technol. 0 (2019) 1–26. https://doi.org/10.1080/09593330.2019.1707882.

[48] B. Wang, Q. Liu, Z. Fan, A Mini Review : Application Progress of Magnetic Graphene Three-Dimensional Materials for Water Purification, 8 (2020). https://doi.org/10.3389/fchem.2020.595643.

[49] C. Liu, H. Liu, T. Xiong, A. Xu, B. Pan, K. Tang, Graphene Oxide Reinforced Alginate/PVA Double Network Hydrogels for Efficient Dye Removal, Polymers (Basel). 10 (2018) 835. https://doi.org/10.3390/polym10080835.

[50] Y. Zhuang, F. Yu, J. Ma, J. Chen, Enhanced adsorption removal of antibiotics from aqueous solutions by modified alginate/graphene double network porous hydrogel, J. Colloid Interface Sci. 507 (2017) 250–259. https://doi.org/10.1016/j.jcis.2017.07.033.

[51] M. Pooresmaeil, S. Javanbakht, S. Behzadi Nia, H. Namazi, Carboxymethyl cellulose/mesoporous magnetic graphene oxide as a safe and sustained ibuprofen delivery bio-system: Synthesis, characterization, and study of drug release kinetic, Colloids Surfaces A Physicochem. Eng. Asp. 594 (2020) 124662. https://doi.org/10.1016/j.colsurfa.2020.124662.

[52] X. Yang, T. Zhou, B. Ren, A. Hursthouse, Y. Zhang, Removal of Mn (II) by Sodium Alginate/Graphene Oxide Composite Double-Network Hydrogel Beads from Aqueous Solutions, Sci. Rep. 8 (2018) 10717. https://doi.org/10.1038/s41598-018-29133-y.

[53] H. Sun, L. Cao, L. Lu, Magnetite / Reduced Graphene Oxide Nanocomposites : One Step Solvothermal Synthesis and Use as a Novel Platform for Removal of Dye Pollutants, 4 (2011) 550–562. https://doi.org/10.1007/s12274-011-0111-3.

[54] A. Mehmood, F. Saleem, A. Khan, N.M. Mubarak, Y.H. Tan, R.R. Karri, Magnetic nanocomposites for sustainable water purification — a comprehensive review, (2021) 19563–19588.

[55] G. Liu, M. Xiao, X. Zhang, C. Gal, X. Chen, L. Liu, S. Pan, J. Wu, L. Tang, D. Clements-Croome, A review of air filtration technologies for sustainable and healthy building ventilation, Sustain. Cities Soc. 32 (2017) 375–396. https://doi.org/10.1016/j.scs.2017.04.011.

[56] O.J. Ajala, J.O. Tijani, M.T. Bankole, A.S. Abdulkareem, A critical review on graphene oxide nanostructured material: Properties, Synthesis, characterization and application in water and wastewater treatment, Environ. Nanotechnology, Monit. Manag. 18 (2022) 100673. https://doi.org/10.1016/j.enmm.2022.100673.

Part I : Synthesis

I. Rapid Oxidation and exfoliation via a thermal shock at different critical temperatures

I.1. Introduction

Considerable effort has been performed to engineer the composition of GO materials to suit specific applications, including reduction by removing oxygen containing groups such as epoxides, hydroxyls, and carboxyls dispersed on its basal planes and edges, and the addition of other functionalities through functionalization.

The synthesis of graphene from graphite oxide has emerged as a promising route for large-scale production. Researchers have been investigating rapid and efficient synthesis protocols unlike other traditional methods. [1] proved rapid exfoliation in a short period of time with less consuming energy using microwave irradiations.

The ability of graphene to self-exfoliate has been demonstrated to be enhanced through the process of functionalization of graphite oxide with dopants, either acids, polymer molecules or activated carbon [2, 3, 4]. The incorporation of a heat sensitive component is also an excellent method for increasing the inner pressure. Excessive gases can be generated when there is a higher concentration of oxygen, which speeds up the exfoliation process [3,5].

Thermal treatment involves subjecting graphite oxide to elevated temperatures where the weakly bonded oxygen functionalities undergo thermal decomposition, releasing gaseous by-products such as CO, CO_2, and water vapor resulting the restoration of sp²-hybridized carbon into a reorganized structure.

In this study we develop novel approach to graphene manufacturing, wherein oxidation-intercalation and reduction occur simultaneously in a single quick process.

For this, natural graphite, intercalation agents and oxidant were simply mixed before thermal shock, where intercalation and exfoliation were all accomplished in few seconds at different temperatures using a tubular furnace.

I.2   Materials

- Graphite (purity of 99% 80 µm of particle size) used in this study was in the form of graphite powder provided by a local company.

- Nitric acid HNO_3 (68%),

- Sulfuric acid H_2SO_4 (98%),

- Potassium permanganate $KMnO_4$,

- Rapid heating was carried out in a tubular furnace provided by Nabertherm GmbH.

I.3 . Protocol

1. 1 g natural graphite (NG), along with volumes of intercalation agents (nitric HNO_3 and sulfuric acid H_2SO_4) and 1 g oxidant (potassium permanganate $KMnO_4$) were easily mixed together using a glass bar at room temperature for a brief period.

2. Heat treatment experiments were carried out in a tubular furnace; provided by Nabertherm GmbH ; under ambient atmosphere conditions employing a gradual heating rate of 10 °C/ min.

3. Subsequently, after 24 h, the resulting mixture was subjected to thermal heat shock treatment in the pre-heated furnace at three distinct critical temperatures (750°C, 820°C, 870°C), enabling rapid accomplishment of oxidation, intercalation and exfoliation processes witting a few seconds.

Based on the different expansion temperatures, the EGs were labelled as GO-750, GO-820 and GO-870.
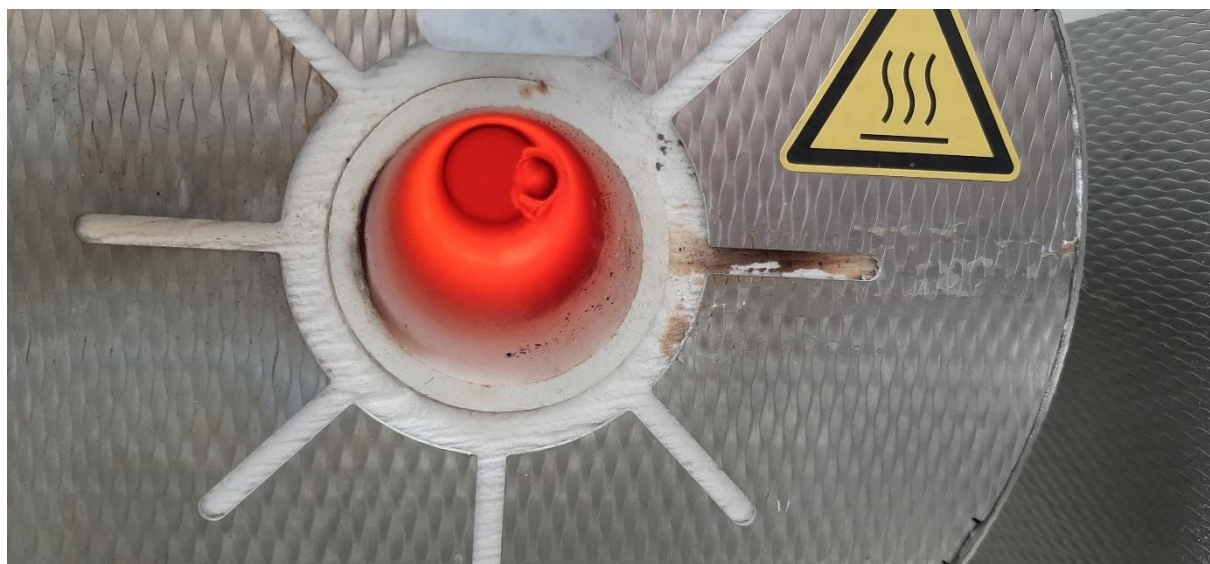
Figure II. 1. Thermal shock via a tubular furnace.

Figure II. 2. GO-750 before thermal shock.

Figure II. 3. Exfoliated GO-750 after thermal shock.
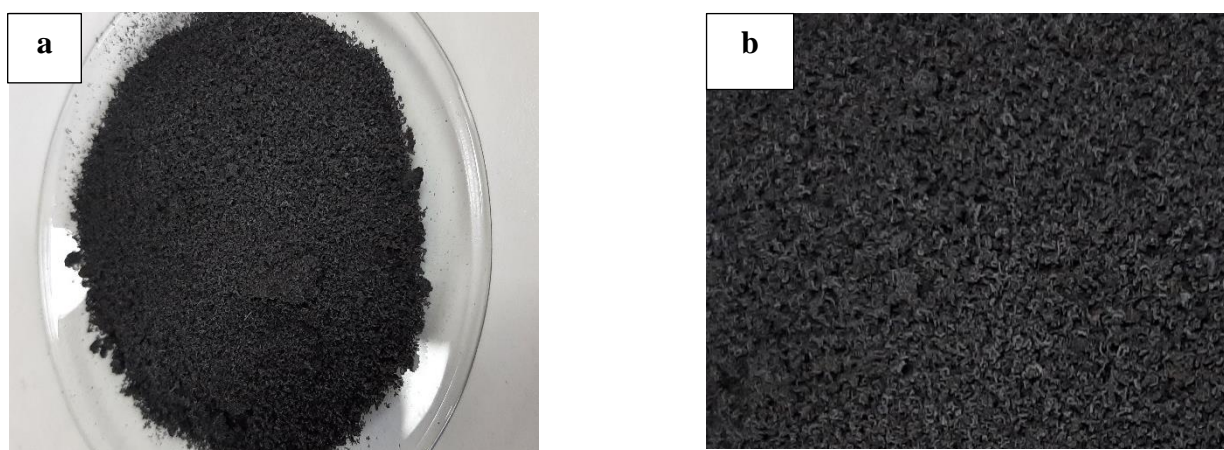
Figure II. 4. (a) Resultant GO-750, (b) Zoomed image of the resultant GO-750.

II . Improved graphene oxide

For purpose of comparison, graphene oxide was synthesized via the improved method of Hummer.

The improved Hummers' method has proved its efficiency with simpler protocol, greater amount of hydrophilic oxidized carbon material with more regular structure and greater amount of basal plane framework retained in addition to higher yielding.

For this, a 9:1 mixture of concentrated H_2SO_4 :H_3PO_4 was added to a mixture of bulk graphite (1 wt equiv) and $KMnO_4$ (6 wt equiv), producing a slight exotherm up to 40 °C. The reaction was then heated to 50 °C and stirred for 6 h. The reaction was then cooled to room temperature and poured onto 400 mL ice with 3 mL of 30% hydrogen peroxide until the colour of the mixture changed to brilliant yellow, indicating fully oxidized graphite. The as-obtained graphite oxide slurry was re-dispersed in DI water and then exfoliated to generate graphene oxide nanosheets by ultrasonication .The filtrate was decanted and the remaining solid material was then washed in succession with 200 mL of distilled water in order to remove remaining acids, and then with 200 mL of 30% HCl to remove metal ions. For each wash, the mixture was decanted away. The resultant aqueous dispersion extended multiple-wash process was vacuum-dried overnight at room temperature [6, 7].
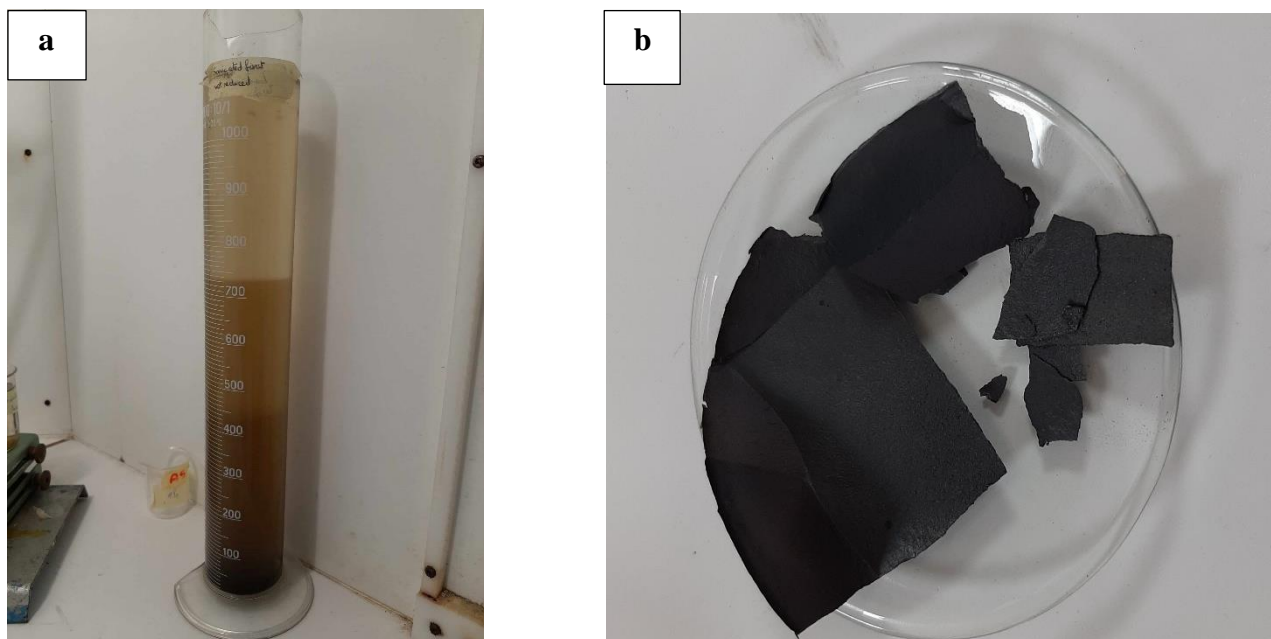
Figure II. 5. (a) Decantation of IGO, (b) IGO.
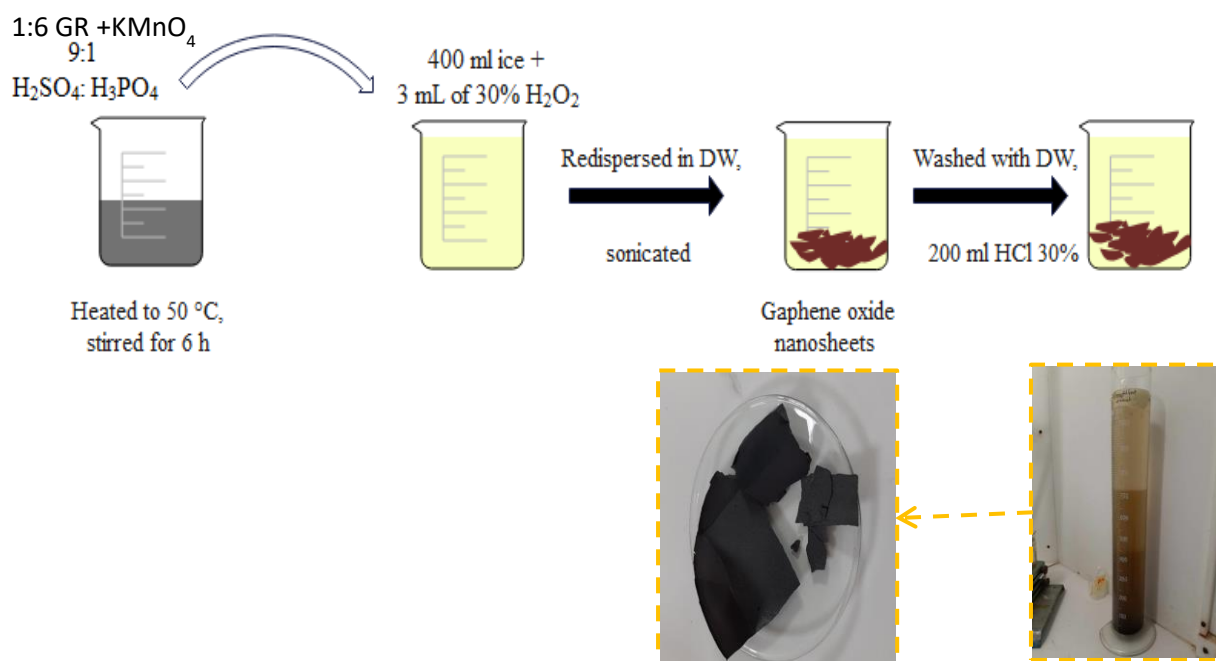
Figure II. 6. Schematic illustration of IGO synthesis

III . Rapid Oxidation via MW irradiations

Natural graphite NG, a volume of a mixture of nitric HNO_3 and sulfuric acid H_2SO_4 with 1 g of potassium permanganate $KMnO_4$ were only simply mixed by a glass bar at room temperature for 3 min in a porcelain dish.

After that, the porcelain dish was directly placed into a domestic MW oven and irradiated at 700W for 60 s. Microwave power facilities the diffusivity of acids among graphite layers [1].

Intercalating graphite flakes with acids is the essential factor. These acids diffuse through the interior of the graphite layers, pushing them apart from one another, improving the exfoliation process.
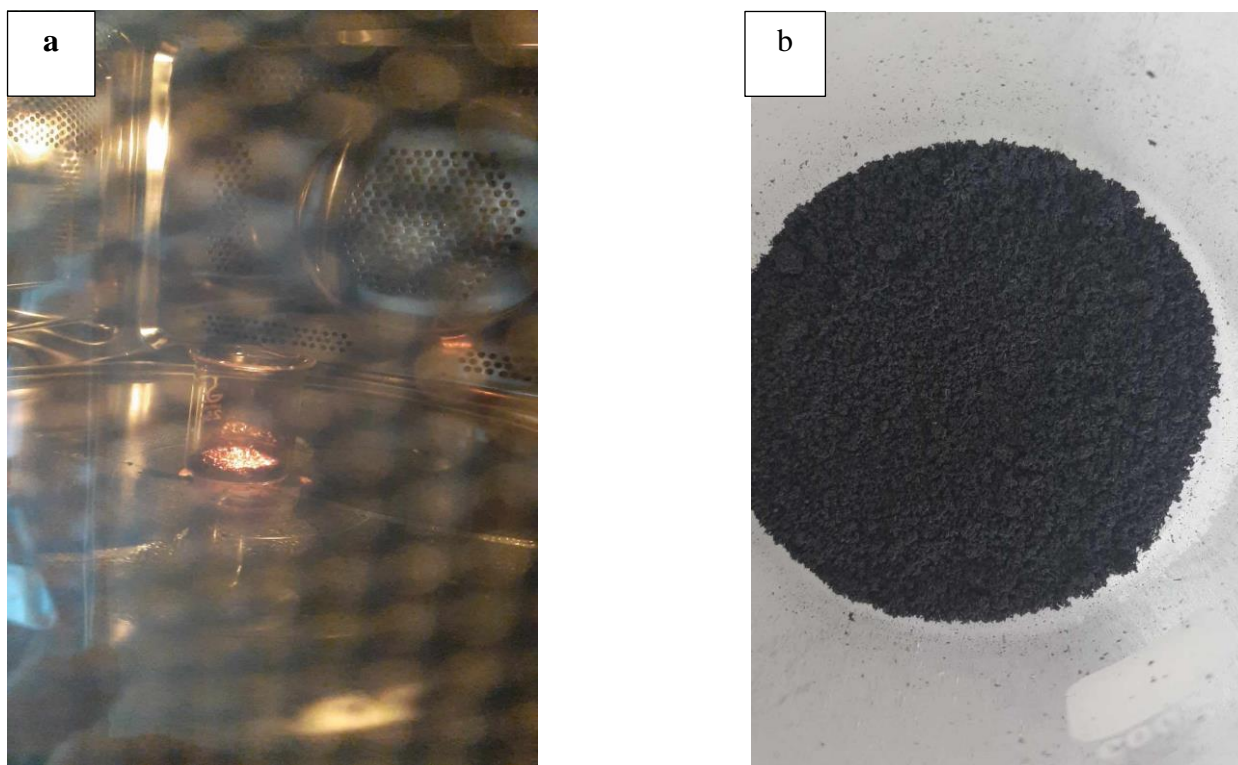
Figure II. 7. (a) Microwave irradiations, (b) Microwave assisted graphene.

IV . Graphene nanocomposite : porous network hydrogel beads (PHB)

IV.1 Introduction

For easier separation of nanomaterial from water after adsorption, preparing nanomaterial hydrogel and polymer composite hydrogel is showed to be useful.

Factors like composition and crosslinking methods of the hydrogels contribute to the overall effectiveness of the hydrogels as adsorbents in environmental remediation as they influence their structure, functional groups, porosity and adsorption mechanisms [8].

Here, we report the synthesis of a sodium alginate/ graphene oxide hydrogels through a facile method, in which graphene was used to form one of the networks in the hydrogel.

IV.2 Mechanism

Hydrogels with a high number of functional groups, such as carboxyl, hydroxyl, and amino groups, have a greater affinity for pollutants through interactions like electrostatic forces, surface complexation, and π–π interactions [8].

The efficiency of the hydrogel beads is controlled by several components including Polyvinyl alcohol, pore formation agent ; calcium carbonate ; and the crosslinking ions $CaCl_2$.

- **Polyvinyl alcohol**

Polyvinyl alcohol (PVA) is a versatile polymer with various applications due to its unique properties. In the context of the study on alginate/graphene porous hydrogel network for enhanced adsorption removal of antibiotics, PVA plays a crucial role in improving the adsorption capacity by increasing abundant hydroxyl and functional groups, thereby improving the overall adsorption efficiency of the hydrogel. Additionally, PVA's ability to prevent agglomerations ensures the structural integrity and prevents the particles from clumping together. Furthermore, PVA's biocompatibility and non-toxic nature make it suitable for biomedical and environmental uses [9, 10].
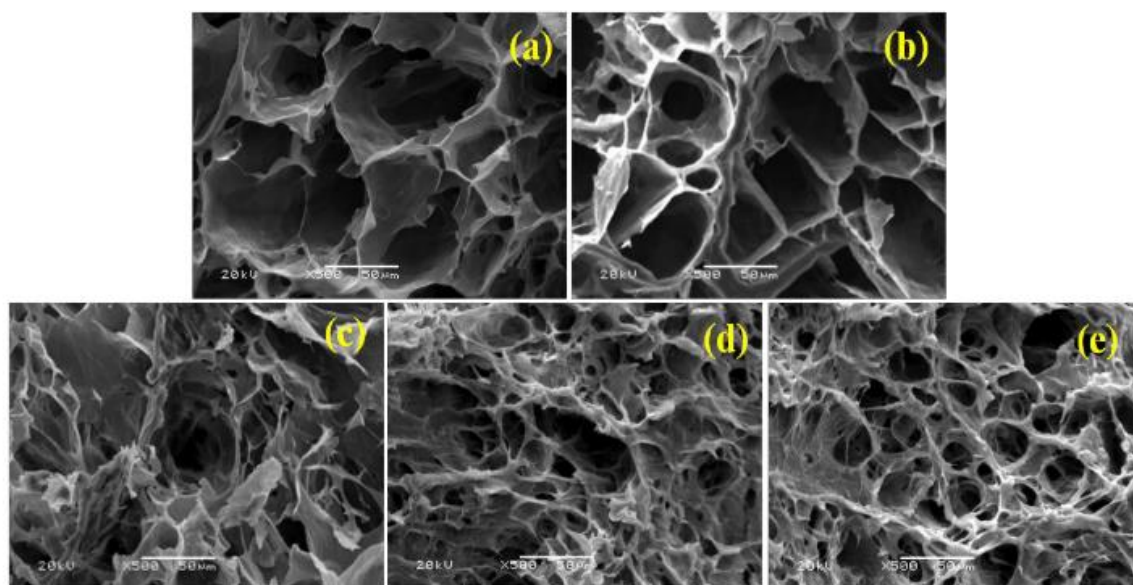
Figure II. 8. SEM images of SA/PVA with different GO loadings: (a) neat SA/PVA; (b) GO1-SA/PVA; (c) GO3-SA/PVA; (d) GO5-SA/PVA; (e) GO7-SA/PVA [11].

- **Calcium carbonate**

The presence of Calcium carbonate $CaCO_3$ is crucial for the pore formation process in the hydrogel structure, where it reacts with hydrochloric acid (HCl) to generate carbon dioxide CO_2 that acts as a pore-forming agent. The resultant $CaCl_2$ produced from the reaction serves as a crosslinking agent

for alginate. $CaCO_3$ influences the specific surface area, pore diameter, and pore volume of the hydrogel, impacting its adsorption capacity for antibiotics [9].
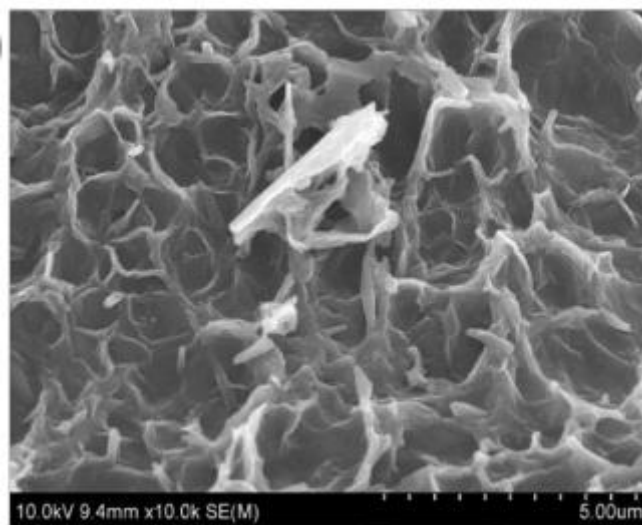
Figure II. 9. SEM image of porous double network hydrogel beads [9].

- **Calcium chloride**

Recently, an increasing number of crosslinked hydrogels properties have been developed [8]. Here, calcium ions from calcium chloride $CaCl_2$ were used to crosslink with sodium alginate chains to form hydrogel beads [12].

IV.3 Experimental method

To obtain porous network hydrogel beads, 1 g sodium alginate was dissolved in 100 mL of distilled water under rigorous stirring. 200 mg PVA and 1 g $CaCO_3$ with 200 mg GO-750 previously synthesized were added to the sodium alginate solution and stirred for 5 h. Then, sodium alginate/PVA/GO solution was slowly dropped into 200 mL of 10 mg/mL $CaCl_2$ solution using a syringe to obtain the PVA/SA/GO network beads.

After that, the obtained network beads were put into 200 mL of 30% HCl solution to produce pores through the following reaction :

$CaCO_3(s) + HCl(aq) = H_2O(l) + CO_2(g) + CaCl_2(aq)$
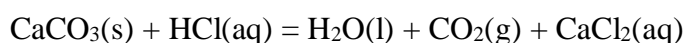
Subsequently, the microspheres were washed several times with distilled water to eliminate the excess of $CaCl_2$ on the beads surface and kept aside for air drying [9, 12].

PVA +
CaCO3   GE-750   Ca ions

Crosslinking   air dry
                                      overnight

Sodium alginate 2%   stir for 5 hours   CaCl2 (10mg/ml)

stir until complete dissolution of SA

After sevral washes

with DW and drying

Porous hydrogel beads   HCl 30%
                                                     Pores forming
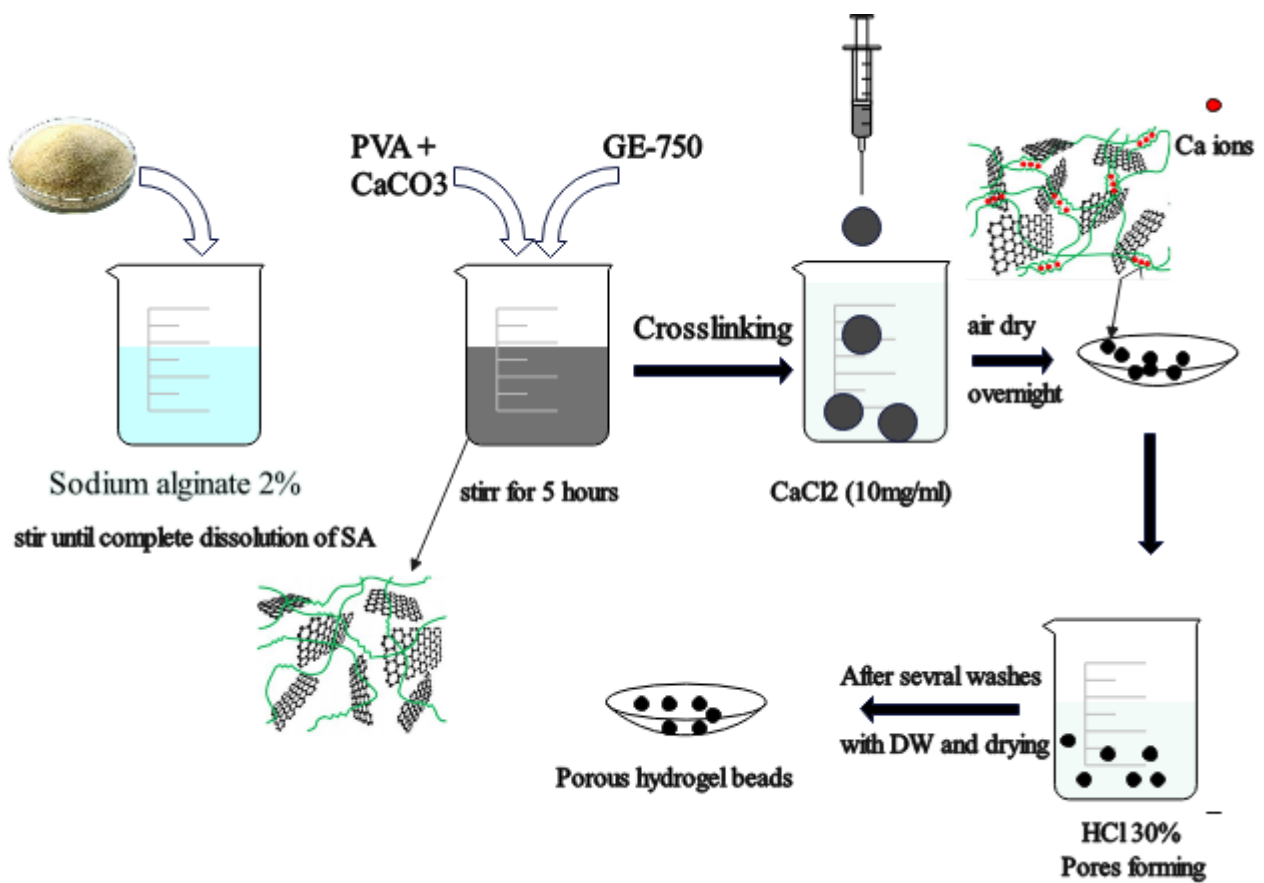
Figure II. 10. Scheme representing the synthesis steps of the hydrogel beads.
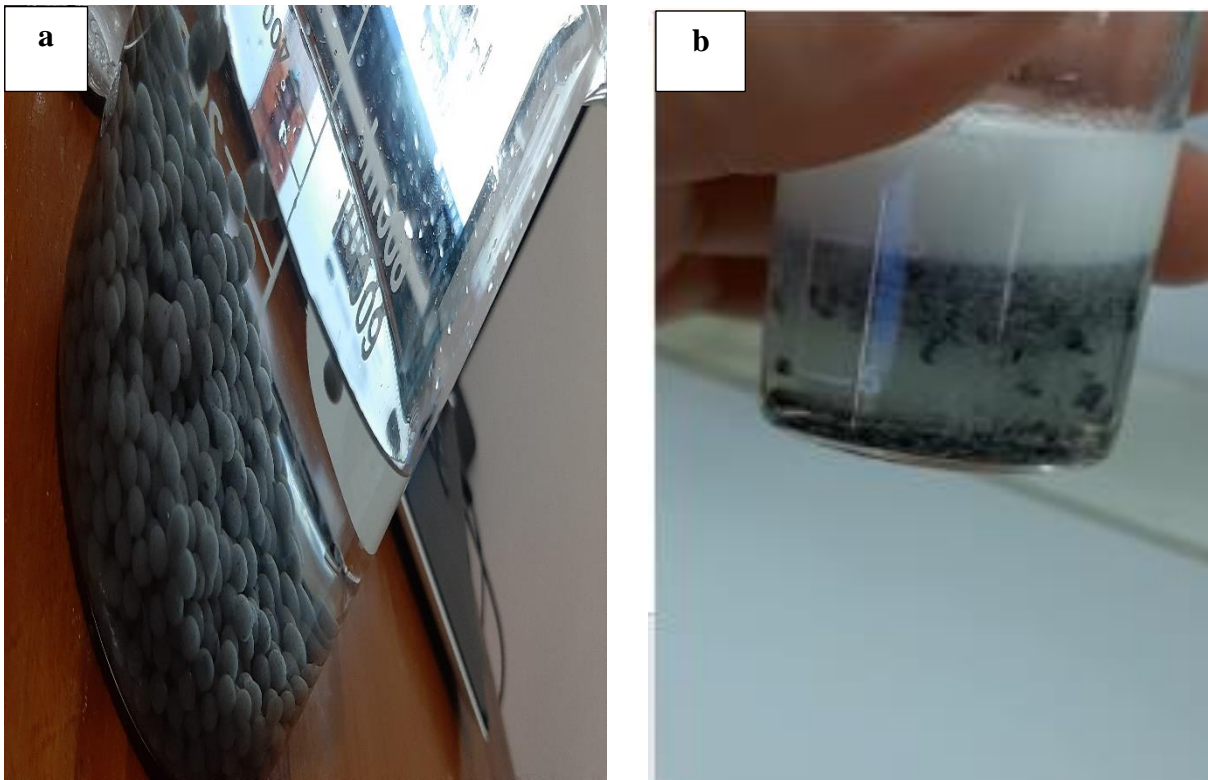
Figure II. 11. (a) GO-750 hydrogel beads, (b) Porous Hydrogel beads.
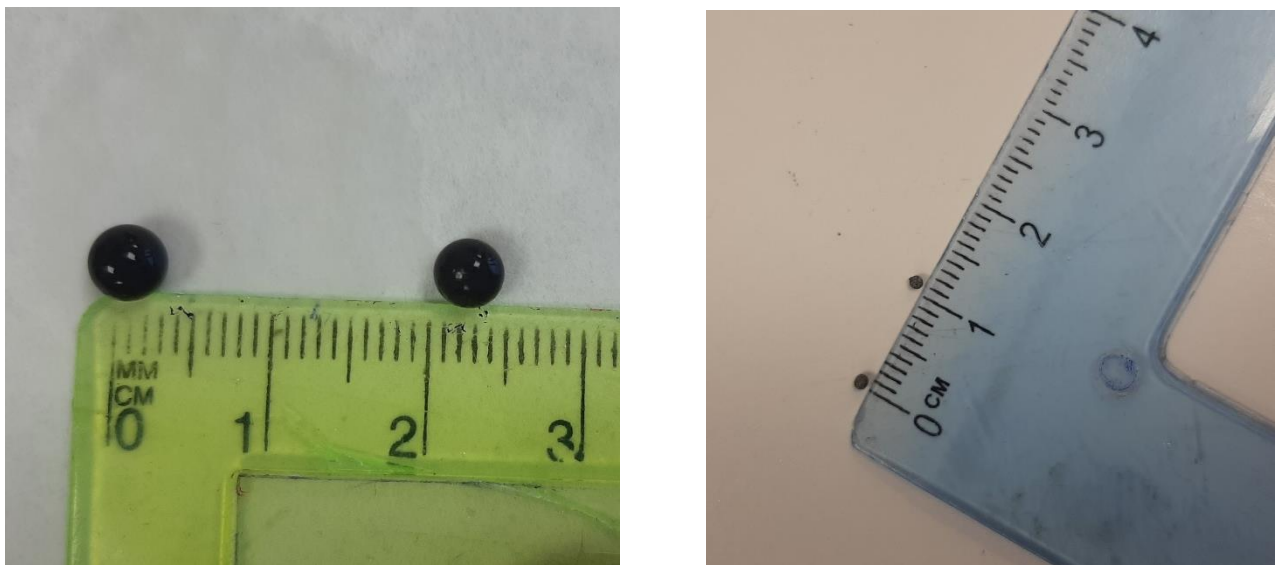
Figure II. 12. Hydrogel beads before and after air drying

V . Magnetic graphene oxide MGO

Currently, graphene is modified through chemical cross-linking or the incorporation of metal oxide nanoparticles in order to enhance its adsorption potential [13]. The synthesis of magnetic graphene oxide involves incorporating magnetic nanoparticles, typically iron oxide (Fe_3O_4) or magnetite, onto the graphene oxide sheets prepared through the co-precipitation of the Fe^{3+} and Fe^{2+} ions. This integration imparts magnetic properties to the graphene oxide, allowing for convenient separation and recovery of the material from wastewater using an external magnetic field.

V.1 . Protocol

IGO–Fe_3O_4 nanocomposites were synthesized following the next procedure :

- First, GO was synthesized by the improved Hummers' method.
- Dispersing IGO in deionized water with a weight : volume ratio of 1:1 w/v respectively and sonicating for about 30 minutes in a conical flask to obtain a homogeneous suspension.
- A ratio of (Fe^{2+} :Fe^{3+} = 1:2), the equivalent of 65 mg of Ferric Chloride $FeCl_3$ and 40 mg of ferrous chloride $FeCl_2 \cdot 4H_2O$, was dissolved in 50 mL of deionized water under constant stirring and added to the previous suspension.
- Fifty millilitres of ammonia solution (25-30%) was then introduced dropwise with vigorous stirring. The pH was controlled between 11 and 12 throughout the reaction.
- This resultant black suspension was continuously stirred for 20 minutes at 85° C followed by cooling down at room temperature.
- The resultant product was filtered and washed with deionized water to remove anionic and cationic impurities [14] and dried in vacuum oven at 70° C to obtain MGO (GO/Fe_3O_4) [15, 16].
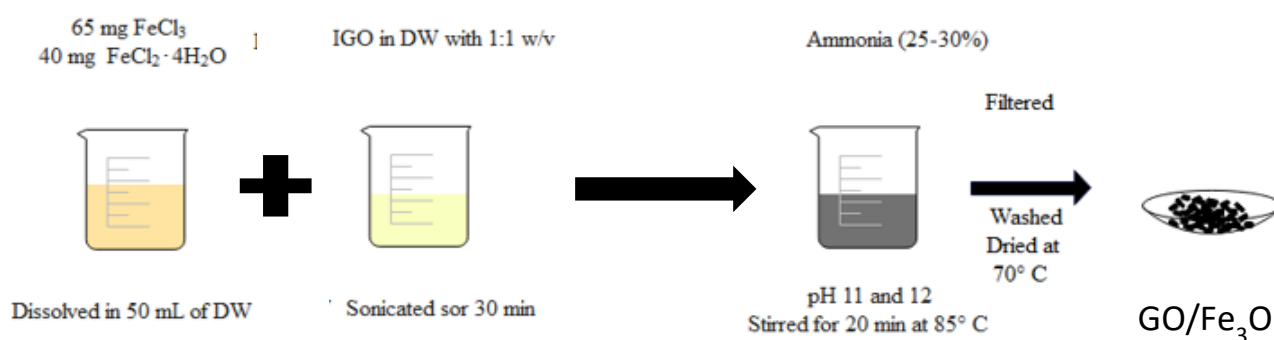
Figure II. 13. Schematic illustration of MGO synthesis

Part II : Characterization

The obtained samples were subjected to analysis using Fourier-transform infrared FTIR spectroscopy in order to determine the surface chemical properties. The interlayer spacing was examined with the help of a X-ray diffraction spectroscopy XRD, while thermogravimetric analyses were carried out to test the thermal behaviour of the as obtained materials.

I.   Fourier-transform infrared spectroscopy analysis

The surface chemical properties were determined by a FTIR using Shimadzu Prestige 21 spectrophotometer with a resolution of 4 cm^{-1} via KBr tablets containing 0.5% of the analyte, with the spectra collected in the range of 4,000 and 400 cm^{-1}.

II. X-ray diffraction analysis XRD

The interlayer spacing of the obtained carbon materials was examined using X-ray diffractometer (600 Miniflex, Rigaku, Japan) equipped with a Cu X-ray tube ($\lambda = 1.54$ Å, 40 kV and 15 mA) was run at with 10°/min scan speed in the range of $2\theta = 5°$ to 80°.

III. Thermogravimetric analysis TGA

Thermogravimetry (TG) were carried out using a TA, SDT Q600 thermal analyser (NETZSCH, Selb, Germany). The heating was conducted in an Al_2O_3 crucible. The stability of samples was analysed at a heating rate of 10°C/min up to 1,000°C under azote gas flow of 50 mL/min.

V.   Number of graphene layers, crystallite size and the graphitization degree

- Crystallite size parameter was calculated using Sherrer's formula with values of K = 0.89 [19].

With D = Kλ/β(0 0 2) cos θ [18]

where D is the average crystallite diameter,

λ is the X-ray wavelength,

θ the angle of Bragg diffraction, and

β the Full width at half maximum (FWHM) of the peak

- The number of graphene layers was estimated from the relation

N = (D/d(0 0 2)*cos θ) + 1

- The graphitization degree (g %) was calculated by the Maire–Mering Equation next bellow [19].

$$g = (3.44 - d_{002})/ (3.44 - 3.354)$$

VI . GO-750, GO-820, GO-870, and the improved graphene oxide characterization

VI.1 FTIR spectra of the improved graphene oxide, graphite and the as obtained carbon materials GO-750, GO-820 and GO-870

The figures II.14 and II.15 represent the FTIR spectrum of the improved graphene oxide, graphite and the as obtained carbon materials GO-750, GO-820 and GO-870.
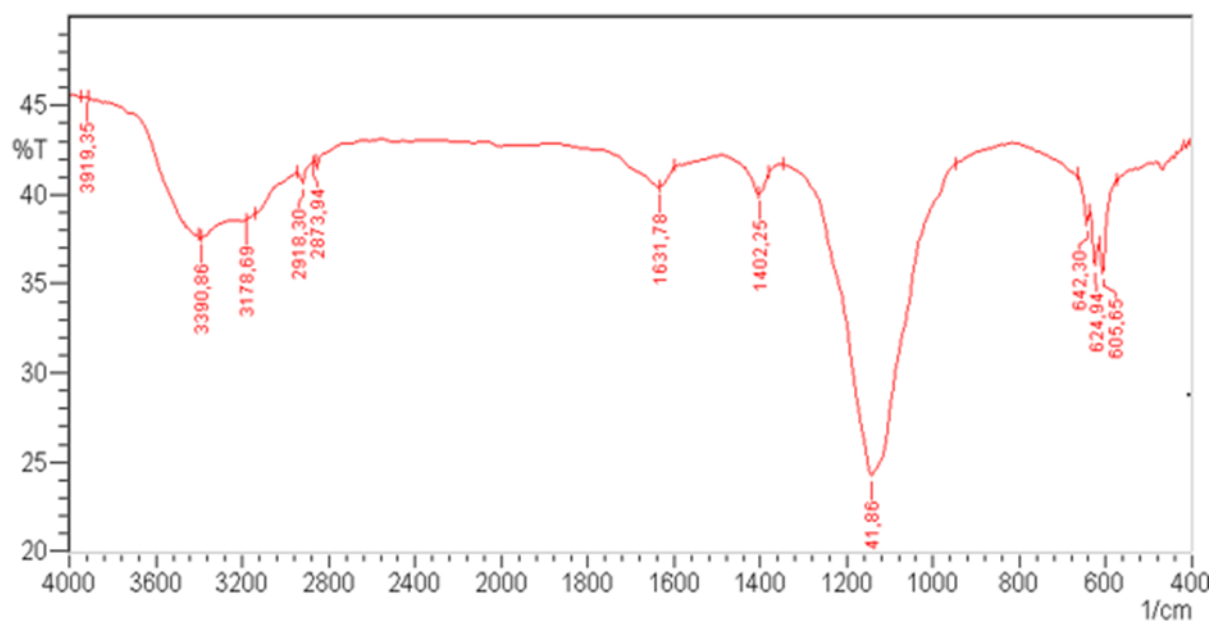
Figure II. 14. FTIR spectra of graphene oxide synthesised via the improved Hummer's method.
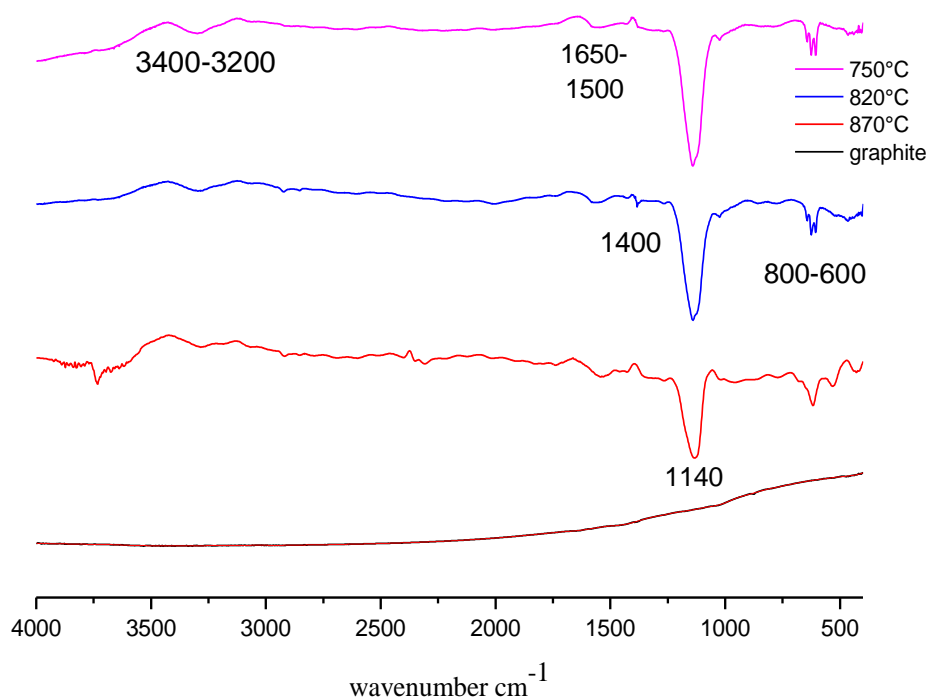
Figure II. 15. Fourier-transform infrared spectroscopy (FTIR) spectra of graphite and the as obtained carbon materials GO-870, GO-820, GO-750.

The visualization of the spectra in figure II.14 and figure II.15 shows the presence of a broad band between 3400 and 3200 cm^{-1} corresponding to the hydrogen elongation vibrations of the hydroxyl groups due to water, carboxyl, phenol or alcohol. While the small bands between 1650 and 1500 cm^{-1} is attributed to elongation vibrations of C=C groups. The small band around 1400 cm^{-1} results from C–H deformation vibrations. The spectra also show an intense band around 1140 cm^{-1} due to deformation vibrations of C–O bonds. The deformation vibration bands between 800 and 600 cm^{-1} correspond to C–H bonds (adjacent =C–H).

Graphite spectrum shows nearly a flat line with no obvious peak, suggesting no significant amount of oxygen functional groups was found in this carbon material [20].

It is also remarkable that the intensity of peaks decreases in function of the exfoliation temperature. Therefore, the oxygen-containing functional groups were partially removed and a lower amounts of functional groups' residue are still remain at the edge and at the basal plane of as obtained materials [21].

VI.2 . Determination of the point zero charge pHzpc

The pH corresponding to the point of zero charge is determined by plotting the experimental data and represented in the following figure.
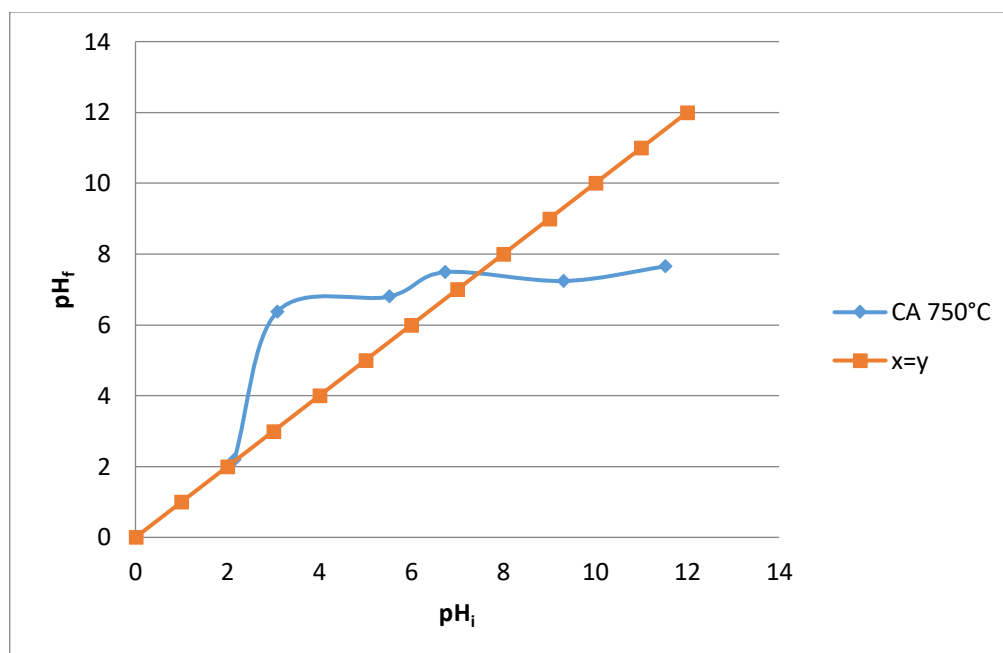
Figure II. 16. Representation of the pHzpc for GO-750 and GO-870.

The pH_{zcp} is the intersection point's value of the graph pH_f vs pH_i [22].

The pH at the point of zero charge (pH_{ZPC}) of GO-750 and GO-870 was found to be 7 and 4.04, respectively, indicating that the synthesised material has amphoteric properties. This behaviour suggests that when the pH of a solution is lower than the pH_{PZC} (point of zero charge), the surface of the adsorbent becomes positively charged. This positive charge is favourable for the adsorption of anions. Otherwise, if the pH of the solution exceeds the pH_{PZC} (point of zero charge), the adsorption of cations is preferred due to the negatively charged surface of the material [23].

IV. Zero Charge Point pH (pH zpc)

The pHzpc refers to the pH value at which there is no positive or negative charge on the surface of the material.

The adsorbent's surface is electrically neutral when the pH is equal to the point of zero charge (pHzpc). When the pH is greater than the pHzpc, it carries a negative charge, but if the pH drops lower the pHzpc, it gains a positive charge.

I. Protocol

In a series of 6 beakers, each containing 50 ml of a 0.01N of NaCl solution at pH adjusted between 2 and 12 with hydrochloric acid or sodium hydroxide solutions. After stirring for 3 hours, the initial pH was measured and 0.15 g of each material was added to each beaker.

After 48 hours stirring, a final pH measurements were taken [17].

VI.3 . X-ray diffraction (XRD) analysis

The next two figures illustrate XDR spectra of pristine graphite, GO-750, GO-820 and GO-870 respectively.
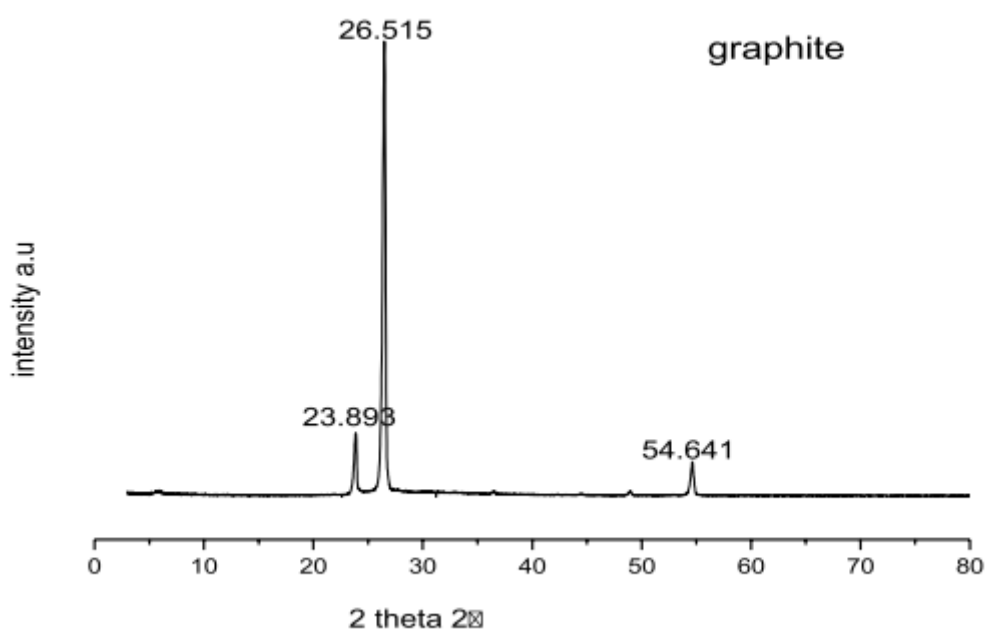
Figure II. 17. XDR spectra of pristine graphite.
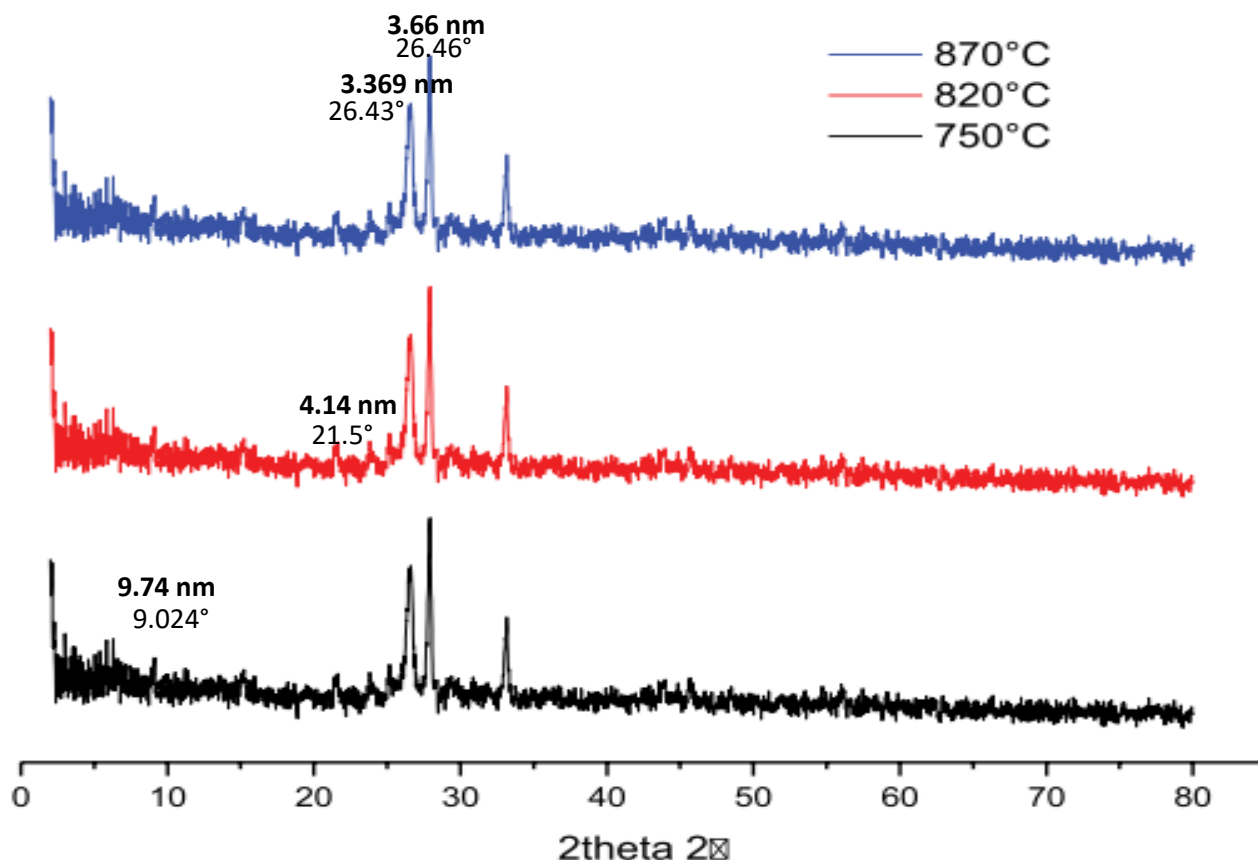
Figure II. 18. XRD of GO-750, GO-820 and GO-870.

Figure II.17 shows X-ray diffraction (XRD) pattern of pristine graphite. It reveals that graphite sample are well arranged with a characteristic sharp (0 0 2) diffraction peak located at $2\theta = 26.515°$ corresponding to an interlayer spacing of $d_{002} = 3.3589$ Å.

Figure II.18 displays the X-ray diffraction (XRD) patterns of the graphene obtained and exposed to temperatures of 750°C, 820°C and 870°C. The oxidation and the exfoliation process is then confirmed by the reappearance of the (d_{002}) diffraction line at $2\theta = 21.5°$, $2\theta = 26.43°$, and $2\theta = 26.46°$, which correspond to lattice spacings of 4.14, 3.369, and 3.66 Å for GO-750, GO-820 and GO-870, respectively.

Both GO-820 and GO-870 have quite similar peak where interlayer distance values are close to 3.35 Å for pristine graphite indicating that carbon materials has been restored considerably with two dimensional ordered stacks after heat treatment [24].

In addition, the XRD patterns of the graphene samples have weak (0 0 2) diffraction peaks with significantly lower intensities, indicating that the lattice structure of graphite is preserved during the

transformation into graphene also the presence of only a few layers in the resulting graphene [25, 26, 27].

Appearance of a new peak at 9.024 After oxidation and exfoliation, illustrating a decrease in graphitization degree and an increase of oxidation degree of GO-750, GO-820 and GO-870. According to Bragg's law, the basal spacing was calculated giving values of 0.974 nm. These values have increased compared with that of graphite 0.335 nm, indicating the disruption of the π–π van der Waals' force between the Graphene sheets during oxidation [3].

The peak sharp C(002) in the as-obtained materials shows that the formation of graphene has not been in single layers [26].

VI.4. Crystallite size, number of carbon layers and graphitization degree of graphite, GO-750, GO-820 and GO-870.

Table II. 1 represents the Crystallite size, number of carbon layers and graphitization degree of graphite, GO-750, GO-820 and GO-870.

Table II. 1. Crystallite size, number of carbon layers and graphitization degree of graphite, GO-750, GO-820 and GO-870.

	Crystallite size in nm	Number of carbon layers	Graphitization degree %
Graphite	28.12	77.29	36.09
GO-750	17.19	51.27	3518
GO-820	12.09	36.06	3610
GO-870	11.38	33.81	36.08

The data corresponded to samples obtained by thermal shock showed the deeper removal of the intercalation compounds from the material making it closer to pure graphite, i.e., material with high graphitization degree [19]. The decrease in crystallite size may be a consequence of defects caused through the heat treatment at higher temperatures when it has decreased from 28 for pure graphite to 17, 12 and 11 nm for GO-750, GO-820 and GO-870.

The number of graphite layers in the obtained materials decrease with increasing heating temperatures indicating good exfoliation into few layers graphene, it went from about 77 layers for graphite to 51, 36 and 33 layers for GO-750, GO-820 and GO-870 respectively.

VI.5 Thermogravimetric analysis

The as prepared graphene materials and graphite samples were subjected to thermal decomposition up to 1,000°C in nitrogen atmosphere to probe thermal characteristics.

The thermogravimetric analysis results illustrations offer useful insights to understand the thermal behaviour of the carbonaceous decomposition of the as-obtained materials.

Figure II. 19 shows that graphite start to decompose at 700°C~1,000°C.

The thermogram of GO-750 in figure II.20 has similarities to that of graphene oxide and reveals three notable thermal events. These events correlate to the evaporation of water below 100°C, and the partial decomposition of some unstable oxygenated functional groups such as epoxide, hydroxyl, and carboxyl between 100°C and 200°C. The carbon skeleton begins oxidative pyrolysis at approximately 400°C with a weight loss of about 11 %. The decomposition of the high amount of oxygen groups and the weaker non-graphitic sp^3 hybridised carbon at 750°C requires less heat energy. Furthermore, third weight loss of about 31% due to successive breakdown of carbon skeleton in the temperature phase range of 400 till 900 C is observed and finally total residual weight obtained at 1000 °C was around 50%.

Figure II.21 and II.22 demonstrates that Graphite, GO-820, and GO-870 exhibit thermographs that are remarkably similar. These materials have an elevated level of thermodynamic stability, as evidenced by their decomposition temperature exceeding 600°C. This can be attributed to their robust 3D carbon network, which consists of numerous layers of graphene held together by strong Van Der Waals forces. Consequently, a significant amount of heat energy is required to disrupt this network [20].
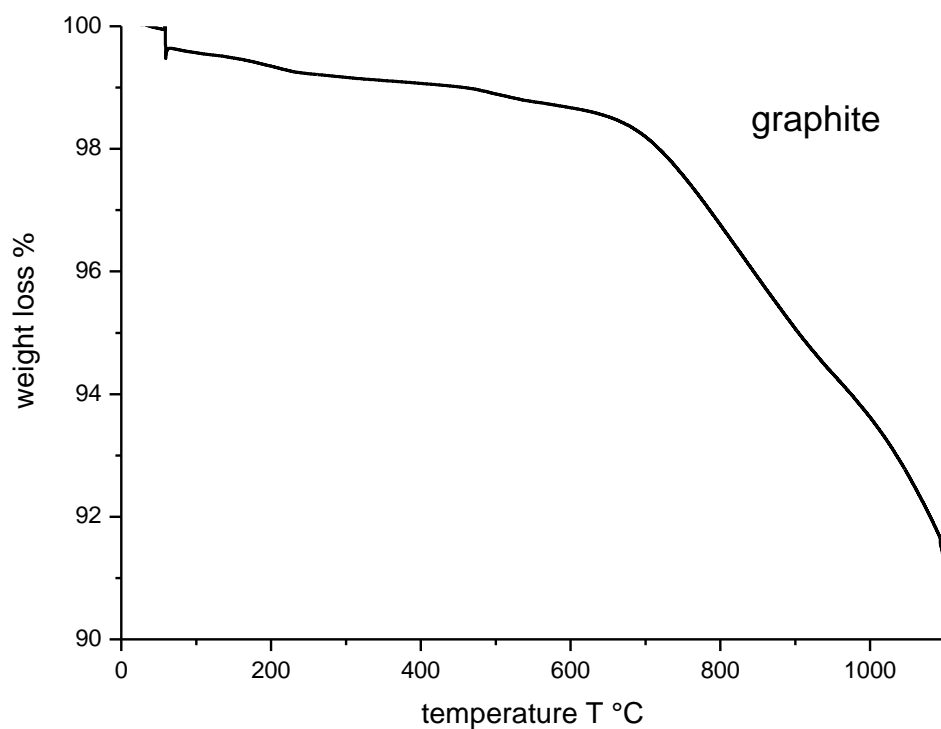
Figure II. 19. Thermogravimetric analysis spectra of graphite.
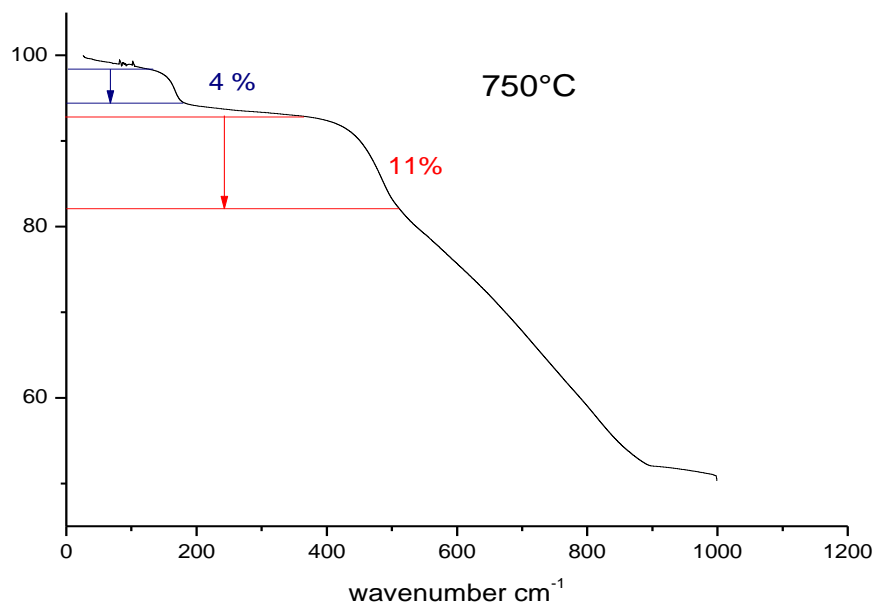
Figure II. 20. Thermogravimetric analysis spectra of GO-750.
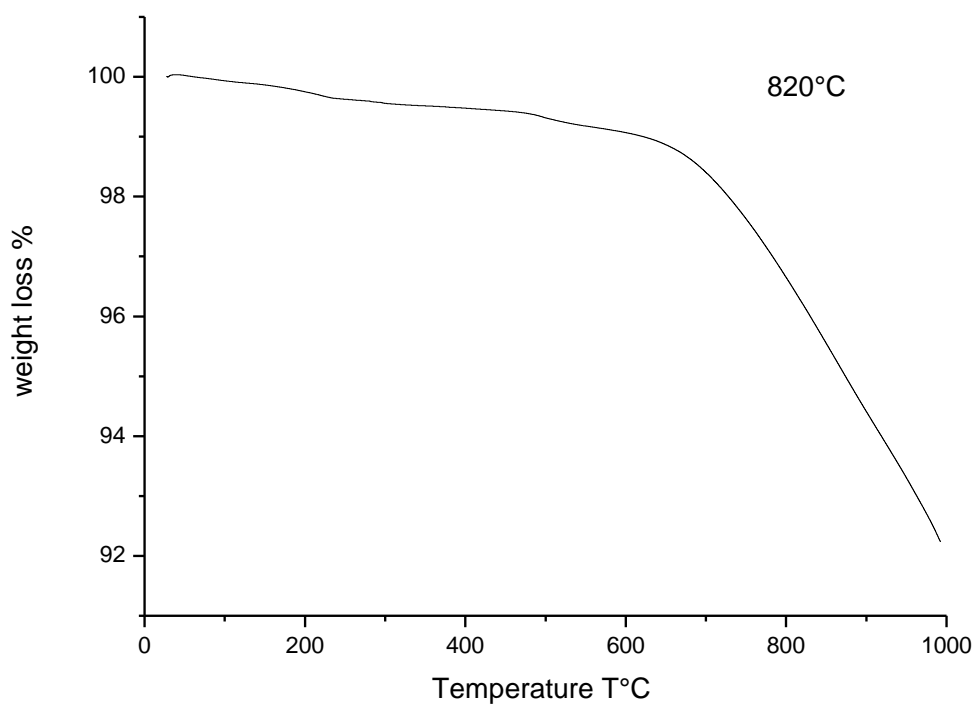
Figure II. 21. Thermogravimetric analysis spectra of GO-820.
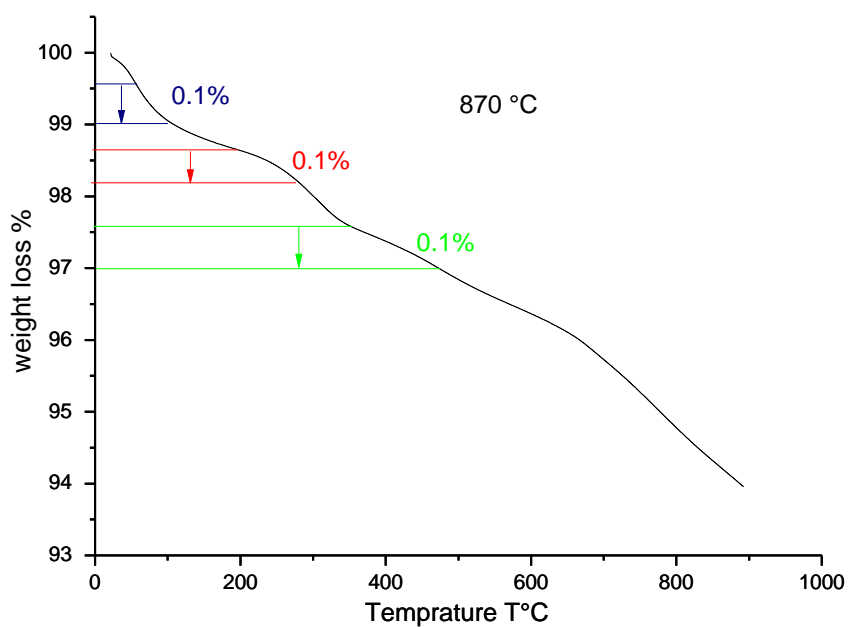
Figure II. 22. Thermogravimetric analysis spectra of GO-870.
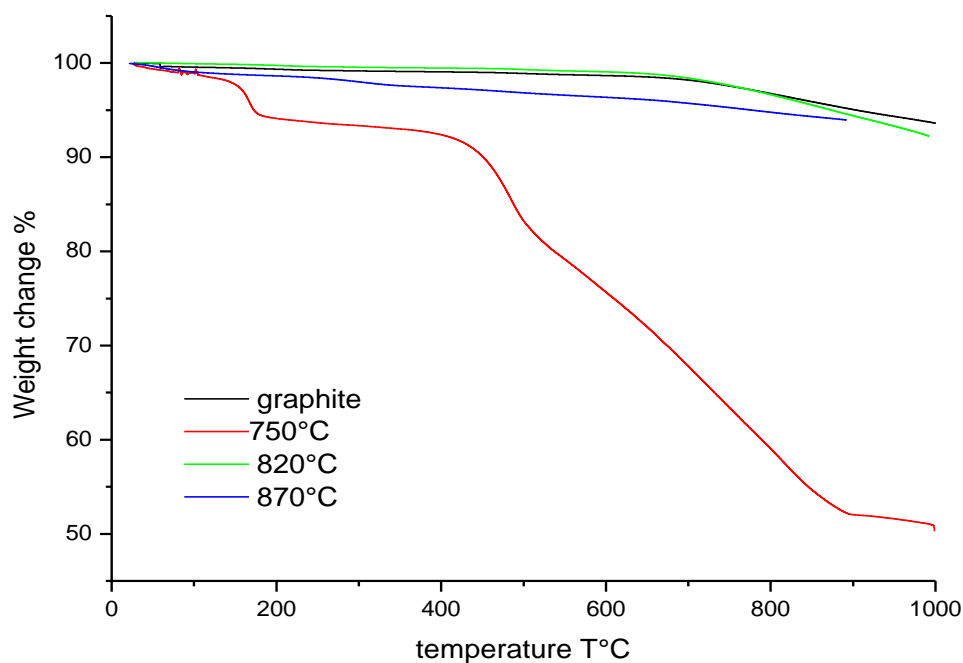
Figure II. 23. Thermogravimetric analysis spectra of graphite, GO-750, GO-820 and GO-870.

VII. MW graphene oxide analysis

VII.1. FTIR analysis

The figure next reveals the FTIR pattern of the microwave assisted synthesis of graphene oxide.
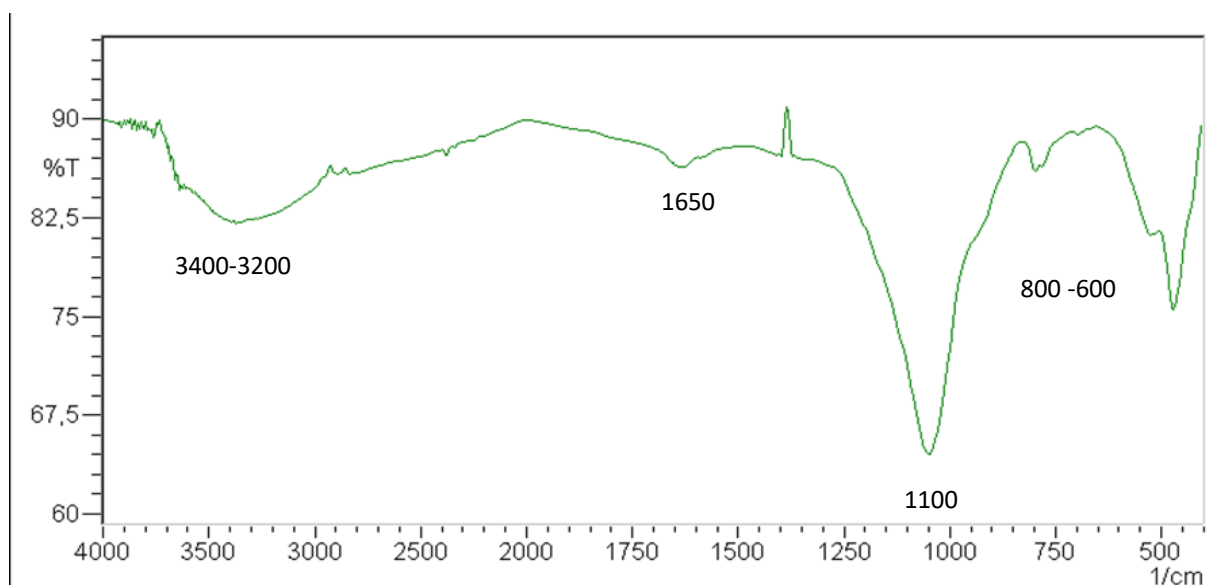
Figure II. 24. FTIR pattern of the microwave assisted synthesis of graphene oxide

The Visualization of the spectrum in figure II.24 shows the presence of a broad band between 3400 and 3200 cm^{-1} corresponding to the hydrogen elongation vibrations of the O–H hydroxyl groups due to water, carboxyl, phenol or alcohol. While the weak band at 1650 cm^{-1} is attributed to elongation vibrations of C=C groups of alcyns. The spectra also show an intense band around 1100 cm^{-1} due to deformation vibrations of C–O bonds. The deformation vibration bands between 800 and 600 cm^{-1} correspond to C–H bonds (adjacent =C–H).

With the presence of all these carboxylic, hydroxyl, epoxide, and carbonyl groups, oxygen molecules (O) were confirmed to be extensively occupied at the edge and basal plane of GO, indicating that graphene was well oxidized in a rapid one step using microwave irradiations [21].

VII.2. X-rays diffraction

The following figure shows the XRD spectra of the obtained sample using microwave irradiations
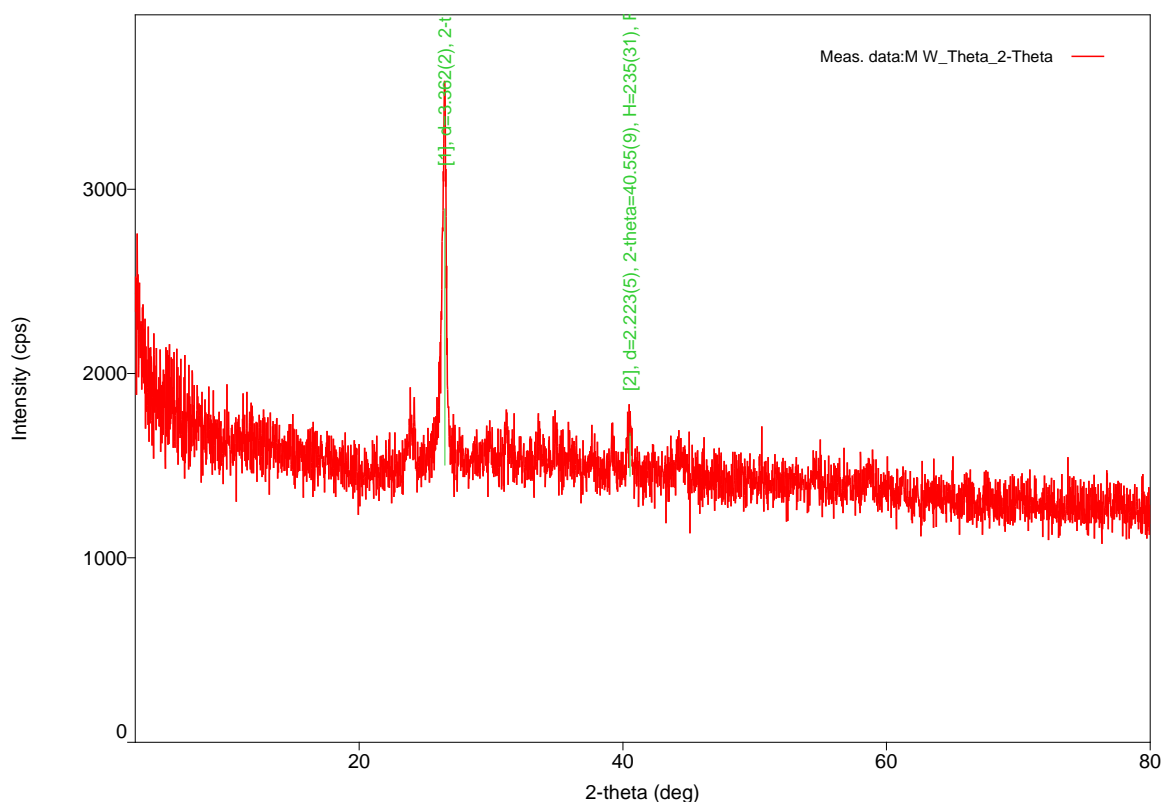
Figure II. 25. DRX spectrum of MW graphene oxide**.**

Figure II.25 shows X-ray diffraction (XRD) pattern of. MW graphene oxide. The figure reveals that MW graphene oxide sample are well arranged with a characteristic sharp (0 0 2) diffraction peak located at 2θ = 26.494° corresponding to an interlayer spacing values of d = 3.3362 Å ascribed to the

reflection from (0 0 2) plane [18], and have a quite similar peak where interlayer distance values are close to 3.35 Å for pristine graphite indicating that some graphite is still remaining in the sample with 2D ordered stacks after heat treatment [24]. While d value of 3,111 Å located at $2\theta = 24.516°$ indicate that some oxygen is still intercalated into the interlayer spacings of graphite. However, the intensity of these peaks is significantly lower in comparison to graphite, which suggests that the resulting graphene has only a few layers [25, 26].

VII.3. Thermogravimetric analysis
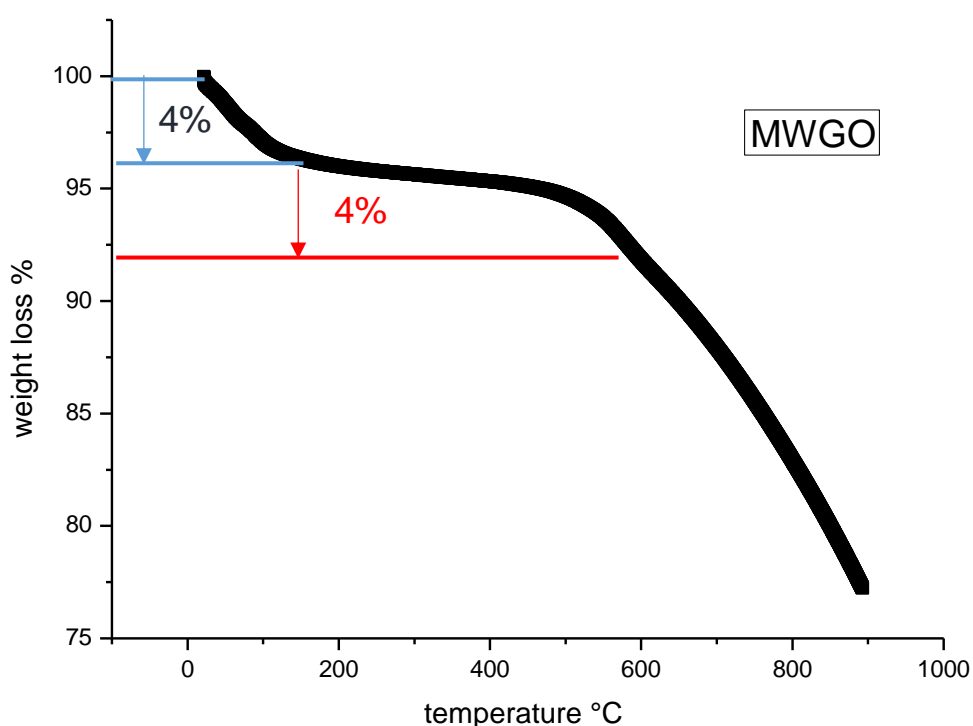
Figure II. 26. Thermogram of MWGO

The thermogram of MWGO (figure II.26) showed to be quite similar to that of GO-750 with three major thermal events. The first one correspond to the evaporation of water below 100°C. and the partial decomposition of some unstable oxygenated functional groups between up to 200°C with a weight loss of 4%. The carbon skeleton begins oxidative pyrolysis at approximatively 400°C with a weight loss of about 4 %. Furthermore. third weight loss of about 19% due to successive breakdown of carbon skeleton in the temperature phase range of 500 five hundred till 900 C is observed. And finally,

a total residual weight obtained at 900 °C was around 73% confirming once again the elevated level of thermodynamic stability.

VIII. Conclusion

The FTIR study indicated that the oxygen-containing functional groups were largely removed, leaving behind trace levels of residue. These functional groups can still be observed at the edge and basal planes of all the produced materials (GO-750, GO-820, GO-870, and MWGO), but their peaks are less intense than those of graphene oxide (IGO), showing that the thermal reduction process was successful.

The XRD examination validated the oxidation and exfoliation process by the reappearance of the (d002) diffraction lines at $2\theta = 21.5°$, $2\theta = 26.43°$, $2\theta = 26.46°$, and $2\theta = 26.49°$, which correspond to lattice spacings of 4.14, 3.369, 3.66 Å and 3.3362 Å for GO-750, GO-820, GO-870 and MWGO, respectively. Furthermore, the XRD patterns of the graphene oxide samples show faint (0 0 2) diffraction peaks with substantially lower intensities, indicating that the graphite lattice structure is preserved during the transition, giving insights that the resultant graphene has a few layers. After heat treatment, GO-820 and GO-870 have similar peak interlayer distance values of 3.35 Å for pure graphite, indicating considerable restoration of carbon materials with two-dimensional ordered stacks.

According to thermogravimetric analysis, GO-750 and MWGO requires less heat to breakdown big oxygen groups and weaker non-graphitic sp3 hybridised carbon. GO-820 and GO-870 thermographs are similar, with a starting breakdown temperature exceeding 600°C, making them the most thermodynamically stable carbon compounds investigated in this study.

References

[1] T. Wei, Z. Fan, G. Luo, C. Zheng, D. Xie, A rapid and efficient method to prepare exfoliated graphite by microwave irradiation, Carbon N. Y. 47 (2009) 337–339. https://doi.org/10.1016/j.carbon.2008.10.013.

[2] E. Freitas, D. Janu, Y. Jaqueline, G. Wernke, G. Maria, M. Demiti, L. Bergamasco, S. Vieira, Chemosphere Application of activated carbon functionalized with graphene oxide for efficient removal of COVID-19 treatment-related pharmaceuticals from water, Chemosphere. 289 (2022) 9. https://doi.org/https://doi.org/10.1016/j.chemosphere.2021.133213.

[3] Y. Hu, C. bao Sun, J. Kou, Exfoliation of poly(ethylene glycol)-intercalated graphite oxide composite in water without sonication, Int. J. Miner. Metall. Mater. 27 (2020) 840–845. https://doi.org/10.1007/s12613-019-1932-4.

[4] M.M.M. Ahmed, T. Imae, J.P. Hill, Y. Yamauchi, K. Ariga, L.K. Shrestha, Defect-free exfoliation of graphene at ultra-high temperature, Colloids Surfaces A Physicochem. Eng. Asp. 538 (2018) 127–132. https://doi.org/10.1016/j.colsurfa.2017.10.074.

[5] C. Zhang, W. Lv, X. Xie, D. Tang, C. Liu, Q.H. Yang, Towards low temperature thermal exfoliation of graphite oxide for graphene production, Carbon N. Y. 62 (2013) 11–24. https://doi.org/10.1016/j.carbon.2013.05.033.

[6] D.C. Marcano, D. V. Kosynkin, J.M. Berlin, A. Sinitskii, Z. Sun, A. Slesarev, L.B. Alemany, W. Lu, J.M. Tour, Improved synthesis of graphene oxide, ACS Nano. 4 (2010) 4806–4814. https://doi.org/10.1021/nn1006368.

[7] G. Wang, X. Shen, B. Wang, J. Yao, J. Park, Synthesis and characterisation of hydrophilic and organophilic graphene nanosheets, Carbon N. Y. 47 (2009) 1359–1364. https://doi.org/10.1016/j.carbon.2009.01.027.

[8] F. Yu, P. Yang, Z. Yang, X. Zhang, J. Ma, Double-network hydrogel adsorbents for environmental applications, Chem. Eng. J. 426 (2021) 131900. https://doi.org/10.1016/j.cej.2021.131900.

[9] Y. Zhuang, F. Yu, J. Ma, J. Chen, Enhanced adsorption removal of antibiotics from aqueous solutions by modified alginate/graphene double network porous hydrogel, J. Colloid Interface Sci. 507 (2017) 250–259. https://doi.org/10.1016/j.jcis.2017.07.033.

[10] Y. Kong, Y. Zhuang, Z. Han, J. Yu, B. Shi, K. Han, H. Hao, Dye removal by eco-friendly physically cross-linked double network polymer hydrogel beads and their functionalized composites, J. Environ. Sci. 78 (2019) 81–91. https://doi.org/10.1016/j.jes.2018.07.006.

[11] C. Liu, H. Liu, T. Xiong, A. Xu, B. Pan, K. Tang, Graphene Oxide Reinforced Alginate/PVA Double Network Hydrogels for Efficient Dye Removal, Polymers (Basel). 10 (2018) 835. https://doi.org/10.3390/polym10080835.

[12] X. Yang, T. Zhou, B. Ren, A. Hursthouse, Y. Zhang, Removal of Mn (II) by Sodium Alginate/Graphene Oxide Composite Double-Network Hydrogel Beads from Aqueous Solutions, Sci. Rep. 8 (2018) 10717. https://doi.org/10.1038/s41598-018-29133-y.

[13] B. Wang, Q. Liu, Z. Fan, A Mini Review : Application Progress of Magnetic Graphene Three-Dimensional Materials for Water Purification, 8 (2020). https://doi.org/10.3389/fchem.2020.595643.

[14] D. Press, Enhanced bioactivity of a GO – Fe 3 O 4 nanocomposite against pathogenic bacterial strains, (2018) 63–66.

[15] Q.- Ain, M.U. Farooq, M.I. Jalees, Journal of Water Process Engineering Application of Magnetic Graphene Oxide for Water Puri fi cation : Heavy Metals Removal and Disinfection, J. Water Process Eng. 33 (2020) 101044. https://doi.org/10.1016/j.jwpe.2019.101044.

[16] M. Pooresmaeil, S. Javanbakht, S. Behzadi Nia, H. Namazi, Carboxymethyl cellulose/mesoporous magnetic graphene oxide as a safe and sustained ibuprofen delivery bio-system: Synthesis, characterization, and study of drug release kinetic, Colloids Surfaces A Physicochem. Eng. Asp. 594 (2020) 124662. https://doi.org/10.1016/j.colsurfa.2020.124662.

[17] T. José, M. Fraga, L. Emely, M. Lima, Z. Santana, B. Souza, M.N. Carvalho, E. Maria, P. De Luna, M.G. Ghislandi, M. Alves, Amino-Fe3O4-functionalized graphene oxide as a novel adsorbent of Methylene Blue : kinetics , equilibrium , and recyclability aspects Amino-Fe 3 O 4 -functionalized graphene oxide as a novel adsorbent of Methylene Blue : kinetics , equilibrium , and recyc, (2019). https://doi.org/10.1007/s11356-018-3139-z.

[18] F.S. Al-Hazmi, G.H. Al-Harbi, G.W. Beall, A.A. Al-Ghamdi, A.Y. Obaid, W.E. Mahmoud, One pot synthesis of graphene based on microwave assisted solvothermal technique, Synth. Met. 200 (2015) 54–57. https://doi.org/10.1016/j.synthmet.2014.12.028.

[19] A.G. Bannov, A. V. Ukhina, E.A. Maksimovskii, I.Y. Prosanov, A.A. Shestakov, N.I. Lapekin, N.S. Lazarenko, P.B. Kurmashov, M. V. Popov, Highly porous expanded graphite: Thermal shock vs. programmable heating, Materials (Basel). 14 (2021) 1–17. https://doi.org/10.3390/ma14247687.

[20] F. Farivar, P. Lay Yap, R.U. Karunagaran, D. Losic, Thermogravimetric Analysis (TGA) of Graphene Materials: Effect of Particle Size of Graphene, Graphene Oxide and Graphite on Thermal Parameters, C. 7 (2021) 41. https://doi.org/10.3390/c7020041.

[21] N.M.S. Hidayah, W. Liu, C. Lai, N.Z. Noriman, C.-S. Khe, U. Hashim, H.C. Lee, Comparison on graphite, graphene oxide and reduced graphene oxide: Synthesis and characterization, in: 2017: p. 150002. https://doi.org/10.1063/1.5005764.

[22] A. Mohseni-bandpi, T.J. Al-musawi, E. Ghahramani, M. Zarrabi, S. Mohebi, S. Abdollahi, Improvement of zeolite adsorption capacity for cephalexin by coating with magnetic Fe 3 O 4 nanoparticles, J. Mol. Liq. 218 (2016) 615–624. https://doi.org/10.1016/j.molliq.2016.02.092.

[23] P. Marin, R. Bergamasco, A. Nivaldo, P. Roberto, S. Hamoudi, Synthesis and characterization of graphene oxide functionalized with MnFe 2 O 4 and supported on activated carbon for glyphosate adsorption in fixed bed column, Process Saf. Environ. Prot. 123 (2019) 59–71. https://doi.org/10.1016/j.psep.2018.12.027.

[24] L. Song, F. Khoerunnisa, W. Gao, W. Dou, T. Hayashi, K. Kaneko, M. Endo, P.M. Ajayan, Effect of high-temperature thermal treatment on the structure and adsorption properties of reduced graphene oxide, Carbon N. Y. 52 (2013) 608–612. https://doi.org/10.1016/j.carbon.2012.09.060.

[25] W. Wu, M. Liu, Y. Gu, B. Guo, H. Ma, P. Wang, X. Wang, R. Zhang, Fast chemical exfoliation of graphite to few-layer graphene with high quality and large size via a two-step microwave-assisted process, Chem. Eng. J. 381 (2020) 122592. https://doi.org/10.1016/j.cej.2019.122592.

[26] R. Siburian, D.R. Sari, J. Gultom, H. Sihotang, S.L. Raja, J. Gultom, M. Supeno, Performance of

graphite and graphene as electrodes in primary cell battery, J. Phys. Conf. Ser. 1116 (2018) 042034. https://doi.org/10.1088/1742-6596/1116/4/042034.

[27] B. Kartick, S.K. Srivastava, I. Srivastava, Green synthesis of graphene, J. Nanosci. Nanotechnol. 13 (2013) 4320–4324. https://doi.org/10.1166/jnn.2013.7461.

Part one : filtration

The objective of this study is to examine the efficiency of the synthesised materials ;GO-750 ; we developed a specialised vertical filtration system in separating water from synthetic wastewater containing malachite green (MG) and Alizarin Red S dyes (ARS).

The filtration system based on a PVC-FPT union and PVC coupling [1], incorporates graphene synthesised at a temperature of 750°C (GO-750) as the filtering material.

A stable mass of 2 g is placed within the assembly by using a support layer of gravel and cotton to prevent material loss. Models of synthetic wastewater containing different molar concentrations (10^{-5} M, 10^{-4} M, and 10^{-3} M) of GM and ARS dyes are employed in order to evaluate the consistency and effectiveness of the filtration system. This analysis provides valuable insights into the potential application of graphene-based filters for efficient removal of dyes from wastewater.

Figure III.1 represent the filtration system.

Figure III. 1. The filtration system.

The permeance recovered at specific time intervals was analysed using UV-visible spectroscopy.

The retention rate of the permeates from the different samples can be determined using the following equation :

$$R(\%)= 1- (\frac{Cp}{C0}) *100 \quad \ldots\ldots\ldots\ldots\ldots (1)$$

Where

- R(%) : retention percentage
- Co : initial concentration of the solution,
- Cp : concentration of the permeate at a defined time.

Cp is calculated according to the Beer-Lambert Law (equation 2), it stated that absorbance is directly proportional to the concentration [2].

A = εLC ……………. (2) where

- A : The absorbance.
- $\mathcal{E}$: The molar absorption coefficient in $L.mol^{-1}.cm^{-1}$
- L : Cell width in cm.
- C : The concentrations of the solution in mol L^{-1}.

I.1 Overview on the two dyes
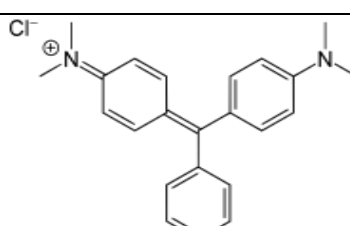
For this investigation, two analytical grade dyes were selected, green malachite MG and alizarin red S ARS. Malachite green is a cationic dye, whereas alizarin red is an anionic one.

I.1.1 Malachite green

a. Physicochemical properties

The physicochemical properties of green malachite are shown in table III.1.

Table III. 1. Physico-chemical characteristics of Green Malachite

Dye name	Green malachite
Molecular weight	364 ,91g /mol
Chemical formula	$C_{23}H_{25}ClN_2$
λ_{max}	617 nm
Chemical structure	
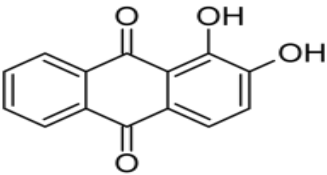
I.1.2. Alizarin Red S

Alizarin Red S is an anionic dye, also known as Alizarin carmine or Red 3 mordant. It is a sulphoconjugated alizarin (1,2-dihydroxy-anthraquinone). The pH of Alizarin Red S is between 4.6 and 6.3, making it an acid dye.

b. Physicochemical properties

The physicochemical properties of Alizarin Red S are shown in table III.2.

Table III. 2. Physico-chemical characteristics of Alizarin Red S.

Dye name	Alizarin Red *S*
Molecular weight	240 ,21 g.mol^{-1}
Chemical formula	$C_{14}H_8O_4$
λ_{max}	500nm
Chemical structure	

II . Scanning and calibration curves

Before obtaining the calibration curve for both malachite green and alizarine red, a scan between 200 and 400 nm is required to determine the wavelength of maximum absorption. The spectra of absorbance as a function of wavelength are shown in figures III.2 and III.3.

II.1 . Optical density of GM

The evolution of GM optical density as a function of wavelength are presented in the figure III.2.
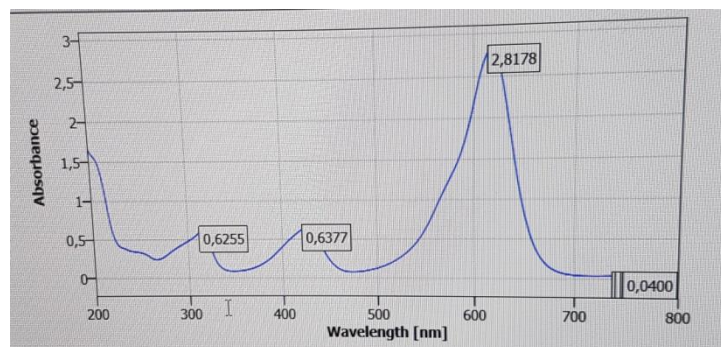
Figure III. 2. Evolution of GM optical density as a function of wavelength.

II.2 . Determining the isosbestic point of Alizarin Red S

An acid-base colour indicator consists of a pair of two coloured substances ; Acid/Base ; which exhibit different forms in their acidic and basic states. The alteration in colour occurs within the colour change region of the indicator. Therefore, the characteristic of the isosbestic point. At this point, the absorption spectra of the colour indicator align, regardless of the pH of the solution.

In order to accomplish this, three volumes of the same analytical concentration were modified to acidic, basic, and neutral pH levels using HCl and NaOH solutions, respectively. The two curves AA and AB cross at a point known as the 'isosbestic point', where the wavelength (represented by λiso) is a distinctive feature of the coloured indication. At the specific wavelength λiso, the molar absorption coefficients are thus identical [3]. The isosbestic point of ARS is represented in figure III.3.
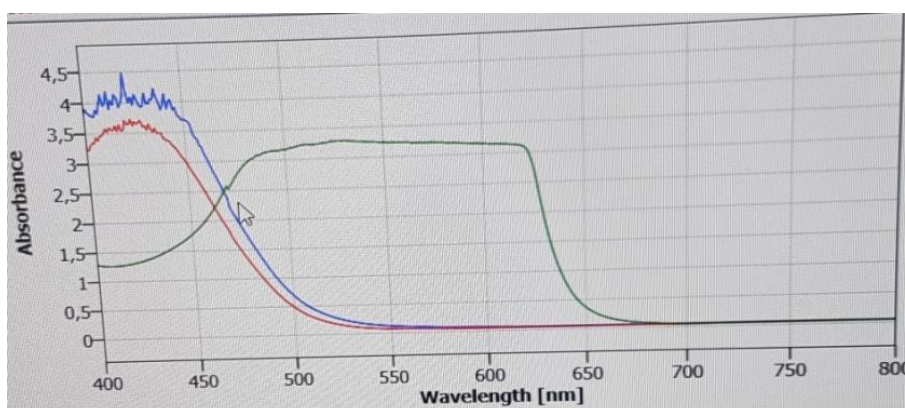
Figure III. 3. Isosbestic point of ARS

It is evident from the spectra that the maximum wavelengths of malachite green and alizarin red S are 617 nm and 480 nm, respectively.

The λ_{max} values will be used to establish the calibration curve for each pollutant and for the next investigations in the work.
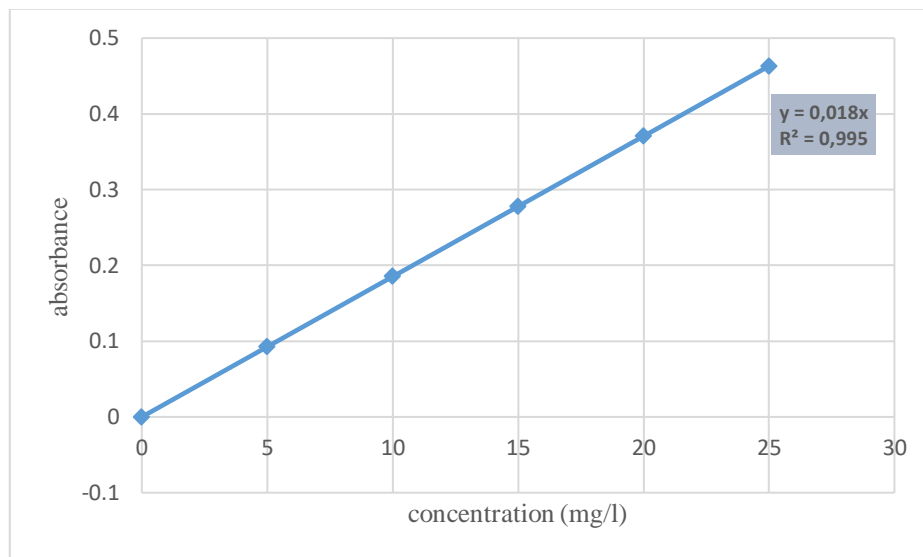
Figure III. 4. GM calibration curve.
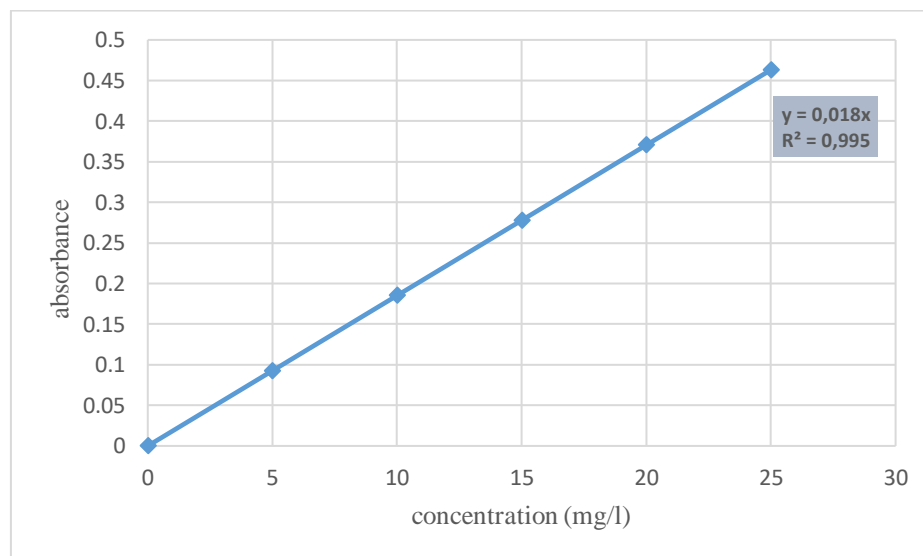
Figure III. 5. ARS calibration curve.

II.3 Conclusion

The retention rate of permeances of GM and ARS solutions through the filtration assembly using GO-750 is given in figure III.6 and III.7 respectively.
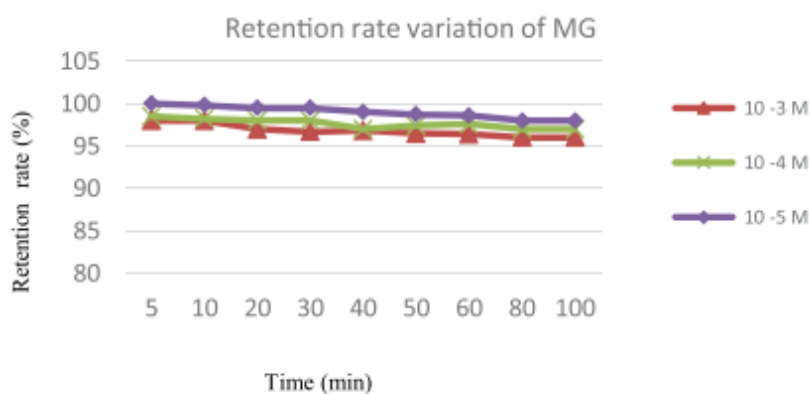
Figure III. 6. Retention rate variation of GM with time on GO-750.

.

Figure III. 7. Retention rate variation of ARS with time on GO-750

The retention rate of the malachite green is nearly perfect ranging from 99% to 100% at concentrations of 10^{-5} M and 10^{-4} M. It initially drops within the first 30 minutes and then remains stable for the duration of the experiment. However, the retention rate of the 10^{-3} M concentration is lower than that of 10^{-4} M and 10^{-5} M concentrations. It varies between 97% and 98%.

Hence, the Alizarin Red S retention rate is consistently between 99% and 100% for the concentrations of 10^{-4} M and 10^{-3} M. This is attributed to the high absorption capacity of the as obtained graphene GO-750.

The absorption of the dye particles may be attributed to the π–π interactions between the GO-750 and the benzene rings of GM and ARS. Furthermore, the binding of the dye particles to the available adsorption sites may be attributed to the Van der Waals' forces and hydrogen bonding [1].

Part II : Cefalexin elimination via adsorption
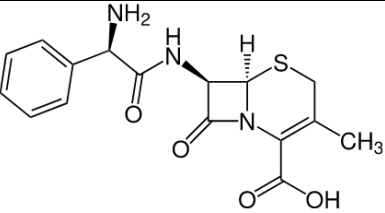
IX. Introduction

The aim of this study is to investigate the possibility of using hydrogel beads prepared from exfoliated graphite treated by thermal shock at 750°C ;GO-750°; and microwave assisted exfoliation for the adsorption of cefalexin from aqueous phases. Numerous parameters are taken into account, such as pH, solution concentration and temperature (thermodynamics). The undertaken work included a kinetic study, modelling of adsorption isotherms and thermodynamic analysis.

II . Physicochemical properties of Cefalexin

The physico-chemical properties of cefalexin are presented in table III.3.

Table III. 3. Physico-chemical properties of Cefalexin.

Cefalexin	
Formula	
Molecular formula	$C_{16}H_{17}N_3O_4S$
Chemical composition	C 55,32 %, H 4,93 %, N 12,1 %, O 18,42 %, S 9,23 %
Class	anti-inflammatory
Molecular weight (g/mol)	347.389
PKa	Strongest Acidic = 3.45 Strongest Basic = 7.23
Abbreviation	CFX
Solubility (mg/mL)	0.297

III . Operational conditions

The adsorption experiments were carried out with a constant solid/liquid ratio. A volume of 20 mL of pollutant solution with a predetermined starting concentration was added to 20 mg of adsorbents (PHB, MWG). The mixture was stirred in a thermostatic bath under constant stirring. The MWG suspension was filtered through a syringe filter of 0.45µm porosity to separate it, while PHB were separated by a simple filtration.

The quantity of adsorbed substance was determined by the difference between the initial concentration and the final concentration. The final concentration enabled the determination of the adsorption isotherms [4].

The equilibrium adsorption capacity (mg/g) represents the amount of adsorbate that is taken per unit mass of adsorbent is given by

$Qe = (Ci – Ce).V/ m$

where

- Ci : initial concentration of the contaminant (mg/L)
- Ce : equilibrium Concentration (mg/L)
- V : volume of the solution (L)
- m : adsorbent quantity (g)

For the kinetic study, Qe and Ce were replaced by Qt and Ct, respectively,

with

- Qt : Quantity adsorbed at time t (mg/g)
- Ct : Concentration at time t (mg/L).

The experimental conditions are described in table III.4.

Table III. 4. Operating conditions considered.

pH				
Temperature (°C)	**Contact time (min)**	**Initial concentration of the contaminant (mg/g)**	**Adsorbent concentration (mg/l)**	**pH of the solution**
25	120	100	1	3 5 7 10
Kinetics				
Temperature (°C)	**Contact time (min)**	**Initial concentration of the contaminant (mg/g)**	**Adsorbent concentration (mg/l)**	**pH of the solution**
25 40 55	5 10 20 30 60 120 180	100	1	7

Temperature (°C)	Contact time (min)	Initial concentration of the contaminant (mg/g)	Adsorbent concentration (mg/l)	pH of the solution
	240			
Adsorption isotherms				
25 40 55	120	100 150 200 250 300	1	7

IV . Calibration curve

A solution with a specific concentration was prepared. Subsequent dilutions were performed to get offspring solutions. The solutions were examined using a Shimadzu 1240 UV-Vis spectrophotometer with a wavelength of 262 nm measured previously through a scan between 200 and 400 nm of the optical density as function of wavelength. figure III.8 represents the calibration curve of CFX.
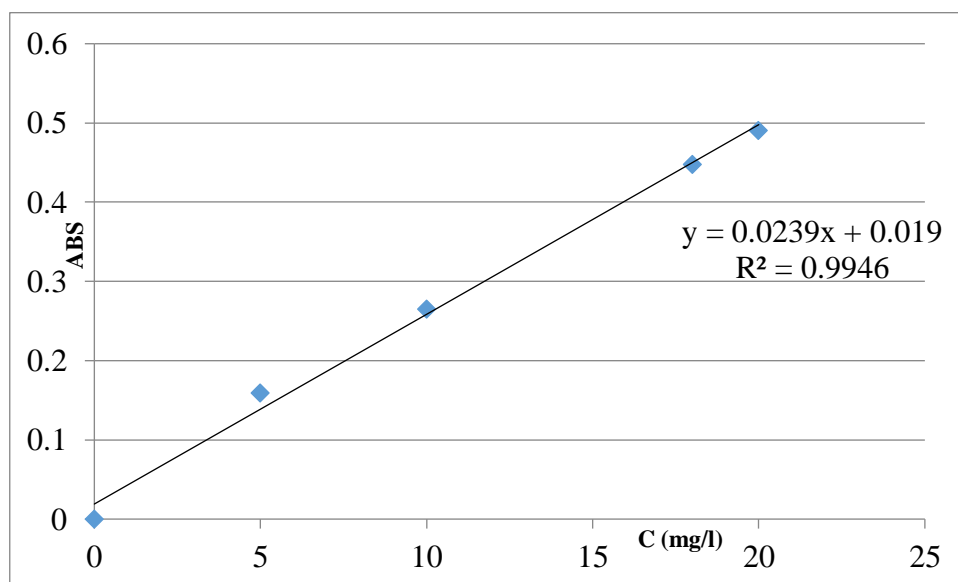
Figure III. 8. Calibration curve of CFX at 262 nm.

The change in optical density is linear with a coefficient of determination, R^2, equal to 0.999 for CFX.

V . pH effect

In order to study the effect of pH, a range from 3 to 10 was considered.

Figures III.9 and III.10 represent the variation of Q_{ads} as function of pH.
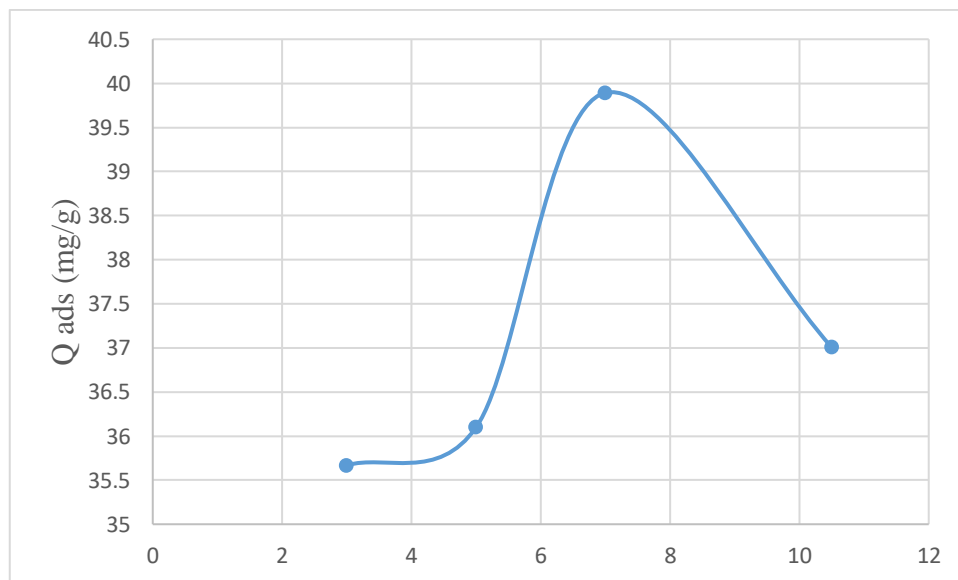
Figure III. 9. Effect of pH on CFX adsorption on PHB.
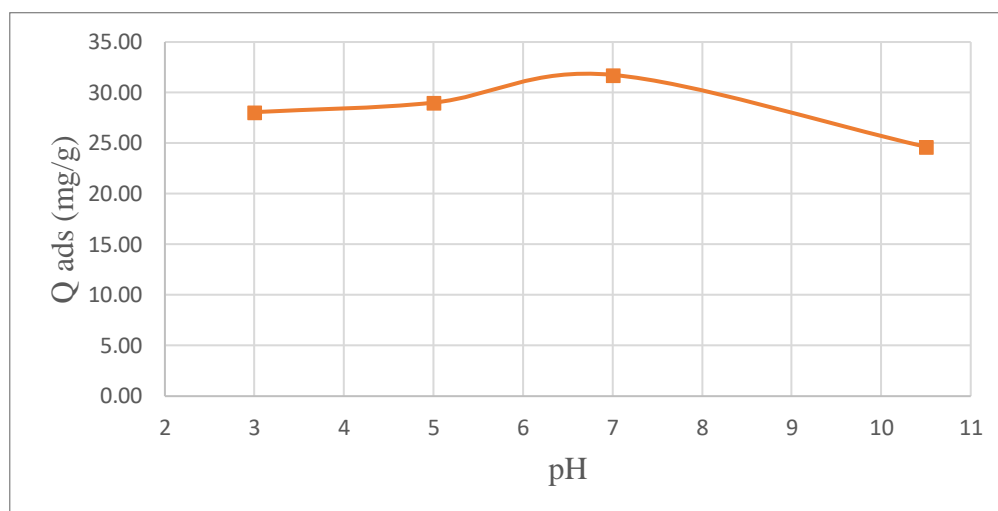
Figure III. 10. Effect of pH on CFX adsorption on MWGO.

When the pH is shifted to alkaline, the ionizable groups (carboxylic and/ or hydroxyl group) on GO-750 and MWG dissociate, and they gain their stronger negative charges. From the values of the pHzpc, it is observed that the adsorbents present negative charges when pH > 7 and positive charges when pH < 7. Cephalexin has a carboxyl group ($pKa_1 \approx 3$) and an amino group ($pKa_2 \approx 7$); thus, at pH less than 3, most of the CFX molecules are in the cationic form, between pH 3 and 7, the molecules behave as zwitterionic and at pH above 7, they have the tendency to be in the anionic form [5]. This indicates that the adsorbate is present predominantly in the zwitterionic or weakly anionic form for the whole range of pHs studied. This is due to the presence of groups that can be ionized or electronically charged, such as carbonyls (C=O), epoxy (C–O–C), and carboxylic acids (COOH), together with groups with protonation facility (electron acceptors), such as amines [5].

Figure III.11 illustrate the molecular structure of CFX and its ionic forms as a function of pH.
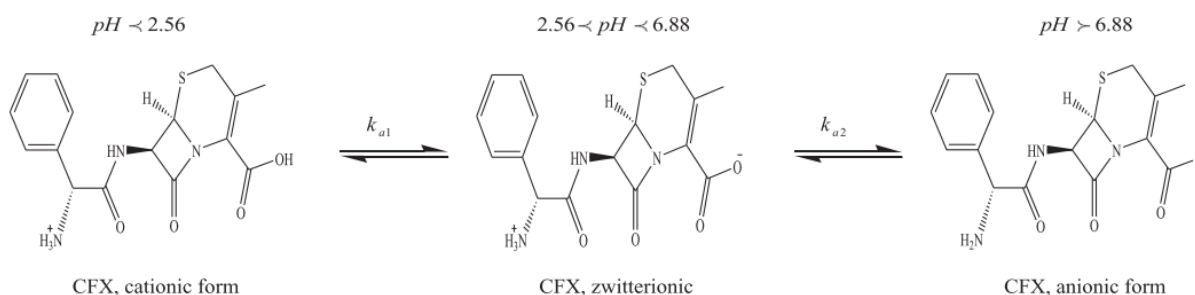
Figure III. 11. Molecular structure of CFX and its ionic forms as a function of pH.

It can be observed in figures III.9 and III.10 that the variation of pHs slightly altered the adsorption capacity and the percentage of CFX antibiotic removed. The most favourable pH to the CFX adsorption was near pH 7 where an adsorption capacity of 39,89 mg g^{-1} and 31,75 mg g^{-1} was obtained for PHB and MWGO respectively. Mohseni-Bandpi et al [6] carried out adsorption studies evaluating the effect of pH from 3 to 11 for the removal of CFX in aqueous solution using natural zeolite and Fe^{3}O^4 magnetic nanoparticles. The best results were obtained at pH 7. Same thing was the result of Mohseni-Bandpi et al [7] investigations on CFX adsorption using zeolite impregnated with manganese oxide nanoparticles. Also, it was observed that the variation of pH discretely affects the adsorption of CFX in carbon nanotubes, which is a material that is very similar to graphene [8].

The results indicate that the adsorption occurs in the anionic form but may also occur with the CFX molecules in the zwitterionic form which is predominant at pH values between 2.56 to 6.88 [9], with the possibility of interactions between the adsorbents' surface and CFX molecules by π-electron-donor–acceptor (EDA) process, electrostatic interaction and hydrophobic interaction [10].

The figure III.12 represent the reactions between carboxyl and carbonyl groups and amine groups on CFX.
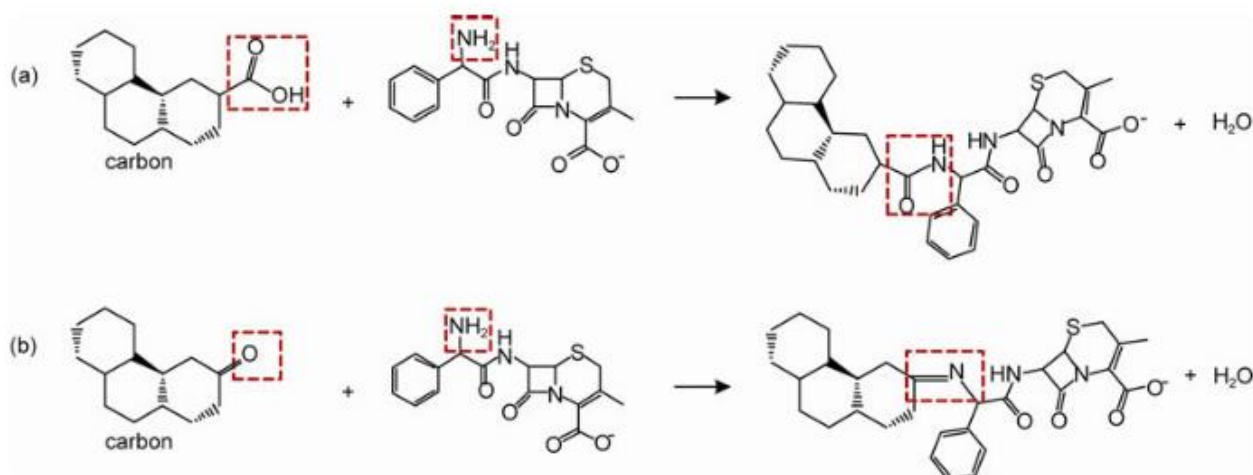
Figure III. 12. Schematic diagrams for (a) reaction between carboxyl groups and amine groups on CFX and (b) reaction between carbonyl groups and amine groups on CFX [11].

We also note that there is a decrease in adsorption by increasing the pH above 7 due to the instability of CFX in alkaline medium and a reduction in sorption at low pH values due to the presence of H$^+$ in solution which competes with CFX in its protonated form.

In addition, the adsorption of CFX on adsorbents rich in surface OH groups (as is our case) occurs preferentially and with greater stability with the horizontally distributed molecules, because in this orientation there is a greater possibility of interaction between the amine groups of CFX and the surface of the adsorbent. However, a vertical orientation of the CFX molecules would cause the molecules to approach the carboxyl group, which is negatively charged in the zwitterionic form [12].

VI   . Kinetics

Kinetics, expressed in terms of the quantity of solute adsorbed as a function of contact time, is one of the most important characteristics defining the efficiency of an adsorption. The speed with which thermodynamic equilibrium is reached is a function of the adsorbate, diffusion rate and the adsorbate-adsorbent interaction.

The evolution of the adsorbed quantity of CFX on PHB and MWGO as a function of stirring time and temperature is shown in figures III.13 and III.14 respectively.
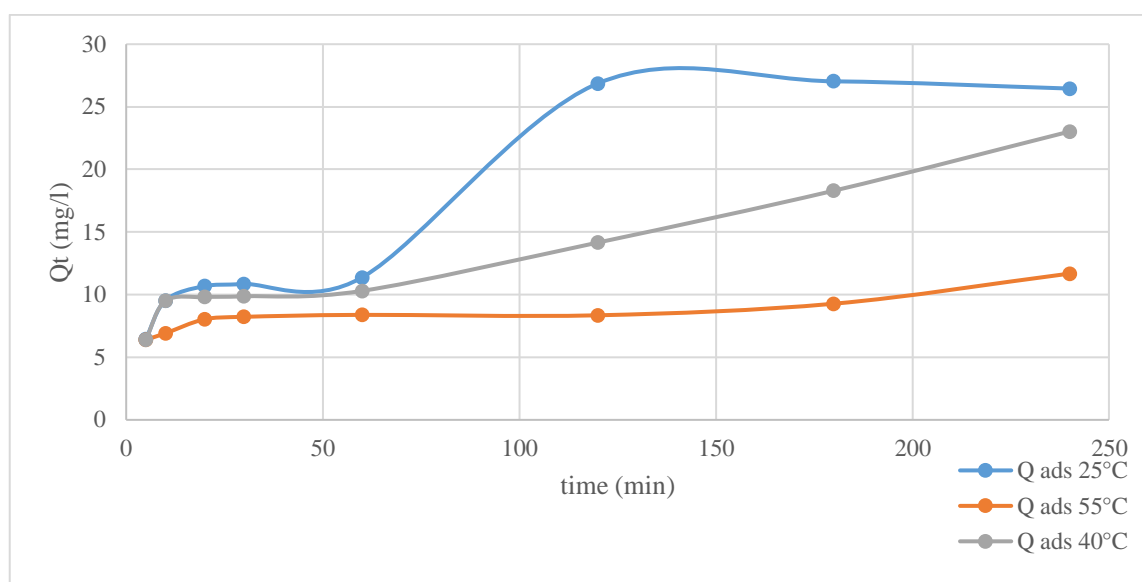
Figure III. 13. Evolution of the quantity of CFX adsorbed on PHB as a function of time and temperature.
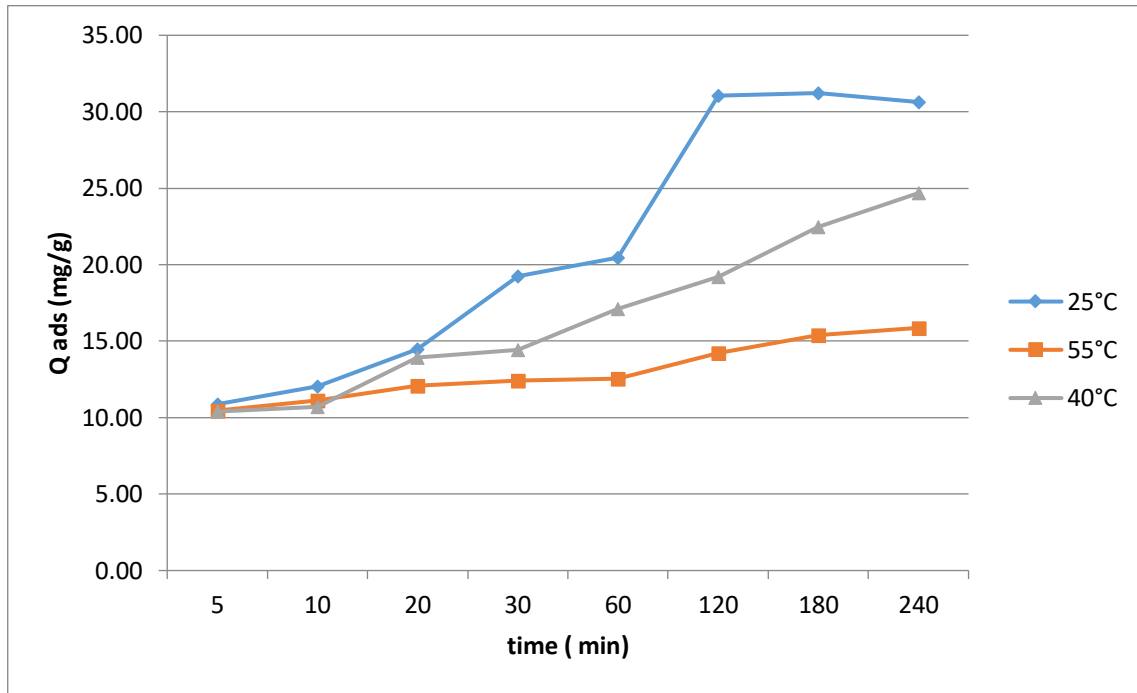
Figure III. 14. Evolution of the quantity of CFX adsorbed on MWGO as a function of time and temperature.

Adsorption of cefalexin CFX was rapid during the first twenty minutes. Equilibrium was reached after 120 minutes of contact, after which the variation was no longer significant. Furthermore, the amount of CFX adsorbed decreases with increasing temperature going from 26,87 to 8,35 mg/g when the temperature increases from 25 to 55°C.

For the rest of our work, we have considered 2 h as the equilibrium time.

The kinetic models have been adjusted to the experimental data acquired. The study employed pseudo-first order models to illustrate the properties of the adsorption process (Lagergren, 1889), and pseudo second order [13], the diffusion kinetics model such as intra-particle diffusion and Elovish.

VI.1 . Pseudo-first order

The equation of pseudo-first order proposed by Lagergren (Lagergren, 1889) can be expressed in equation 3 as :

dQt /dt = K$_1$ (Qe - Qt) …………(3)

where : Qt = 0 at t = 0.

The equation can be integrated as follows :

$\log (Qe - Qt) = \log Qe - (K_1 \cdot t / 2{,}303)$

where

- Qt is the adsorption capacity of CFX in time t (mg g^{-1}),
- Qe is the adsorption capacity at equilibrium (mg g^{-1}),
- t is the reaction time (min),
- K_1 is the adsorption rate constant of pseudo-first order (min^{-1})

If the kinetics follow the pseudo-first order model, plotting $\log (Qe-Qt)$ as a function of time will result in a straight line with a slope of - $K_1/2.303$ and a y-intercept of $\log Qe$. The linearization parameters are listed in tables III.5 and III.6.

Table III. 5. Adsorption parameters of CFX according to the pseudo-first order model on PHB.

Pseudo first order				
Temperature (°C)	Qe_{exp} (mg g^{-1})	Qecal (mg g^{-1})	K_1 (min^{-1})	R^2
25	26.8690	23.2809	0.0179	09174
40	23.0295	16.1398	0.0062	0.9298
55	11.683	4.4514	0.0034	0.7279

Table III. 6. **A**dsorption parameters of CFX according to the pseudo-first order model on MWGO.

Pseudo first order				
Temperature (°C)	Qe$_{exp}$ (mg g^{-1})	Qe$_{cal}$ (mg g^{-1})	K$_1$ (min^{-1})	R^2
25	31.0591	23.3292	0.00368	0.9149
40	20.1941	10.8268	0.0322	0.9752
55	13.5401	3.0190	0.00598	0.8611

We observe that this model does not fully describe our isotherms, since coefficients of determination, R^2, of approximately 0.9174, 0.9298 and 0.7279 has been obtained.

VI.2 . Pseudo-second-order model

The pseudo-second-order model is demonstrated in equation (4) as follows [13]

$$dQt/dt = K_2 (Qe - Qt)^2 \ldots\ldots\ldots(4)$$

By integrating equation (5) and noting that $Q_t = 0$ at t= 0, the equation obtained after rearrangement becomes:

$$t/Qt = (1/K_2.Qe^2) + t/Qe \ldots\ldots\ldots(5)$$

where

- Qt is the adsorption capacity of CFX at time t (mg g^{-1}),
- Qe is the adsorption capacity at equilibrium (mg g^{-1}),
- t is the reaction time (min),
- K$_2$ is the pseudo- second-order adsorption rate constant (g mg^{-1} min^{-1})

The initial rate of adsorption h, when $t \rightarrow 0$ is defined as : $h = K_2 .Qe^2$.

Qe, K_2 and h are obtained from the slope and y-intercept of the linear plot of t/Qt versus t. The kinetic parameters are presented in tables III.7 and III.8 .

Table III. 7. Adsorption parameters of CFX on PHB according to the pseudo-second order model.

Pseudo-second order					
Temperature (°C)	Qe_{exp} (mg g^{-1})	Qecal (mg g^{-1})	H (mg g^{-1}min^{-1})	K_2 (g mg^{-1} min^{-1})	R^2
25	26.8690	30.6748	1.1036	0.0011	0.9797
40	23.0295	21.8818	0.8140	0.0017	0.9730
55	11.683	10.3093	1.1057	0.0104	0.9841

Table III. 8. Adsorption parameters of CFX on MWGO according to the pseudo-second order model.

Pseudo-second order					
Temperature (°C)	Qe_{exp} (mg g^{-1})	Qe_{cal} (mg g^{-1})	H (mg g^{-1}min^{-1})	K_2 (g mg^{-1} min^{-1})	R^2
25	31.0591	34.0136	0.0762	0.0014	0.9890
40	20.1941	24.6305	0.0591	0.0024	0.9932
55	13.5401	16.1812	1.4138	0.0051	0.9928

The results show that the pseudo-second order model fits our kinetic data adequately. The values of R^2 values are > 0.97. A fairly good match between the experimental and calculated adsorbed quantities. Same results was found in other studies. This model states that the rate of reaction depends on the amount of solute adsorbed on the surface of the adsorbent and the equilibrium adsorbed amount.

VI.3. Intra-particle diffusion model

The intra-particle diffusion rate model is applied to porous materials.

It was proposed by Weber and Morris who indicated that, in the case where adsorption is influenced by intra-particle diffusion, the retention of an adsorbate (Qt) varies linearly with $t^{1/2}$, according to the equation (6).

$$Qt = K_{id} \cdot t^{1/2} + 1 \ldots\ldots\ldots(6)$$

Where K_{id} is the intra-particle diffusion rate constant (mg/g.min$^{1/2}$), the intercept, l, gives information about the thickness of the boundary layer : a large value of value of l corresponds to a thick boundary layer.

The parameters of the intra-particle diffusion model relating to the adsorption of CFX are shown in tables III.9 and III.10 respectively.

Table III. 9. Parameters relating to CFX on PHB according to the intra-particle diffusion model

Temperature (°C)	Qe_{exp} (mg g^{-1})	l (mg g^{-1})	K_{id} (min^{-1})	R^2
25	26,8690	3.1256	1.7047	0.9183
40	23.0295	5.3298	0.339	0.8734
55	11.683	4.297	1.0723	0.9283

Table III. 10. Intra-particular diffusion for CFX adsorption on MWGO.

Temperature (°C)	Qe_{exp} (mg g^{-1})	l (mg g^{-1})	K_{id} (mg g^{-1} min$^{-1/2}$)	R^2
25	31.0591	6.9503	2.0376	0.9712
40	20.1941	8.5167	1.0299	0.982
55	13.5401	9.124	0.4349	0.9766

The values of 'l' that give an idea of the boundary layer thickness are all positive ($l \neq 0$) for all the systems considered. This implies that intra-particle diffusion is not the only factor responsible for the adsorption rate, but it is involved.

In the case of the adsorption when MWGO is used as adsorbent, the intra-particle diffusion model describes well our experimental data with R^2 values that exceed 0,97. In the contrary for adsorption on PHB where R^2 are relatively weak.

VI.4 Elovich model

The Elovich equation is one of the most commonly used equations. It is suitable for systems with heterogeneous adsorbent surfaces. It applies when dealing with an activated process, meaning that adsorption is enhanced by an increase in temperature. It is expressed as follows [14]:

$dQt/dt = \alpha \exp(-\beta Qt)$

To simplify this equation, Chien and Clayton [15] assume $\alpha\beta t \gg 1$.

Applying the conditions: $Q_t = 0$, at $t = 0$ and $Q_t = Q_t$, at $t = t$, the equation becomes :

$Qt = \frac{1}{\beta}\ln(\alpha.\beta) + \frac{1}{\beta}\ln t$

where :

Q_t : Quantity adsorbed at time t (mg/g)

α : Initial adsorption rate (mg/g min)

β : Desorption constant according to the Chien and Clayton equation (g/mg).

The results relating to the Elovich model are given in the following tables III.11 and III.12 respectively.

Table III. 11. Elovich model for CFX adsorption on PHB.

Elovich model				
Temperature **(°C)**	**Qe$_{exp}$** **(mg g^{-1})**	**α** **(mg g^{-1} min$^{-1/2}$)**	**β** **(g mg^{-1})**	**R^2**
25	26.8690	2.7439	0.1619	0.8491
40	23.0295	46.7867	0.9331	0.7135
55	11.683	3.1155	0.2829	0.8126

Table III. 12. Elovich model for CFX adsorption on MWGO.

Elovich model				
Temperature **(°C)**	**Qe$_{exp}$** **(mg g^{-1})**	**α** **(mg g-1 min$^{-1/2}$)**	**β** **(g mg^{-1})**	**R^2**
25	65.3608	5.1278	0.1662	0.8322
40	2.6789	8.6105	0.2760	0.9714
55	13.0735	100.1193	0.6284	0.9203

We note that the Elovich model is not suitable overall, because the values of R^2 are not suitable. This means that the adsorption of CFX is a non-activated process. An increase in temperature would not favour the fixation of these pharmaceutical molecules.

VII. Adsorption isotherms

Adsorption isotherms for CXF at 25, 40 and 55°C are shown in figures III.11 and III.12, in terms of the quantity adsorbed per gram of adsorbent, Qe (mg/g), as a function of the concentration of the solute remaining in solution at equilibrium, Ce (mg/L). Following the previous kinetic study, an equilibrium time of 120 min was considered for further work.

VII.1 . Isotherms' explanation

Various adsorption models, such as Langmuir, Freundlich, Redlich-Peterson, Langmuir-Freundlich, etc., have been developed to analyse experimental data and predict the adsorption mechanism and the interactions between the adsorbate and adsorbent (such as monolayer, multilayer, homogeneous, heterogeneous, lateral interaction, etc.). The coefficient of determination, R^2, is a reliable statistical method for determining the most appropriate model. Isotherms relative to CFX adsorption on PHB and MWGO are represented in figures III.15 and III.16.
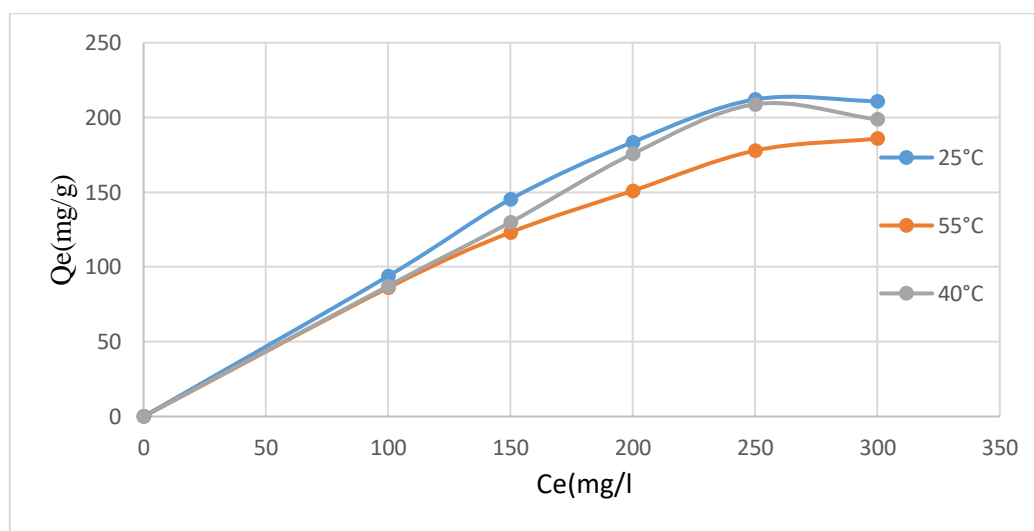
Figure III. 15. Isotherm relative to CFX adsorption on PHB.
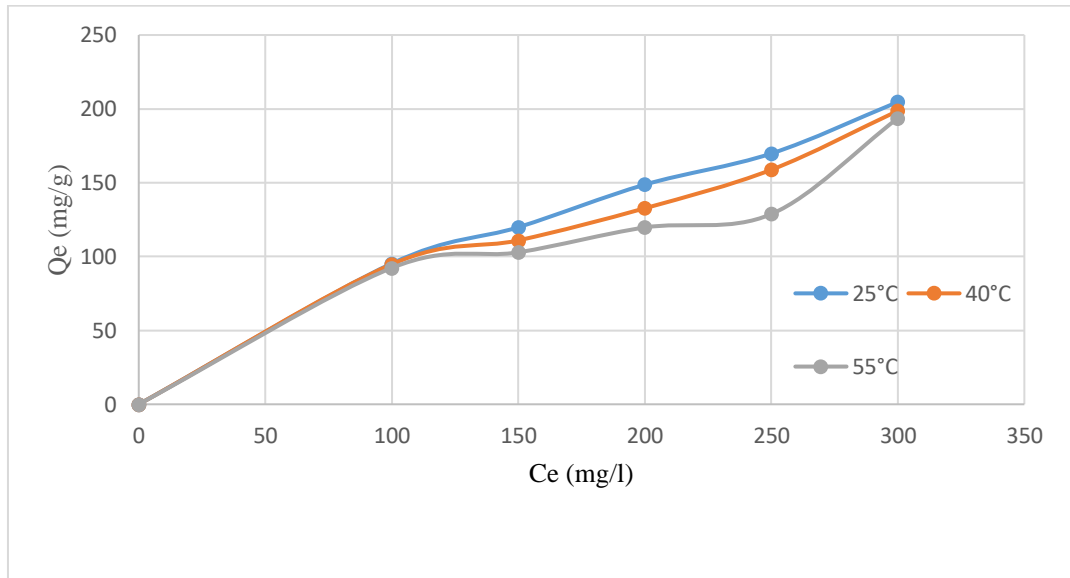
Figure III. 16. Isotherm relative to CFX adsorption on MWGO.

VII.2 . The Langmuir isotherm

The Langmuir adsorption isotherm model is the most commonly researched model. It assumes that a monolayer of adsorbate molecules forms uniformly on the adsorbent, without any lateral interactions between them. The equation (7) formulated by Langmuir is represented as

$$\frac{Qe}{Qm} = \frac{KlCe}{1+KlCe} \dots\dots\dots\dots(7)$$

With:

Q_e : Quantity adsorbed at equilibrium (mg/g)

Q_m : Quantity adsorbed at saturation (capacity of a monolayer) (mg/g)

C_e : Equilibrium concentration (mg/L)

K_L: Adsorption equilibrium constant, dependent on temperature and experimental conditions (L/mg).

VII.2.1 Linear form of Langmuir's isotherm for CFX adsorption

The linear form of the Langmuir isotherm is represented by the following equation

$C_e/Q_e = 1/Q_m.K_L + C_e / Q_m \dots\dots\dots\dots$ (8)

If the given equation is validated, then when plotted in the coordinates of $C_e/Q_e = f(C_e)$, the resulting graph should be a straight line with a slope of $1/Qm$ and an intercept of $1/Qm.K_L$. The linearization settings for CFX are provided in tables III.13 and III.14.

Table III. 13. Linearisation parameters of the Langmuir model relative to the CFX on PHB.

T (°C)	Qm (mg/g)	K_L (L/mg)	R^2
25	217.3913	0.0083	0.9977
40	212.7659	0.0098	0.9915
55	208.3333	0.0079	0.9950

Table III. 14. Linear parameters of Langmuir isotherm for CFX adsorption on MWGO.

T (°C)	Qm (mg/g)	K_L (L/mg)	R^2
25	209.3913	0.0072	0.9934
40	201.4530	0.0087	0.988
55	198.3400	0.0076	0.9952

We constat that the Langmuir model is appropriate for describing the adsorption isotherms, as all of the R^2 values exceed 0,99 and 0,98 for PHB and MWG respectively.

For all temperatures, the maximum adsorbed capacity Q_m determined by the Langmuir equation decreased with the temperature of the thermostatic bath, once again confirming the exothermic nature of cephalexin adsorption. Same adequality was found by Wernke et all [5] using graphene oxide as adsorbent. The Langmuir model suggests adsorption of a homogeneous and monolayer nature.

VII.3. Freundlich isotherm

The Freundlich model has been extensively used to describe the adsorption data on a heterogeneous adsorbent surface with several types of sites with different energies, distributed according to exponential law as a function of the adsorption's heat. This model is usually employed in order to characterise solution-solid systems.

The non-linear form of the Freundlich isotherm is given by the following equation :

$$Q_e = K_F \, Ceq^{\frac{1}{n}} \ldots\ldots\ldots(9)$$

Whereas the linear form follows the next equation

$$\text{Log } Q_e = \log K_F + \frac{1}{n} \log C_{eq} \ldots\ldots\ldots(10)$$

With

Q_e: Equilibrium adsorption capacity (mg/g)

C_e : Concentration at equilibrium (mg/L)

K_F : Constant representing the adsorption capacity (L/g)

n : Constant representing the adsorption intensity

VII.3.1 linear form of Freundlish isotherm for CFX adsorption

When adsorption follows the Freundlich model, the plot of ln Qe vs ln Ce gives a straight line with a slope of 1/n and a y intercept of ln K_F. The linearization parameters are represented in the tables III.15 and III.16 respectively.

Table III. 15. Linearisation parameters of the Freundlich model relative to the CFX on PHB.

T (°C)	K_f (Lg^{-1})	n	R^2
25	14.84	2.41	0.9862
40	14.36	2.31	0.9723
55	11.71	2.24	0.9631

Table III. 16. Linearisation parameters of the Freundlich model relative the adsorption of CFX on MWGO.

T (°C)	K_f (Lg^{-1})	n	R^2
25	12.02	1.83	0.8962

| 40 | 10.89 | 1.62 | 0.9513 |
| 55 | 09.18 | 1.76 | 0.9605 |

VIII . Thermodynamic parameters

The characteristics of the adsorption process, such as spontaneity, nature and applicability of the adsorbent, were determined using thermodynamic functions such as the variations in standard free energy ($\Delta G°$), enthalpy ($\Delta H°$) and entropy ($\Delta S°$), and evaluated graphically from the Van't Hoff equation as a function of temperature and the adsorption distribution coefficient (K_d) using the following equations :

$K_d = Q_e / C_{eq}$ …………(11)

$Ln\ Kd = \Delta S° /R - \Delta H° /T$ …………(12)

$\Delta G° = RTlnKd = T\Delta S° - \Delta H°$

ΔH^0 : Enthalpy variation (kJ mol^{-1})

ΔS^0 : Entropy variation (J mol^{-1} K^{-1})

K_d : Distribution coefficient (L g^{-1})

The thermodynamic coefficients related to the process of adsorption of CFX on PHG and on MWGO are represented in tables III.17 and III.18 respectively. As it is shown, all $\Delta G°$ values are negative, this indicates a spontaneous feasible reaction. Further, if $\Delta G°$ lies between − 20 to 0 kJ/mol, a physisorption is assumed to be an operative mechanism [16]. So with values -20 < -14.650 ; -15.386 ; -16.12 < 0 and 20 < -10.913 ; -11.462; -12.010 < 0 for PHB and MWGO respectively confirm a physisorption.

Table III. 17. Thermodynamic parameters for CFX adsorption on PHB.

ΔH(Kj/mol)	ΔS (J·mol^{-1}·K^{-1})	ΔG (Kj/mol)		
		25°C	40°C	55°C
-0.032	0.049	-14.650	-15.386	-16.121

Table III. 18. Thermodynamic parameters of CFX adsorption on MWGO.

ΔH(Kj/mol)	ΔS (J·mol^{-1}·K^{-1})	ΔG (Kj/mol)		
		25°C	**40°C**	**55°C**
-0.012	0.037	-10.913	-11.462	-12.010

The results demonstrate that ΔH is negative, indicating that an exothermic adsorption process has occurred. [12] results are similar to the current findings. The positive ΔS value indicates an increase in entropy at the solid/solution interface due to the internal structure of the adsorption.

IX.   Comparison with other adsorbents

Since our work focuses on cephalexin, we have reviewed some publications concerning the adsorption of this product in table III.19.

Table III. 19. Adsorption of diclofenac by different adsorbents.

Materials	Q$_{max}$ mg g^{-1}	References
GO	164.35	[12]
AC prepared from loofah sponge	55.11	[17]
Natural zeolite	16.1	[7]
Zeolite coated with manganese oxide nanoparticles	24.5	[7]
Walnut shell-based activated carbon	233	[9]
Bauxite	112	[18]
Palygorskite	12	[18]
Chitin–AC	245.19	[19]

X.   Conclusion

From this adsorption study, we opted for a comparative study to compare two of the synthesized materials : the porous hydrogel beads based of graphene exfoliated at 750°C and the microwave exfoliated graphene. We found that both materials are effective in removing cefalexin antibiotic from

aqueous solutions. Results were close with almost the same operational conditions. The optimum pH for this adsorption was 7. The study of adsorption isotherms led us to consider the Langmuir model as the most appropriate for describing these adsorption phenomenon's, based on high correlation coefficients R^2 values ; that exceed 0,98 ; and a maximum adsorption capacity of 217.39 mg/g for the hydrogel network and 209.46 mg/g for the MWGO. The thermodynamic study revealed that the adsorption process was spontaneous and exothermic. We can conclude that the synthesised materials are efficient to eliminate organic molecules like CFX from aqueous solutions.

References

[1]   M. Zhao, M.T. Yang, M. Singh, T. Overturf, Y. Gao, G. Silva Hernandez, S. Ahmed, S. Banerjee, Fabrication and characterization of a water purification system using activated carbon and graphene nanoplatelets: Toward the development of a nanofiltration matrix, Water Environ. Res. 93 (2021) 1530–1542. https://doi.org/10.1002/wer.1535.

[2]   I. Ali, A. Arsh, X.Y. Mbianda, A. Burakov, E. Galunin, I. Burakova, E. Mkrtchyan, A. Tkachev, V. Grachev, Graphene based adsorbents for remediation of noxious pollutants from wastewater, Environ. Int. 127 (2019) 160–180. https://doi.org/10.1016/j.envint.2019.03.029.

[3]   S.S. Hemdan, A.M. Al Jebaly, F.K. Ali, Importance of isosbestic point in spectroscopy : a review صخلملا يئانيبلا مسر لا سفن لع ةينورتكلالا فايطالا نم ةعومجم يف ةدوجوملا كتسبوزيالا ةطقن نكمي لوطلا سفن ناكلتمي : Abstract (2019). ,نينوكم نيب نازتا ةلاح لدي يلع دوجو ةيئاملا ليلاحملا يف يئايميكلا لعافتل ةطقن مادختخ https://doi.org/10.37376/1571-000-062-004.

[4]   F. Salaa, S. Bendenia, G.L. Lecomte-Nana, A. Khelifa, Enhanced removal of diclofenac by an organohalloysite intercalated via a novel route: Performance and mechanism, Chem. Eng. J. 396 (2020) 125226. https://doi.org/10.1016/j.cej.2020.125226.

[5]   G. Wernke, Q.L. Shimabuku-Biadola, T.R.T. dos Santos, M.F. Silva, M.R. Fagundes-Klen, R. Bergamasco, Adsorption of cephalexin in aqueous media by graphene oxide: kinetics, isotherm, and thermodynamics, Environ. Sci. Pollut. Res. 27 (2020) 4725–4736. https://doi.org/10.1007/s11356-019-07146-y.

[6]   A. Mohseni-bandpi, T.J. Al-musawi, E. Ghahramani, M. Zarrabi, S. Mohebi, S. Abdollahi, Improvement of zeolite adsorption capacity for cephalexin by coating with magnetic Fe 3 O 4 nanoparticles, J. Mol. Liq. 218 (2016) 615–624. https://doi.org/10.1016/j.molliq.2016.02.092.

[7]   M.R. Samarghandi, T.J. Al-Musawi, A. Mohseni-Bandpi, M. Zarrabi, Adsorption of cephalexin from aqueous solution using natural zeolite and zeolite coated with manganese oxide nanoparticles, J. Mol. Liq. 211 (2015) 431–441. https://doi.org/10.1016/j.molliq.2015.06.067.

[8]   S. Aghamiri, Batch Adsorption of Cephalosporins Antibiotics from Aqueous Solution by Means of Multi-Walled Carbon Nanotubes Batch Adsorption of Cephalosporins Antibiotics from Aqueous Solution by Means of Multi-Walled Carbon Nanotubes, (2017).

[9]   G. Nazari, H. Abolghasemi, M. Esmaieli, Batch adsorption of cephalexin antibiotic from aqueous solution by walnut shell-based activated carbon, J. Taiwan Inst. Chem. Eng. 000 (2015) 1–9. https://doi.org/10.1016/j.jtice.2015.06.006.

[10]   S. Yadav, A. Asthana, A.K. Singh, R. Chakraborty, S.S. Vidya, Methionine-Functionalized Graphene Oxide / Sodium Alginate Bio-Polymer Nanocomposite Hydrogel Beads : Synthesis , Isotherm and Kinetic Studies for an Adsorptive Removal of Fluoroquinolone Antibiotics, (2021).

[11]   L.I.U. Weifeng, X.I.E. Huijun, Z. Jian, Z. Chenglu, Sorption removal of cephalexin by HNO 3 and H 2 O 2 oxidized activated carbons, 55 (2012) 1959–1967. https://doi.org/10.1007/s11426-011-4488-3.

[12]   G. Wernke, Q.L. Shimabuku-biadola, T. Rhuna, M.F. Silva, M.R. Fagundes-klen, Adsorption of cephalexin in aqueous media by graphene oxide : kinetics , isotherm , and thermodynamics, (2019).

[13]   Y.S. Ho, G. Mckay, Pseudo-second order model for sorption processes, 34 (1999) 451–465.

[14] S.H. Chien, W.R. Clayton, Application of Elovich Equation to the Kinetics of Phosphate Release and Sorption in Soils 1, (1955) 1–4.

[15] M.J.D. Low, KINETICS OF CHEMISORPTION OF GASES ON SOLIDS, (1960).

[16] C. Sutherland, and mechanistic insights, Desalin. Water Treat. 318 (2024) 100357. https://doi.org/10.1016/j.dwt.2024.100357.

[17] Q. Kong, Y. Wang, L. Shu, M. Miao, Isotherm , kinetic , and thermodynamic equations for cefalexin removal from liquids using activated carbon synthesized from loofah sponge, 3994 (2015). https://doi.org/10.1080/19443994.2015.1052991.

[18] S. Giannoulia, A.G.T.C.A. Aggelopoulos, Exploration of cephalexin adsorption mechanisms onto bauxite and palygorskite and regeneration of spent adsorbents with cold plasma bubbling, Appl. Water Sci. 14 (2024) 1–18. https://doi.org/10.1007/s13201-024-02101-w.

[19] W.A. Khanday, M.J. Ahmed, P.U. Okoye, E.H. Hummadi, B.H. Hameed, Bioresource Technology Single-step pyrolysis of phosphoric acid-activated chitin for efficient adsorption of cephalexin antibiotic, Bioresour. Technol. 280 (2019) 255–259. https://doi.org/10.1016/j.biortech.2019.02.003.

General conclusion

The synthesized graphene has exhibited exceptional adsorption properties, making it an ideal candidate for water treatment applications. By harnessing its high surface area and unique physical and chemical properties, graphene can effectively remove heavy metals, organic compounds, and other impurities from contaminated water sources through adsorption and filtration processes.

The use of high temperature in the synthesis of graphene has proven to be an effective method for producing high-quality graphene materials. This method allows for the control of graphene's size, shape, and defect density, leading to enhanced adsorption capabilities.

This research proposes a promising, cost-effective and scalable approach to thermally exfoliate graphite into few layers of graphene. Our method involves a unique high-temperature shock treatment in a tubular furnace, enabling simultaneous oxidation, intercalation, and exfoliation within a matter of seconds. The heat sensitive component increased the inner pressure within basal spacing and facilitated its exfoliation into well exfoliated nanosheets. Three critical temperatures ; 750°C, 820°C and 870°C ; were selected carefully in order to see their impact on the exfoliation process. Furthermore, the impact of expansion temperature on the physicochemical properties of the resulting carbonaceous materials was taken in investigations.

The efficiency of exfoliation was additionally investigated using microwave irradiations.

The FTIR analysis confirmed that the oxygen-containing functional groups were partially eliminated, leaving behind a small amounts of residue. These functional groups can still be found at the edge and basal plane of all the obtained materials (GO-750, GO-820, GO-870 and MWGO) , but their peaks are less intense compared to those of graphene oxide (IGO), indicating a successful thermal reduction process.

The XRD analysis confirmed the oxidation and the exfoliation process by the reappearance of the (d_{002}) diffraction line at $2\theta = 21.5°$, $2\theta = 26.43°$, $2\theta = 26.46°$ and $2\theta = 26.49°$ which correspond to lattice spacings of 4.14, 3.369, 3.66 Å and 3.3362 Å for GO-750, GO-820, GO-870 and MWGO respectively. In addition, the XRD patterns of the graphene samples have weak (0 0 2) diffraction peaks with significantly lower intensities, indicating that the lattice structure of graphite is preserved during the transformation proving to the few- layer feature of the resultant graphene. After heat treatment,

General conclusion

GO-820 and GO-870 exhibit similar peak interlayer distance values of 3.35 Å for pure graphite, showing significant restoration of carbon materials with two-dimensional ordered stacks.

According to the thermogravimetric analyses indicate that GO-750 and MWGO needs less heat to decompose large oxygen groups and weaker non-graphitic sp^3 hybridised carbon. GO-820 and GO-870 have similar thermographs with a starting decomposition temperature above 600°C, making them the most thermodynamically stable carbon materials studied in this work.

In order to examine the efficiency of the synthesised materials a specialised vertical filtration system in separating water from synthetic wastewater containing malachite green (MG) and Alizarin Red S dyes (AR).

The retention of malachite green is consistently between 99% and 100% at concentrations of 10^{-5} M and 10^{-4} M. Nevertheless, at a concentration of 10^{-3} M, the retention rate fluctuates between 97% and 98%. Therefore, the retention of Alizarin Red S permeates recorded is in the order of 99% up to 100% for the concentrations 10^{-4} M and 10^{-3}M. This is due to the good absorption capacity of the activated carbon.

Single network hydrogel beads and the microwave assisted exfoliated graphene were successfully synthesized and tested for the elimination of an antibiotic ; Cefalexin ; from aqueous solutions. This adsorption worked best at pH 7. After studying adsorption isotherms, we decided the Langmuir model best described this phenomenon due to its high correlation coefficients R^2 values close to unit and maximum adsorption capacity of 217.39 mg/g and 209.46 mg/g for the porous hydrogel network and MWG respectively. The thermodynamic analysis showed exothermic and spontaneous adsorption. The synthesised materials can effectively remove organic compounds like CFX from aqueous solutions. This underscores the potential of graphene-based materials in addressing the pressing challenges of water pollution and scarcity.

Future research should focus on investigating the process of graphite exfoliation into defect-free single-layer graphene at high temperatures. This could lead to environmentally friendly and economically effective methods for addressing freshwater and wastewater cleanup initiatives.